ARCHIVES OF ACOUSTICS
12, 3–4, 159–175 (1987)

SIMILARITY FUNCTIONS OF ACOUSTIC PATTERNS AS INDICES OF THE OBJECTIVE QUALITY EVALUATION OF SPEECH TRANSMISSION

CZESŁAW BASZTURA

Institute of Telecommunication and Acoustics
Wrocław Technical University
(50–317 Wrocław, ul. B. Prusa 53/55)

This study is concerned with a new, objective quality evaluation of speech transmission through telephone lines. The conception of the studies is based on the assumption of equivalency between the results of subjective and objective measurements. A special purpose of the study was to investigate the efficiency of the similarity function of the acoustic patterns of signals as an indice of the objective quality evaluation of speech transmission. Altogether, the usefulness of 8 functions of similarity were investigated, such as the Hamming, Euclid, Minkowski, Tanimoto, Chebyshev, Camberra distances, χ-square and directional cosine. The obtained preliminary results indicate for some similarity functions good agreement with subjective results obtained by the subjective method.

1. Introduction

The telephone communication is the fundamental kind of speech-based communication. The development of telephone networks, accompanied by the simultaneous increase in the quality requirements set by users of these systems, makes more and more distinct the necessity of elaborating effective methods for quality measurements of telephone systems and lines. The quality and faithfulness of transmission of messages by telephone links depend both on subjective factors brought about by users and also on the objective physical parameters of tele-transmission systems.

Keeping in with CCITT recommendations, the national and international telephone systems are standardized, in terms of their quality, according to the criterion of loudness [21, 22].

Another important criterion of the quality evaluation of telephone transmission is the clearness or intelligibility as measured by the articulation method [16, 17]. The clearness measurement by the articulation method is carried out by a team of operators. The measurement consists in the transmission and detection of appropriate articulation lists made up from elements of speech (logatoms, words). On the basis

of these two basic criteria of loudness and clearness, many methods have been developed, which are objectivized to a greater or lesser extent [1, 2, 3, 7, 9, 11, 12, 16, 17, 18, 19]. Most of them involve numerous faults preventing their use on a larger scale.

The difficulties occurring in the solution of the objectivization problem consist in the fact that the objective measurement system should take into account not only the main characteristics of the standard (reference) system, the physical characteristics of the speech signal, but also the physiological properties of hearing, determining the subjective sensation of loudness or clarity (intelligibility). Since the measurement methods concerned with the quality of speech transmission which are based on the criterion of clearness, or that of intelligibility, are the methods which ensure better agreement with users' evaluations, most objective methods, including the present one, are now devoted to the objectivization of measurements, taking as the reference (comparative) measure subjective measurements of clearness [1, 6, 9, 17].

The complexity of the problem of objectivization of subjective evaluations of clearness or intelligibility implies a different approach to its solution. This is manifested, e.g., in the applied method, in the number and kind of studied interferences, in the ways of the signal parametric representation, measurement methods and algorithms of objective estimation.

T. B. BARNWELL, in studies [1, 2, 3], carried out investigations on the effective objective measure correlated with subjective evaluations. He studied a relatively wide spectrum of distortions arising in both discrete transmission (APCM, ADPCM, LPC etc), and analogue transmission (band filtration, noise interference, clippering, echo etc.). As the subjective measure, Barnwell applied the DAM measure (Diagnostic Acceptability Measure) [19]. As objective measures, he used 4 classes of measures:

– the measure of spectral distance, where the distortions were measured in the domain of frequency;

– the parametric measures of distance, where the parametric distances were measured between the patterns of distorted and undistorted speech signals;

– noise measures used for noised signals;

– complex measures which were a linear combination of other measures.

The results which Barnwell obtained ensured a large degree of agreement between objective and subjective measures. Their basic fault is the complicated character of measurement methods and the resulting difficulty involved in applying them in more general operations.

Among other studies, one should mention, e.g., those by W. J. HARTMANN [9], L. R. RABINER [11], D. L. RICHARDS [12] and R. VISWANATHAN et al. [18].

In most general terms, objective methods for the quality evaluation ef speech transmission can be divided into:

– methods using a test (natural or artificial) signal, and

– methods which do not a test signal.

Previously, most methods for the quality evaluation of speech transmission were based on the use of a test signal as a carrier of information about the degree of signal

distortion. Moreover, this signal was a natural or artificial one with the statistics of certain parameters being close to the natural-speech signal [1, 2, 3, 9, 11, 18]. Some papers were concerned with calculation methods based on the results of physical measurements of the parameters of a telephone line. On this basis, it was possible to determined objective measures as correlated with subjective reference measures [7, 12].

In elaborating an objective method for the quality evaluation of the transmission of a speech signal, one should bear in mind the fact that subjective clearness measurements can be replaced only if the principle of equivalency between the results of subjective and objective measurements is satisfied. The comparative basis for this equivalence is the subjective measure, which is understandable if one takes into account the fact that human beings are users of the studied tele-transmission systems. The way of the articulation of transmitted signals and also the perception of these signals by hearing organs also exert an influence on the quality evaluation of transmission. To make the results of subjective measurements to depend to the largest extent only on the physical parameters of a telephone line, logatom lists are used as the linguistic test material, ensuring the elimination of semantic information [20].

The performed studies were based on the a priori assumption saying that there exists some correlation between the objective measure M_r and the subjective measure of the quality evaluation of speech transmission M_s. As the objective measure M_r, the probability degree between the test signal at the output from the investigated line and the signal assumed as a standard one was assumed (Fig. 1). In particular, the

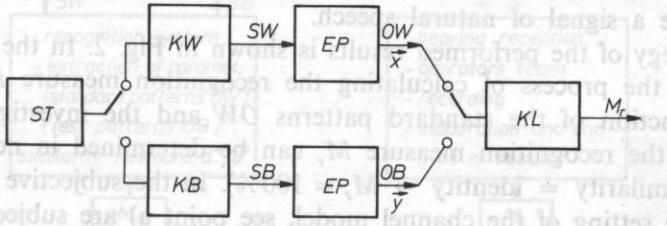

Fig. 1. Block scheme of the system for the objective measurement of speech transmission using the measure of recognition of acoustic patterns: ST – test signal (original), KW – standard channel, SW – standard signal, KB – ivestigated channel, SB – investigated signal, EP – extractor of parameters, OB, OW – studied and standard patterns, KL – classifer, M_r – recognition measure

standard signal can be the transmitted as original signal. At the output of the studied line, the test signal contains information about distortions and interferences introduced by telephone lines, having an effect on the transmission quality, i.e., on the evaluation of the quality of the line.

In investigations of this type, the fundamental problem is to separate out such information; in other words, to create specific acoustic patterns of a signal at the output of the studied line OB and to compare it with the standard pattern OW. Some

of the indices serving in determining the mutual relations of the images *OB* and *OW* are known as similarity functions [4, 8, 14], applied in the automatic recognition of speech and voices.

2. Research method

2.1. *Main assumptions*

For further considerations, the following basic assumptions and definitions were presumed:

a) the investigated objects are typical telephone lines alternatively called telephone channels, represented to ensure the repeatability of subjective and objective measurements, by an adjustable physical model of a telephone channel [5];

b) the reference criterion of the quality of speech transmission, and at the same time the quality criterion of the k-th telephone channel, is the logatom articulation index measured according to ISO recommendations [20];

c) the objective measurement (estimation) of articulation is the procedure aimed at some equivalent transformation determined from the set K of channels (in fact, from sets of measurable groups of parameters describing these channels), or otherwise, patterns (x, y) and the values of the indices M_r;

d) it was assumed that the principle of maximum agreement of physical conditions should be applied with objective measurements and the existing conditions for subjective reference measurements;

e) the principle was assumed that resulting from the previous condition the test signal will be a signal of natural speech.

The strategy of the performed results is shown in Fig. 2. In the objective part, there occurs the process of calculating the recognition measure M_r namely the similarity function of the standard patterns *OW* and the investigated ones *OB*. Particularly, the recognition measure M_r can be determined in normalized form (maximum similarity = identity $\rightarrow M_r = 100\%$). In the subjective part, the same links (for the setting of the channel model, see point a) are subject to subjective measurements using a crew of operators (transmitters and receivers) and by means of appropriate logatom lists [20]. The calculated mean articulations index, assumed as the subjective measure M_s, are references for the objective measure M_r.

2.2 *Similarity functions*

Similarity functions serve in determining the relation between two patterns, i.e. the standard pattern of the signal *OW* and the investigated image *OB*. Similarity functions can have the form of the distance function $d^{\alpha}(x, y)$ or of the nearness function $b^{\alpha}(x, y)$ (where α denotes the kind of the possibility function). Between the distance and nearness functions, with some assumptions, there exist unique relations,

such as

$$b^{\alpha}(x, y) = \frac{1}{d^{\alpha}(x, y)} \qquad d^{\alpha}(x, y) \neq 0, \tag{1}$$

$$b^{\alpha}(x, y) = \exp[-d^{\alpha}(x, y)]. \tag{2}$$

In automatic speech recognition, the distance functions, also called briefly distances, are more broadly used. Below, expressions are given for the distance and nearness functions used in the studies.

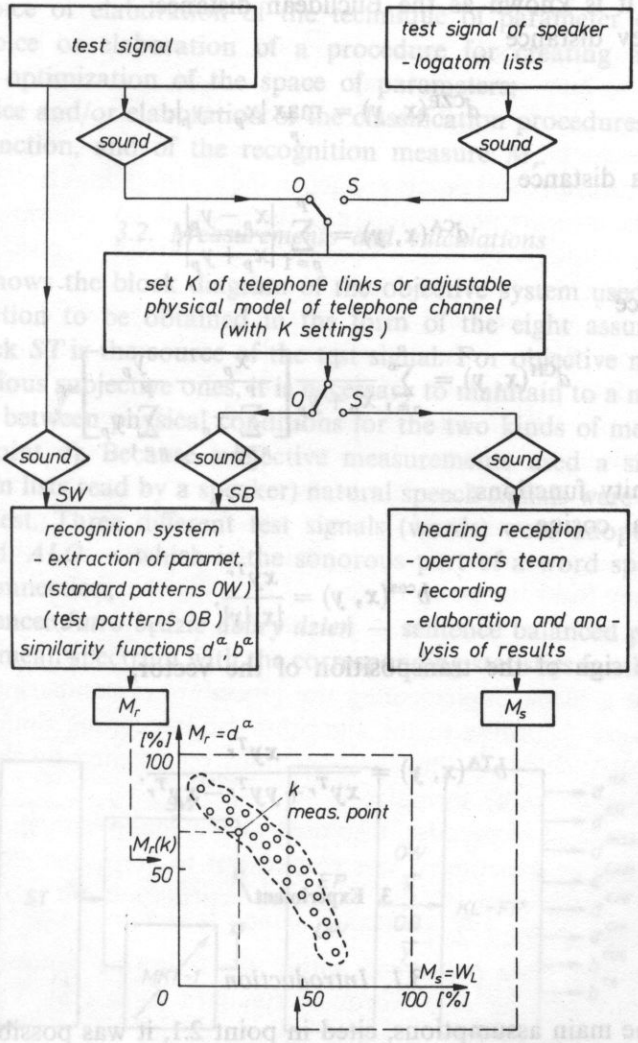

Fig. 2. Block scheme of the "learning" of the objective system. O — objective measurements, S — subjective measurement of articulation

Distance functions:

a) Minkowski distance

$$d^{\mathrm{MI}}(x, y) = \Big[\sum_{p=1}^{P} |x_p - y_p|^r\Big]^{1/r} \qquad r \geqslant 1, \tag{3}$$

where $p = 1, 2, \ldots, P$, where P is the dimension of the parameter vector constituting the image, x_p is the p-th component of the vector which is the standard pattern (OW) an y_p is the p-th component of the vector which is the investigated pattern (OB) for $r = 1$ $d^{\mathrm{MI}}(x, y)$ it is known as the Hamming, or street distance [15], and for $r = 2$, it is known as the Euclidean distance;

b) Chebyshev distance

$$d^{\mathrm{CZE}}(x, y) = \max_{p} |x_p - y_p|, \tag{4}$$

c) Camberra distance

$$d^{\mathrm{CA}}(x, y) = \sum_{p=1}^{P} \frac{|x_p - y_p|}{|x_p + y_p|}, \tag{5}$$

d) χ^2-distance

$$d^{\mathrm{CH}}(x, y) = \sum_{p=1}^{P} \frac{1}{x_p + y_p}\left[\frac{x_p}{\sum_{p=1}^{P} x_p} - \frac{y_p}{\sum_{p=1}^{P} y_p}\right], \tag{6}$$

and the proximity functions:

e) directional cosine

$$b^{\cos}(x, y) = \frac{xy^{T_r}}{|x|\,|y|}, \tag{7}$$

where T_r is the sign of the transposition of the vector,

f) Tanimoto

$$b^{\mathrm{TA}}(x, y) = \frac{xy^{T_r}}{xy^{T_r} + yy^{T_r} - xy^{T_r}}. \tag{8}$$

3. Experiment

3.1. Introduction

By taking the main assumptions, cited in point 2.1, it was possible to carry out experimental studies and analysis attempted at the verification of the hypothesis concerned with the possibility of using the similarity functions of acoustic patterns in

the objective evaluation of the speech transmission quality. The first, at the same time the fundamental, problem was the creation of the space of observations (the space of parameters) which was representative from the point of view of the information of interest. In the process of evaluation of the speech transmission quality, the space of observations should contain information about the degree of distortion and interference of the transmitted speech signal. In the carrying out of the experiment, the first step consisted in choosing the appropriate test signal.

The other steps included:

a) the choice of physical quantities representing the desired set of information;

b) the choice of a set (or sets) of parameters of the signal;

c) the choice or elaboration of the technique of parameter extraction;

d) the choice or elaboration of a procedure for creating acoustic patterns including the optimization of the space of parameters;

e) the choice and/or elaboration of the classification procedures and the related probability function, and of the recognition measure M_r.

3.2. Measurements and calculations

Figure 3 shows the block diagram of the objective system used, permitting the similarity function to be obtained in the form of the eight assumed probability functions. Block *ST* is the source of the test signal. For objective measurements to replace the tedious subjective ones, it is necessary to maintain to a maximum degree the agreement between physical conditions for the two kinds of measurements (see chapter 2.1, point d). Because subjective measurements used a signal of natural speech (logatom lists read by a speaker) natural speech signals were also included in the objective test. Three different test signals (words) were adopted;

a) the word: *ALO* – which is the sonorous part of a word spoken in making a telephone connection,

b) the sentence: *Jutro będzie dobry dzień* – sentence balanced phonetically and in terms of the mean spectrum with the corresponding statistics for the Polish speech [10],

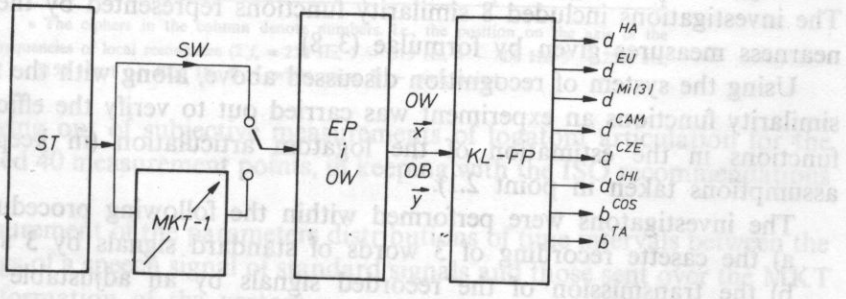

Fig. 3 Simplified block scheme of the amplified objective system for the evaluation of speech transmission quality

c) the sentence: *Sprawdzenie przydatności funkcji podobieństwa do oceny jakości transmisji sygnału mowy.*

The above mentioned test signals were recorded by 3 male speakers (with each speaker recording all 3 words). MKT – 1 is a physically adjustable model of a telephone link permitting (in repeatable way) the setting of various values of the main sets of parameters for typical telephone links [5, 21, 22]. In the further part of this paper, these sets of parameters will be called measurement points. The investigations included 40 measurement points which represented just as many corresponding typical telephone links. The sets of parameters contained the following quantities:

– the frequency band;
– the signal-to-noise ratio (white and pink noise): [s/noise];
– the signal-to-hum ratio; [s/hum]; and
– different types of the amplitude response of the channel the position of local resonances [corrector].

The full set of measurement points applied in the investigations is shown in Table 1.

In choosing the measurement points, e.g., the principle of uniform distribution of these points was followed so that it could cover as broad as possible a range of logatom articulation the (10–97%, see Table 1).

EP and *OW* is a measurement block extracting selected physical parameters of the standard signal *SW* and the investigated one *SB*, and forming the standard patterns *OW* of data in the form of the vector of parameters $\boldsymbol{x}$ and that of the investigated patterns *OB* of data in the form of the vector of parameters $\boldsymbol{y}$.

In the present investigations, the extractor of the parameters $\boldsymbol{x}$ and $\boldsymbol{y}$ was a system implementing the procedure of measurement of the distribution of time intervals between zero crossings of a speech signal. This kind of parametrization of the signal was chosen because of its simple implementation in a real time and the sufficient efficiency from the point of view of carrying the characteristic features of a speech signal, namely distortions, interference, individual features etc. [4, 6, 7, 8].

KL – FP is a block implementing the procedure of comparing standard and investigated images according to the algorithm for calculating similarity functions. The investigations included 8 similarity functions represented by the distance and nearness measures given by formulae (3–8).

Using the system of recognition discussed above, along with the assumed eight similarity functions an experiment was carried out to verify the efficiency of these functions in the estimation of the logatom articulation (in keeping with the assumptions taken in point 2.1).

The investigatons were performed within the following procedure:

a) the casette recording of 3 words of standard signals by 3 speakers;

b) the transmission of the recorded signals by an adjustable model of the telephone channel MKT–1, i.e., by 40 settings of it (measurement points – see Table 1);

Table 1. Set of parameters for measurement points used in the experiment

K	band boundary frequency [Hz]	S/noise [dB]	S/hum [dB]	corrector * ch-ki-	logatom articulation W_L [%]
1	2	3	4	5	6
1	200-4000	> 40dB	40	-	96.3
2	200-4000	B+12	40	2,3,7,8	86.8
3	200-4000	B+6	40	2,3,7,8	78.2
4	200-4000	B+3	40	2,3,7,8	70.4
5	200-4000	B 0	40	2,3,7,8	64.1
6	200-4000	B-3	40	2,3,7,8	32.4
7	300-4000	B+9	40	–	74.3
8	300-4000	B+3	40	–	83.7
9	300-4000	B-3	40	–	41.6
10	300-4000	B-9	40	–	29.2
11	600-2000	>40	40	–	93.4
12	600-2000	B+12	40	–	83.7
13	600-2000	B+6	40	–	77.2
14	600-2000	B+3	40	–	56.1
15	600-2000	B 0	40	–	58.5
16	600-2000	B-3	40	–	36.7
17	400-2500	B+15	40	–	85.6
18	400-2500	B+6	40	–	72.2
19	400-2500	B+3	40	–	699.5
20	400-2500	B 0	40	–	53.8
21	400-2500	B-2	40	–	51.4
22	400-2500	B-4	40	–	42.4
23	400-2500	B-6	40	–	19.1
24	400-2500	B-9	40	–	18.4
25	400-2500	B-12	40	–	9.1
26	400-2500	R-3	40	–	27.9
27	400-2500	R-6	40	–	55.4
28	400-2500	R-9	40	–	26.2
29	400-2500	>40	40	–	80.8
30	400-2500	>40	40	–	82.9
31	400-2500	>40	+3	3,4,6,7	84.5
32	400-2500	B+12	+6	3,4,6,7	64.2
33	400-2500	B+12	+3	3,4,6,7	70.7
34	400-2500	B+6	-2	3,4,6,7	48.7
35	400-2500	B+6	-3	3,4,6,7	62.0
36	400-2500	B+6	+6	3,4,6,7	59.0
37	400-2500	B+3	+6	3,4,6,7	58.8
38	400-2500	B+3	+3	3,4,6,7	65.2
39	400-2500	B-3	-3	–	32.1
40	400-2500	R-6	0	–	19.9

* The ciphers in the column denote numbers, i.e., the position on the axis of the frequencies of local resonances (2 f_0 = 250 Hz, 3 – 315 Hz, 4 – 400 Hz, 5 – 2500 Hz, 7 – 3150 Hz, 8 – 4000 Hz, B – white noise, R – pink noise).

c) the carrying out of subjective measurements of logatom articulation for the above-mentioned 40 measurement points, in keeping with the ISO recommendations [20];

d) the measurement of the parameters distributions of time intervals between the zero – crossings of a speech signal of standard signals and those sent over the MKT – 1 and the formation of the vectors

$$X = \{x_1, x_2, \ldots, x_p \ldots x_p\}^T r, \quad P = 7. \tag{9}$$

Table 2. Values of the components of the vector of standard signals x and the patterns y of the measurement points. Patterns of expressions of three speakers for the third word, k – channel number, W_L – articulation measured subjectively

k		$x_{k,0}$							
		$x_{k,1}$ $y_{k,1}$	$x_{k,2}$ $y_{k,2}$	$x_{k,3}$ $y_{k,3}$	$x_{k,4}$ $y_{k,4}$	$x_{k,5}$ $y_{k,5}$	$x_{k,6}$ $y_{k,6}$	$x_{k,7}$ $y_{k,7}$	W_L [%]
standard $k=0$	1	1448	411	163	266	444	206	48	
	2	2077	661	234	380	299	40	18	100
	3	2139	645	253	461	428	108	32	
1	1	1365	681	251	335	471	243	28	
	2	2262	1191	311	416	361	62	80	96
	3	2294	1087	298	507	464	64	41	
2	1	1287	1420	544	511	189	170	12	
	2	1633	1576	427	473	102	29	6	93
	3	1629	1666	580	698	108	54	11	
3	1	2574	1089	347	368	420	181	2	
	2	2551	1865	442	450	304	39	1	86
	3	2591	1812	453	530	409	38	1	
4	1	1796	1487	469	413	269	109	3	
	2	2712	2362	635	731	122	52	6	78
	3	2796	2341	615	690	199	62	2	
5	1	2032	1609	518	413	269	27	9	
	2	2993	2681	731	409	122	12	6	69
	3	3029	2591	690	503	199	34	12	
6	1	2317	2041	646	418	226	28	4	
	2	3081	2912	850	398	92	12	2	58
	3	3185	2873	815	500	175	12	3	
7	1	2514	2344	753	381	134	16	2	
	2	3223	3097	872	364	62	11	3	32
	3	3318	3145	386	468	123	11	2	
8	1	2022	1479	473	415	380	31	12	
	2	2801	2104	569	478	242	3	2	74
	3	2823	1966	508	585	355	11	7	
9	1	2297	1818	560	397	252	111	19	
	2	3029	2583	683	408	143	71	21	61
	3	2950	2398	671	570	244	84	40	
10	1	2643	2342	679	338	119	20	4	
	2	3355	2979	829	321	61	11	2	41
	3	2980	880	438	102	16	7		

As an example, Table 2 gives values of the standard vector for 3 speakers, the 3rd word and control vectors (for 10 measurement points);

e) the setting in motion of the programme of the classifer $KL - FP$ reading in the vectors $\boldsymbol{x}$, and the calculation of 8 similarity functions and the polynomial approximation for the calculated similarity functions and the values of the subjectively measured logatom articulation W_L;

f) analysis of the results.

The calculations of the similarity functions and the polynomial approximation were implemented on MC Odra 1304, using purpose-constructed subprogrammes.

The first of the elaborated subprogrammes implemented the calculations of the distance between the investigated vectors $\boldsymbol{y}$ from the standard one $\boldsymbol{x}$.

The other subprogramme implemented the polynomial approximation of points lying on the plane: the logatom articulation $W_L = M_s$, given by the distance function $d^\alpha = M_r$. The least squares method was used by polynomials of different degrees, from 1 to 5. In this way, for each word and each similarity function, the following dependence was obtained:

$$W_L = [s^\alpha(x, y)]. \tag{10}$$

Another subprogramme made it possible to represent graphically the inverse dependence

$$d^\alpha(x, y) = f(W_L) \tag{11}$$

approximating too, the points by least squares method by polynomials with degrees of 1 to 5. Dependencies (10) and (11) make it possible to verify the degree of agreement of subjective measurements ($W_L = M_s$) and objective ones ($d^\alpha = M_r$)

4. The research results and conclusions

The performed experimental results, calculations and analyses made it possible to obtain quite an ample set of results. The chosen characteristic results will be presented in greater detail, including the functional relations $W_L = f(d^\alpha)$, making it possible to evaluate the usefulness of the studied functions d^α.

Figures 4 and 5 show some typical graphic dependencies on the function approximating the dependence $W_L = f(d^\alpha)$ for chosen kinds of distances and for words 1 and 3. Comparing the usefulness of the particular functions as arguments facilitating the mapping of the logatom articulation W_L dependence 10 one can state that:

a) The Hamming distance gives good mapping W_L for all test signals, particularly for the approximation with a third-degree polynomial.

E.g., for the word "ALO"

$$W'_L = 0.929 \cdot 10^2 - 0.121 \cdot 10^{-1} d^{\mathrm{HA}} + 0.151 (d^{\mathrm{HA}})^2 - 0.631 \cdot 10^{-10} (d^{\mathrm{HA}})^3. \tag{12}$$

b) For Euclidean and Minkowski distances ($r = 3$)(MI(3)) the best agreement in the mutual mapping between M_r and M_s was obtained just as for the Hamming distance for the longest word and for all higher degrees of the approximating polynomials. For example, for the third word and third degree of the polynomial it was obtained that

$$W'_L = 90.2 - 0.184 \cdot 10^{-1} d^{\mathrm{EU}} + 0.364 \cdot 10^{-5} (d^{\mathrm{EU}})^2 - 0.239 \cdot 10^{-9} (d^{\mathrm{EU}})^3, \tag{13}$$

and

$$W'_L = 89.6 - 0.203 \cdot 10^{-1} (d^{\mathrm{MI(3)}}) + 0.448 \cdot 10^{-5} (d^{\mathrm{MI(3)}})^2 - 0.327 \cdot 10^{-9} (d^{\mathrm{MI(3)}})^3. \tag{14}$$

c) The Chebyshev distance, just as the Minkowski distance, gives good unique

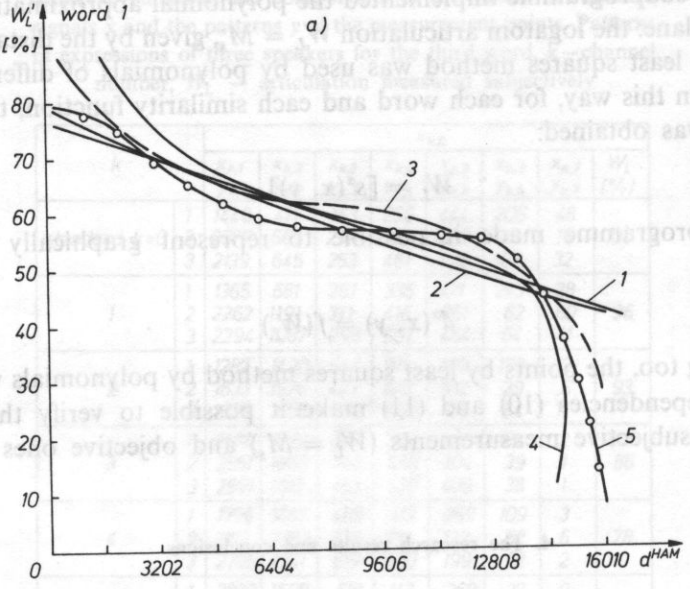
a)
W_L' word 1
[%]
80
70
60
50
40
30
20
10
0
3202
6404
9606
12808
16010 d^{HAM}
1
2
3
4
5

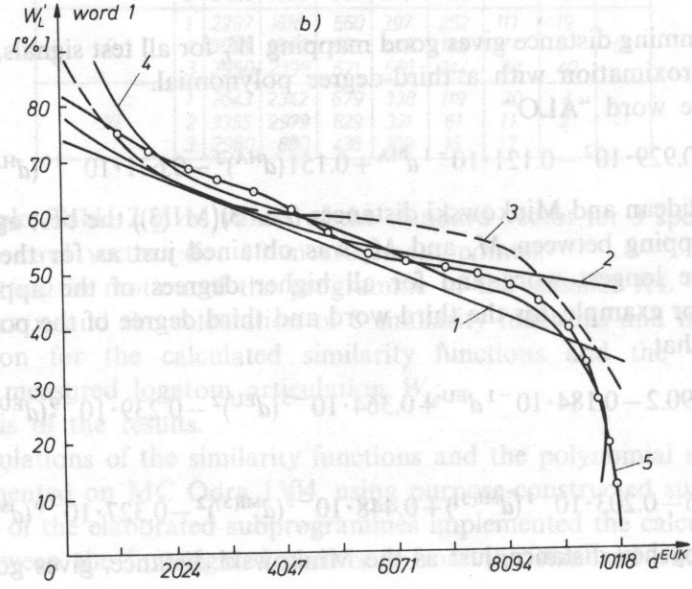
b)
W_L' word 1
[%]
80
70
60
50
40
30
20
10
0
2024
4047
6071
8094
10118 d^{EUK}
1
2
3
4
5

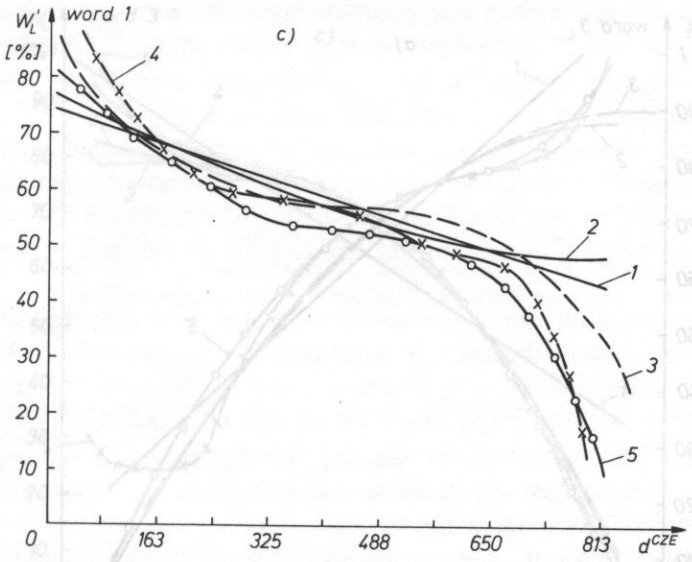

Fig. 4. Plots of functions approximating the logaton articulation $W_L = f(d^n)$ for word 1 and polynomial degrees a) Hamming distance, b) Euclidean distance, c) Chebyshev distance

mapping W_L, particularly for the third word and higher degrees of the approximating polynomial.

d) The Camberra distance and χ^2 give results either ambiguous or ones covering too small a range of logatom articulation.

e) The proximity functions of the directional cosine and Tanimoto do not make it possible to obtain unique mappings of logatom articulation (Fig. 5d), resulting mainly from the very forms of these functions.

In summary, it can be stated that the best effects were obtained by using as similarity functions the Hamming, Euclidean, Minkowski ($r = 3$) and Chebyshev distances. The best results were obtained for the third message (the longest one), and good agreement was provided already by the approximation with polynomials of the third degree. Here, it is interesting to note that, although graphically they represent the desired character of mapping, approximations with polynomials of the first and second degrees constitute hardly inaccurate approximation, particularly for small and large logatom articulations. The other similarity functions, i.e., the directional cosine, Tanimoto, Camberra and χ^2 give weak, or unambiguous, mappings for the applied patterns of acoustic signals. No significant changes were observed for differences in the values of similarity functions for particular speakers.

In evaluating the results, it is interesting to note three assumptions and restrictions made in the performed experiment, which, at this stage of research do not permit one to draw the final quantitative conclusions, namely ones related, e.g. to the values of the coefficients of approximating functions.

The first restriction involves the way of introducing a signal into a telephone link

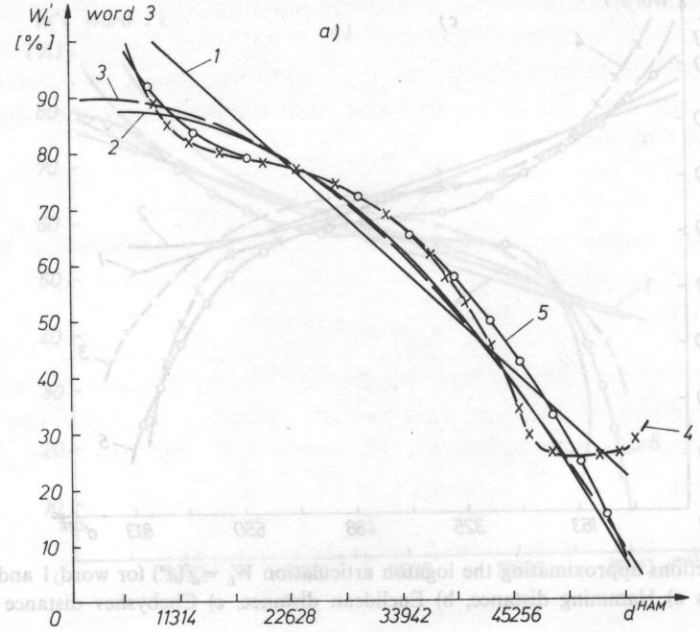
W_L' [%]
word 3
a)
1
2
3
4
5
90
80
70
60
50
40
30
20
10
0
11314
22628
33942
45256
d^{HAM}

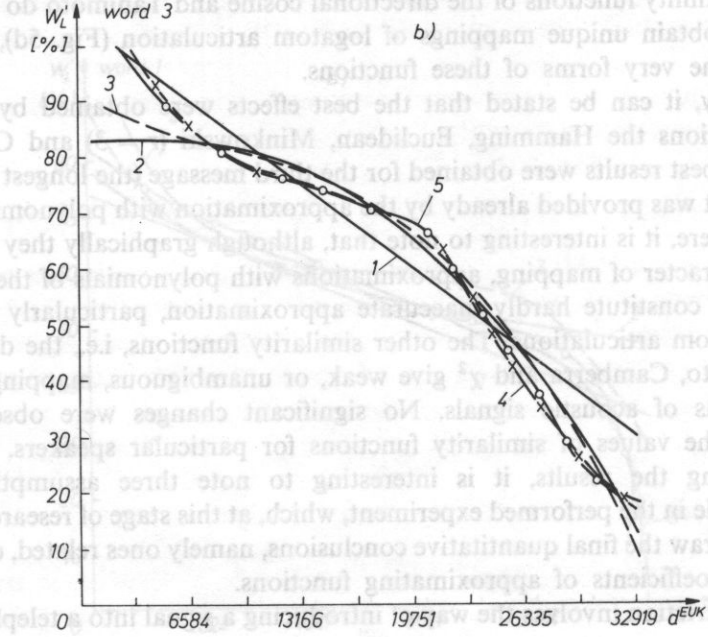
W_L' [%]
word 3
b)
1
2
3
4
5
90
80
70
60
50
40
30
20
10
0
6584
13166
19751
26335
32919
d^{EUK}

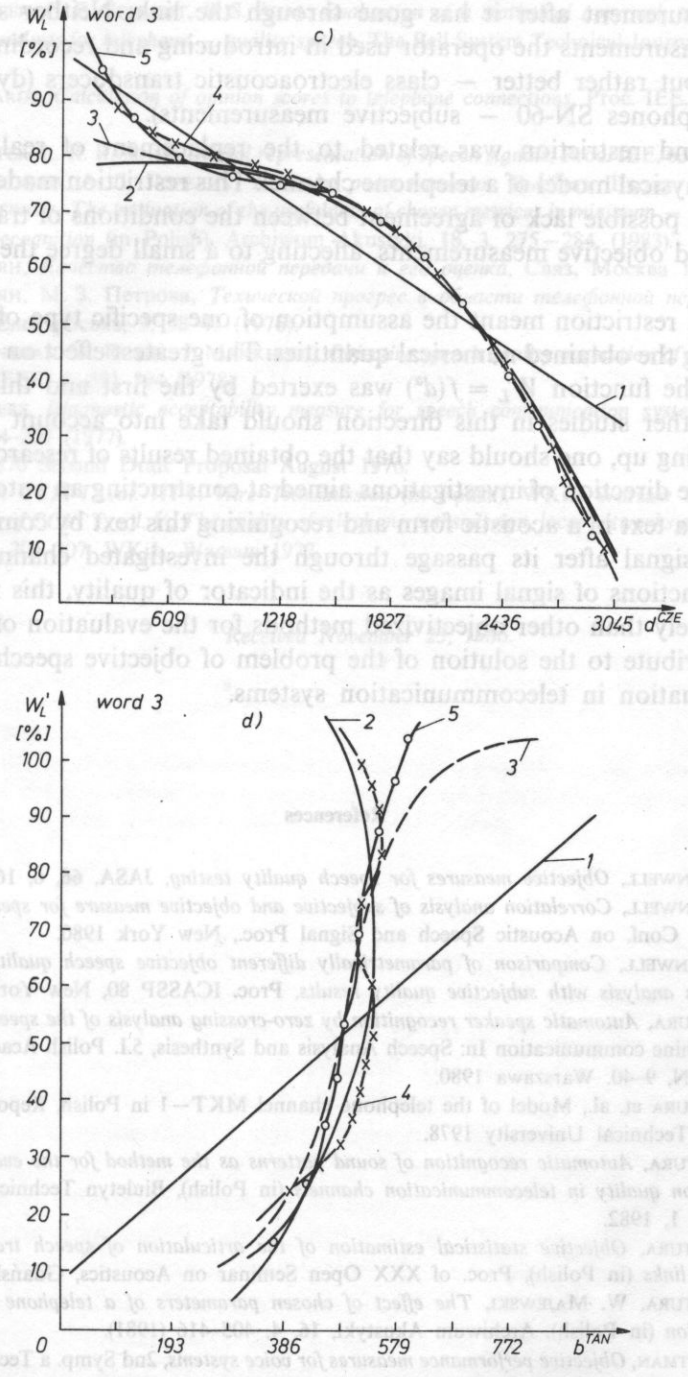

Fig. 5. Plots of functions approximating the logatom articulation $W_L = f(d^n)$ for word 3 and polynomial degrees 1-5: a) Hamming distance, b) Euclidean distance, c) Chebyshev distance, d) Tanimoto proximity function

and its measurement after it has gone through the link. Neither subjective nor objective measurements the operator used in introducing and recording test signals, telephones, but rather better – class electroacoustic transducers (dynamic microphone, headphones SN-60 – subjective measurements).

The second restriction was related to the replacement of real links by an adjustable physical model of a telephone channel. This restriction made it possible to eliminate the possible lack of agreement between the conditions of transmission for subjective and objective measurements, affecting to a small degree the results of the studies.

The third restriction meant the assumption of one specific type of parametrization, affecting the obtained numerical quantities. The greatest effect on the numerical values and the function $W'_L = f(d^\alpha)$ was exerted by the first and third restriction, therefore further studies in this direction should take into account these aspects.

In summing up, one should say that the obtained results of research confirm the validity of the direction of investigations aimed at constructing an automatic devices transmitting a text in a acoustic form and recognizing this text by comparing it with a standard signal after its passage through the investigated channel. Using the similarity functions of signal images as the indicator of quality, this method could more effectively than other objectivized methods for the evaluation of transmission quality contribute to the solution of the problem of objective speech transmission quality evaluation in telecommunication systems.

References

[1] T. P. BARNWELL, *Objective measures for speech quality testing*, JASA, **66**, 6, 1658–1663 (1979).

[2] T. P. BARNWELL, *Correlation analysis of subjective and objective measure for speech quality*, Proc. IEEE Int. Conf. on Acoustic Speech and Signal Proc., New York 1980.

[3] T. P. BARNWELL, *Comparison of parametrically different objective speech quality measures using correlation analysis with subjective quality results*, Proc. ICASSP 80, New York 1980.

[4] Cz. BASZTURA, *Automatic speaker recognition by zero-crossing analysis of the speech signal*, Chapt.: Man machine communication In: Speech Analysis and Synthesis, 5.I. Polish Academy of Sciences, IPPT PAN, 9–40, Warszawa 1980.

[5] Cz. BASZTURA et. al., Model of the telephone channel MKT–1 in Polish, Report I-28/R-139/79, Wrocław Technical University 1978.

[6] Cz. BASZTURA, *Automatic recognition of sound patterns as the method for the evaluation of speech transmission quality in telecommunication channels* (in Polish), Biuletyn Techniczny Ministerstwa Łączności 1, 1982.

[7] Cz. BASZTURA, *Objective statistical estimation of the articulation of speech transmitted through telephone links* (in Polish), Proc. of XXX Open Seminar on Acoustics, Gdańsk 503–506, 1983.

[8] Cz. BASZTURA, W. MAJEWSKI, *The effect of chosen parameters of a telephone channel on voice identification* (in Polish), Archiwum Akustyki, **16**, 4, 405–416 (1981).

[9] W. J. HARTMAN, *Objective performance measures for voice systems*, 2nd Symp. a Techn. Exhibition on Electromagn. Compact Proc. IEEE, 521–524 Montreux, June 1977.

[10] W. MAJEWSKI, *A phonetic test for subjective measurements of reference attenuation* (in Polish), Przegląd Telekomunikacyjny, **8**, 237–240 (1979).

[11] L. R. RABINER, C. E. SCHMIDT, B. S. ATAL, *Evaluation of a statistical approach to voices univocal – silence analysis for telephone – quality speech*, The Bell System Technical Journal, **56**, 3, 455–481 (1977).

[12] D. I. RICHARDS, *Calculation of opinion scores to telephone connections*, Proc. IEE, **121**, 5, 313–323 (1974).

[13] R.W. SCHAFER, L. R. RABINER, *Digital representation of speech signals*, Proc. IEE, **63**, 662–675 (1975).

[14] В. А. СКРИПКИН, А. Л. ГОРЕЛИК, *Методы розпознавания*, Высшая Школа, Москва 1977.

[15] R. TADEUSIEWICZ, *The evaluation of the usefulness of chosen metrices in minimum – distance methods of speech recognition* (in Polish), Archiwum Akustyki, **18**, 3, 275–284, (1983).

[16] Г. В. ВЕМЯН, *Качество телефонной передачи и его оценка*, Связ, Москва 1970.

[17] Г. В. ВЕМЯН, М. З. Петрова, *Техической прогрес в области телефонной передачи мечевых сигналов*, Електросвяз, 3, 38–41 (1976).

[18] R. VISAWANTHAN, W. RUSSEL, J. MAKKHOUL, *Objective speech quality evaluation of narrowband LPC Vocoders*, IEEE, **6**, 591–594 (1978).

[19] W. D. VOIERS, *Diagnostic acceptability measure for speech communication systems*, Proc. IEEE ICASP, 204–207 (1977).

[20] ISO/DP 4870 Second Draft Proposal August 1976.

[21] *Green Book CCITT, vol. III-1: Wire Transmission* (in Polish), WKiŁ Warsaw 1971.

[22] *Green Book of CCITT, vol. V: The quality of telephone transmission, local networks and telephone sets* (in Polish), 204–207, WKiŁ, Warsaw 1977.

Received November 25, 1986.

ARCHIVES OF ACOUSTICS
12, 3–4, 177–197 (1987)

ACOUSTIC FILTERS WITH A PERFORATED TUBE

GERARD BRZÓZKA

Institute of Machine Construction and Operation of the Engineering College in Zielona Góra
(65–246 Zielona Góra, ul. Podgórna 50)

A method of calculating acoustic properties of a low-pass filter with a perforated side baffle separating two wave-guides with constant cross-section areas is proposed. It is based on the principle of segmentation of the wave-guide into a series of elementary models which describe properties of acoustic element related to individual rows of perforation and segments of acoustic wave-guides, and on the description of acoustic properties of these models with the application of a transmission matrix with its properties of a chain matrix. Also relationships are given from which acoustic properties of a perforated baffle can be determined for a discrete parameter model at a laminar flow through orifices of the perforation.

Moreover, a calculation model for determining generally applied measures – insertion loss and transmission loss – was proposed on the basis of the transmission matrix of an acoustic filter determined with the presented method.

1. Introduction

Acoustic filters with perforated tubes are generally used to attenuate noise in systems with motion of a medium. They are constructed as analogues of low-pass elctric wave filters which as a rule operate in misfit conditions.

During the last period a very convenient and univocal description of filters transmission properties with the use of a chain matrix [1, 12, 16], in foreign literature called also a transmission matrix, was introduced. The term – transmission matrix – will be used in this paper. It is simple to determine hitherto applied attenuation measures, such as transmission loss TL or insertion loss IL, for a given transmission matrix at definite filter installation conditions [16, 17]. A description with a chain matrix is the most convenient description due to general usage of a cascade connections of individual filter elements [11].

Hitherto applied models have been developed for conditions of sound propagation in a medium at rest [7, 8]. However in practice the velocity of the motion of the medium is substantial and hence measurement results stray considerably from so obtained theoretical estimations.

On the basis of experimental and theoretical studies performed during the last several years [14] SULLIVAN formulated a physical and mathematical model which made it possible to determine elements of the transmission matrix of a filter with perforated channel at known value of the acoustic impedance of the perforated surface. In his earlier paper [2] SULLIVAN formulated propositions of calculating this impedance for a discrete parameter model. This would make it possible to estimate analytically elements of the transmission matrix, as a consequence.

This paper presents an outline of a physical model and mathematical model of determining elements of the transmission matrix of the described above type of filter. The impedance of the perforated surface is described in the form of a discrete parameter model and other elements of wave-guides are described with the application of a distributed parameter model. Because of several editorial errors in mathematical models presented in literature, it seems advisable to present the full model in this paper. Also relationships which enable the determination of generally applied attenuation measures – TL and IL – are described.

2. Outline of physical model

The diagram of the physical model is presented in Fig. 1, on the assumption that conditions of plane wave propagation are satisfied in channels. This model was developed on the basis of Sullivan's propositions [14]. Two channels with cross-sections S_1 and S_2, are connected on a segment with length L by several rows of perforations. Acoustic impedances are arbitrarily determined at the beginning of the segment $Z_{1,N+1}$, $Z_{2,N+2}$ and at its end – $Z_{1,1}$ and $Z_{2,1}$. An individual j-row of the perforation has a joint surface of S_{0j} and ratio of perforations related to this

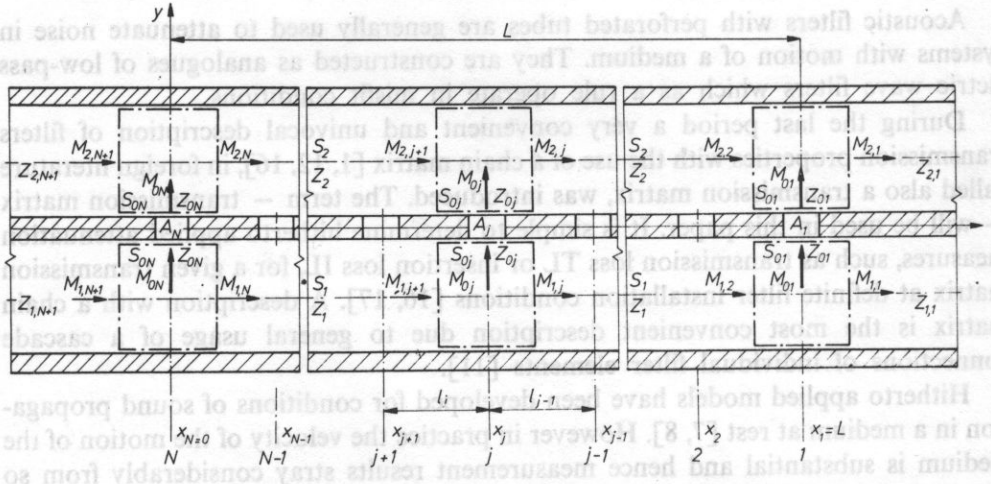

Fig. 1. Diagram of an acoustic filter with a perforated tube

surface σ_j ratio of the joint surface of orifices and the perforated surface. The flow of the medium in channels is determined by Mach numbers $M_{1,j}$, $M_{1,j+1}$ with relation to wave-guide 1, M_{2+j}; $M_{2,\ j+1}$ with relation to wave-guide 2, and M_{0j} with relation to the flow between channels in terms of surface S_{0j}. It is assumed that the value of acoustic admittance of perforations A_j is known.

The acoustic element located accordingly in wave-guide 1 and 2, connected together by orifices of the perforation can be isolated for every row of perforations. Every particle is connected with neighbouring acoustic element in the wave-guide. Segments of wave-guides 1 and 2 with lengths l_{j-1} and l_j are such connections. Taking into consideration mentioned above assumptions an analogue diagram of the filter under consideration (Fig. 1) is presented in Fig. 2. Acoustic parameters of individual elements of the model are described.

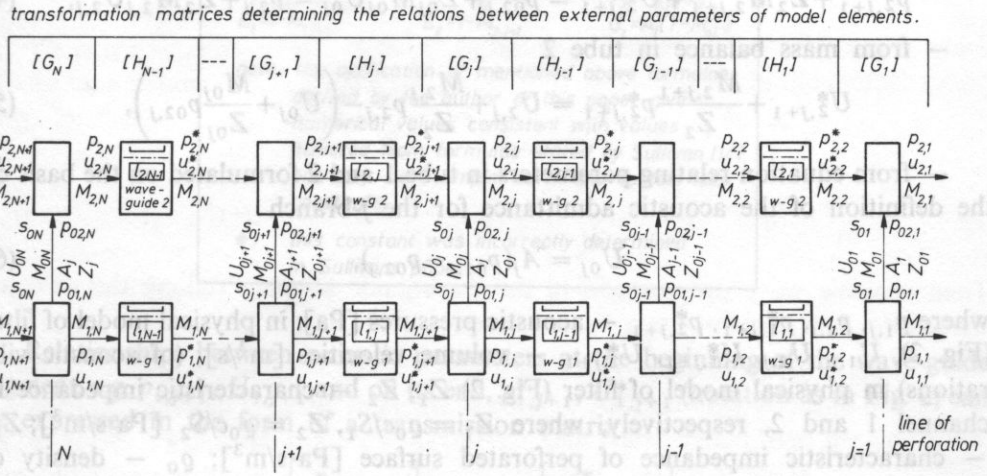

Fig. 2. Diagram of an analogous system of acoustic wave-guides with a common perforated side baffle

3. Mathematical model

The total amplitude of linear velocity on the perforated surface S_{0j} can be expressed by [14]

$$u_c = M_{0j}\, c + U_{0j}/S_{0j}, \tag{1}$$

where U_{0j} — volume acoustic velocity in the perforation orifice [m^3/s], c — sound velocity in the medium [m/s]. It is assumed that Mach numbers for the flow in channels and flow between channels in rows of perforations, M_{0j}, are known from separate hydrodynamic calculations of these channels.

Relations describing dependencies in such a model of a j-branch can be determined from an energy and mass balance in volumes of acoustic elements in channels 1 and 2, if we assume that there are no internal acoustic energy sources in

these volumes and that acoustic pressure and velocity undergoe isentropic processes. On the basis of SULLIVAN's considerations [14] and for the above mentioned assumptions the mathematical model of a j-branch of orifices can be presented in the following form:

– from energy balance in tube 1

$$p^*_{1,j+1}+Z_1 M_{1,j+1}\cdot U^*_{1,j+1} = p_{01,j}+Z_{0j}M_{0j}U_{0j} = p_{1,j}+Z_1 M_{1,j}U_{1,j} \tag{2}$$

– from mass balance in tube 1

$$U^*_{1,j+1}+\frac{M_{1,j+1}}{Z_1}p^*_{1,j+1} = U_{1,j}+\frac{M_{1,j}}{Z_1}p_{1,j}+\left(U_{0j}+\frac{M_{0j}}{Z_{0j}}p_{01,j}\right), \tag{3}$$

– from energy balance in tube 2

$$p^*_{2,j+1}+Z_2 M_{2,j+1}+U^*_{2,j+1} = p_{02,j}+Z_{0j}M_{0j}U_{0j} = p_{2,j}+Z_2 M_{2,j}U_{2,j}, \tag{4}$$

– from mass balance in tube 2

$$U^*_{2,j+1}+\frac{M_{2,j+1}}{Z_2}p^*_{2,j+1} = U_{2,j}+\frac{M_{2,j}}{Z_2}p_{2,j}-\left(U_{0j}+\frac{M_{0j}}{Z_{0j}}p_{02,j}\right), \tag{5}$$

– from equation relating parameters in tube 1 and 2 formulated on the basis of the definition of the acoustic admittance for the j-branch

$$U_{0j} = A_j(p_{01,j}-p_{02,j}), \tag{6}$$

where $p_{1,j}$, $p_{2,j}$, $p^*_{1,j+1}$, $p^*_{2,j+1}$ – acoustic pressures [Pa]; in physical model of filter (Fig. 2), $U_{1,j}$, $U_{2,j}$, $U^*_{1,j+1}$, $U^*_{2,j+1}$ – volume velocities [m^3/s]; (of acoustic vibrations) in physical model of filter (Fig. 2) Z_1, Z_2 – characteristic impedance in channel 1 and 2, respectively, where $Z_1 = \varrho_0 c/S_1$, $Z_2 = \varrho_0 c/S_2$ [Pa·s/m^3]; Z_{0j} – characteristic impedance of perforated surface [Pa·s/m^3]; ϱ_0 – density of medium [kg/m^3]; $p_{01,j}$, $p_{02,j}$ – acoustic pressure [Pa]; at the boundary of the perforation orifice in tube 1 and 2, respectively, U_{0j} – volume velocity in a perforation orifice [m^3/s]; A_j – acoustic admittance of perforations (a complex number in general [m^3/(Pa·s)]).

The transmission matrix for the j-branch, expressed in the form of a chain matrix, can be noted as follows

$$\begin{bmatrix} p^*_{1,j+1} \\ U^*_{1,j+1} \\ p^*_{2,j+1} \\ U^*_{2,j+1} \end{bmatrix} = [G_j] \begin{bmatrix} p_{1,j} \\ U_{1,j} \\ p_{2,j} \\ U_{2,j} \end{bmatrix} \tag{7}$$

and elements of this (4×4) matrix can be determined from equations (2)–(6). Equations from which elements of this matrix can be determined are presented in Table 1.

Table 1

element denotation	calculation formula	element denotation	calculation formula
G_{11}	$1-B_3G_1/E_1$	G_{21}	G_1/E_1
G_{12}	$B_1-B_3[1-B_1(B_2-G_1)]/E_1$	G_{22}	$[1-B_1(B_2-G_1)]/E_1$
G_{13}	B_3G_1/E_1	G_{23}	$-G_1/E_1$
G_{14}	$B_3C_1G_1/E_1$	G_{24}	$-C_1G_1/E_1$
G_{31}	C_3G_1/E_2	G_{41}	$-G_1/E_2$
G_{32}	$B_1C_3G_1/E_2$	G_{42}	$-B_1G_1/E_2$
G_{33}	$1-C_3G_1/E_2$	G_{43}	G_1/E_2
G_{34}	$C_1-C_3[1-C_1(C_2-G_1)]/E_2$	G_{44}	$[1-C_1(C_2-G_1)]/E_2$

$B_1=M_{1,j}Z_1$ *) $B_2=M_{1,j}/Z_1$ $B_3=M_{1,j+1}Z_1$

$C_1=M_{2,j}Z_2$ $C_2=M_{2,j}/Z_2$ $C_3=M_{2,j+1}Z_2$

$E_1=1-M_{1,j+1}^2$ $E_2=1-M_{2,j+1}$ $G_1=A_j(1-M_{oj}^2)$

note: the application of mentioned above formulae derived by the author of this paper give numerical values consistent with values achieved from formulae stated by Sullivan [14], but they have simpler form and contain less constants.

*) this constant was incorrectly determined in Sullivans paper

Relationships between acoustic parameters at the beginning of the wave-guide segment, e.g. $p_{1,j+1}$, $U_{1,j+1}$ and on its end, $p^*_{1,j+1}$, $U^*_{1,j+1}$ (notation as in Fig. 2) can be expressed in the form of a transmission matrix

$$\begin{bmatrix} p_{1,j+1} \\ U_{1,j+1} \end{bmatrix} = [\mathrm{H}] \begin{bmatrix} p^*_{1,j+1} \\ U^*_{1,j+1} \end{bmatrix}.$$

A distributed parameter model in the form of an equation of plane wave propagation in a wave-guide [7, 16] can be used to determine calculation formulae for elements of this matrix. Acoustic pressure and velocity are equal to:

$$p_1(x) = P_1 e^{-ikx}, \quad U_1(x) = \frac{P_1}{Z_1} e^{-ikx},$$

where: P_1 – pressure amplitude of acoustic wave in wave-guide 1, [Pa], Z_1 – characteristic impedance of wave-guide, [Pa·s/m^3], k – wave number, [m^{-1}]; $k = \omega/c$, ω – angular velocity (pulsation), [rad/s]; $\omega = 2\pi f$, f – frequency, [Hz], c – velocity of sound propagation in the medium at rest, [m/s], x – coordinate of the reference system along the wave-guide axis (as in Fig. 1).

Taking the motion of the medium into consideration, the velocity of sound propagation in terms of coordinate x will change by a value equal to the velocity of

the motion of the medium – v (convection of the acoustic wave in the medium). Thus, sound velocity of a progressive wave c^+ and reflected wave c^- can be determined from relationships:

$$c^+ = c+v = c(1+v/c) = c(1+M_{1,j+1}),$$
$$c^- = c-v = c(1-v/c) = c(1-M_{1,j+1}).$$

In consequence wave numbers and wave impedances will change also:

– for a progressive wave

$$k^+ = \frac{\omega}{c^+} = \frac{\omega}{c(1+M_{1,j+1})} = \frac{k}{1+M_{1,j+1}},$$
$$Z_1^+ = \frac{\varrho_0 c^+}{S_1} = \frac{\varrho_0 c}{S_1}(1+M_{1,j+1}) = Z_1(1+M_{1,j+1}),$$

– for a reflected wave

$$k^- = \frac{\omega}{c^-} = \frac{\omega}{c(1-M_{1,j+1})} = \frac{k}{1-M_{1,j+1}},$$
$$Z_1^- = \frac{\varrho_0 c_1^-}{S_1} = \frac{\varrho_0 c}{S_1}(1-M_{1,j+1}) = Z_1(1-M_{1,j+1}).$$

Then acoustic wave propagation in the wave-guide segment (taking the reflected wave into consideration) can be expressed as follows:

$$p_1(x) = P_1^+ \cdot e^{-ik^+x} + P_1^- \cdot e^{ik^-x},$$
$$U_1(x) = \frac{1}{Z_1(1-M_{1,j+1}^2)}[(1-M_{1,j+1})P_1^+ \cdot e^{-ik^+x} - (1+M_{1,j+1})P_1^- \cdot e^{ik^-x}],$$

where: P_1^+ – amplitude of progressive wave, [Pa], P_1^- – amplitude of reflected wave, [Pa].

Including parameters at the begining and the end of a considered wave-guide segment in given above formulae, we achieve the following system of equations:

$$p_{1,j+1} = p_1(x_{j+1}), \qquad U_{1,j+1} = U_1(x_{j+1}),$$
$$p_{1\,j+1}^* = p_1(x_j), \qquad U_{1,j+1}^* = U_1(x_j).$$

When constants P_1^+ and P_1^- are eliminated and several simple algebraic conversions are performed, then formulae for elements of the transmission matrix [**H**] are obtained. According to the author's considerations [6] these formulae have the following form:

$$H_{11} = F_1(\cos\alpha_1 + iM_{1,j+1}\sin\alpha_1)$$
$$H_{12} = iF_1 z_1(1-M_{1,j+1}^2)\sin\alpha_1$$

$$H_{21} = i\frac{F_1}{Z_1}\sin\alpha_1$$

$$H_{22} = F_1(\cos\alpha_1 - iM_{1,j+1}\sin\alpha_1)$$

where: α_1 – phase shift, [rad],

$$\alpha_1 = \frac{k \cdot l_{1,j}}{1 - M_{1,j+1}^2},$$

k – wave number of the medium at rest ($v = 0$), [m^{-1}], $l_{1,j}$ – length of considered wave-guide segment, [m], F_1 – auxiliary function related to the motion of the medium

$$F_1 = \cos(M_{1,j+1} \cdot \alpha_1) - i\sin(M_{1,j+1} \cdot \alpha_1).$$

There is a necessity of introducing a notation in the form of a (4×4) matrix which would take parameters in both wave-guides into consideration in the muffler model (Fig. 2):

$$\begin{bmatrix} p_{1,j+1} \\ U_{1,j+1} \\ p_{2,j+1} \\ U_{2,j+1} \end{bmatrix} = [\mathbf{H}_j] \begin{bmatrix} p^*_{1,j+1} \\ U^*_{1,j+1} \\ p^*_{1,j+1} \\ U^*_{2,j+1} \end{bmatrix}. \tag{8}$$

considered segments of wave-guides 1 and 2 are not connected (this does not concern connections between acoustic elements in rows of perforations), acoustic parameters at the beginning of wave-guide 1: $p_{1,j+1}$, $U_{1,j+1}$ are independent from parameters on the end of wave-guide 2: $p^*_{2,j+1}$, $U^*_{2,j+1}$. Thus, it can be noted:

$$H_{13} = H_{14} = H_{23} = H_{24} = 0.$$

Other elements of the $[\mathbf{H}_j]$ matrix are obtained by assigning derived relationships to parameters describing acoustic wave propagation in wave-guide 2. Table 2 presents these formulae.

The transmission matrix for the whole filter (which describes the relationship between acoustic parameters in the last, $N+1$, and first row of orifices) can be noted as:

$$\begin{bmatrix} p_{1,N+1} \\ U_{1,N+1} \\ p_{2,N+1} \\ U_{2,N+1} \end{bmatrix} = [\mathbf{T}] \begin{bmatrix} p_{1,1} \\ U_{1,1} \\ p_{2,1} \\ U_{2,1} \end{bmatrix}. \tag{9}$$

Taking advantage of properties of a chain matrix, the transmission matrix for the filter can be determined from successive multiplications of transmission matrices

Table 2

element denotation	calculation formula	element denotation	calculation formula
H_{11}	$F_1(\cos\alpha_1 + iM_{1,j+1}\sin\alpha_1)$	H_{21}	$i\frac{F_1}{Z_1}\sin\alpha_1$
H_{12}	$iF_1Z_1(1-M_{1,j+1}^2)\sin\alpha_1$	H_{22}	$F_1(\cos\alpha_1 - iM_{1,j+1}\sin\alpha_1)$
H_{13}	0	H_{23}	0
H_{14}	0	H_{24}	0
H_{31}	0	H_{41}	0
H_{32}	0	H_{42}	0
H_{33}	$F_2(\cos\alpha_2 + iM_{2,j+1}\sin\alpha_2)$	H_{43}	$i\frac{F_2}{Z_2}\sin\alpha_2$ *)
H_{34}	$iF_2Z_2(1-M_{2,j+1}^2)\sin\alpha_2$	H_{44}	$F_2(\cos\alpha_2 - iM_{2,j+1}\sin\alpha_2)$

where:

α_1, α_2 - phase shifts, [rad]

$$\alpha_1 = \frac{k \cdot l_{1,j}}{1-M_{1,j+1}^2} \qquad \alpha_2 = \frac{k \cdot l_{2,j}}{1-M_{2,j+1}^2}$$

k - wave number, $[m^{-1}]$; $k = \omega/c$; $\omega = 2\pi f$

ω - angular velocity, [rad/s]; f - frequency, [Hz],

$l_{1,j}, l_{2,j}$ - length of wave-guide segments between rows of perforations in wave-guide 1 and 2, respectively, [m],

Z_1, Z_2 - wave impedance in wave-guide 1 and 2, respectively, $[Pa \cdot s/m^3]$,

$M_{1,j+1}, M_{2,j+2}$ - Mach number behind the j-row of perforations /Fig.1 and 2/ in wave-guides 1 and 2, respectively,

F_1, F_2 - auxiliary functions,

$$F_1 = \cos(M_{1,j+1}\alpha_1) - i\sin(M_{1,j+1}\alpha_1) = e^{-iM_{1,j+1}\alpha_1}$$

$$F_2 = \cos(M_{2,j+1}\alpha_2) - i\sin(M_{2,j+1}\alpha_2) = e^{-iM_{2,j+1}\alpha_2}$$

note: Sullivan [14] introduced simplifications in his formulae which do not influence significantly calculation results for low Mach numbers (less than 0.1); besides, the formula for element H_{43} marked */ is given incorrectly.

$[\mathbf{G}_j]$ and $[\mathbf{H}_j]$

$$[\mathbf{T}] = \prod_{j=1}^{N} [\mathbf{H}_j]\,[\mathbf{G}_j], \tag{10}$$

where:

$$[\mathbf{H}_N] = [\mathbf{I}],$$

$[\mathbf{I}]$ — unit matrix.

It is necessary to know the value of the acoustic admittance of perforations in order to calculate dependencies given in Table 1. As it was done by SULLIVAN [15] it can be calculated from formula (13) on the basis of specific acoustic resistance Θ_0

and specific acoustic admittance χ_0 of perforations determined from investigations. If we do not have mentioned above experimental data, then these quantities be estimated from known theoretical models.

4. The determination of the admittance of a perforated surface for a discrete parameter model

The acoustic impedance of a single orifice in a perforated baffle can be determined from formulae describing the discrete parameter model of a perforated plate [18]

$$Z_d = \frac{4\varrho_0}{\pi d^2}\left\{2\sqrt{2\omega\nu}\left[\frac{h}{d}+\left(1-\frac{\pi}{4}\cdot\frac{d^2}{b^2}\right)\right]+i\omega h_{ef}\right\},^{(1)} \tag{11}$$

where $d < 0.06\cdot\lambda$; ω – angular velocity (pulsation) [rad/s]; $\omega = 2\pi f$; f – frequency, [Hz]; λ – length of acoustic wave, [m], $\lambda = c/f$; ϱ_0 – density of medium [kg/m^3]; ν – kinematic viscosity of medium, [m^2/s], in order to consider losses due to heat exchange between condensed and rarefied places in the medium it is suggested that this coefficient should be increased by 114% [9]; d – diameter of orifices [m], b – scale of perforation orifices, [m], h – thickness of perforated plate (baffle), [m]; h_{ef} – effective length of orifices of the perforation, including the mass of the medium adjoining the orifice; according to source material [18]

$$h_{ef} = h+0.85\left(1-\frac{d}{2b}\right)\cdot d.$$

Applying the above formula to the j-row of perforations and considering dimensionless specific resistance and reactance of perforations, we have

$$Z_j = Z_{0j}(\Theta_{0j}+i\chi_{0j})/\sigma_j,$$

where: Θ_{0j} – specific acoustic resistance of perforation, χ_{0j} – specific acoustic reactance of perforations.

Substituting formulae for characteristic impedance of the perforated surface Z_{0j} and for the ratio of perforation σ_j

$$Z_{0j} = \frac{\varrho_0 c}{S_{0j}} \qquad \sigma_j = \left(\frac{\pi d^2}{4}\right)/b^2,$$

in above relationships, comparing both sides of the relationships and after several algebraic conversions we reach the following notation of the specific acoustic

---

(1) The denotation of the coefficient of dynamic viscosity which does not satisfy dimensional relationships was given mistakenly in source materials in [18].

resistance and reactance of perforations

$$\Theta_{0j} = \frac{4\sqrt{\pi f\nu}}{c}\left[\frac{h}{d}+(1-\sigma_j^2)\right],$$
$$\chi_{0j} = \frac{2\pi f}{c}h_{ef,j}. \tag{12}$$

On the basis of considerations presented in paper [2] the author suggests that the formula including the Fok function for effective length of an orifice of the perforation should be applied

$$h_{ef,j} = h+\frac{\pi}{4\varphi(d/b_j)}\cdot d$$

where: $\varphi(d/b_j)$ – Fok function which according to the author's approximation can be expressed by the following formula

$$\varphi(d/b_j) = \frac{1.5\,d/b_j+0.48}{0.9-d/b_j} \quad \text{for} \quad d/b_j < 0.9,$$
$$\varphi(d/b_j) = 0 \quad \text{for} \quad d/b_j \geqslant 0.9.$$

According to author's own computational verifications, given above formulae for specific acoustic resistance and reactance of the perforation (12) present good consistence with results of empirical research [10, 13, 15] which were within author's means, within the range of applicability of the theory of propagation of acoustic waves with infinitely small amplitudes, i.e. for acoustic pressure levels practically below 120 dB.

The acoustic admittance of the j-row of perforations, A_j, can be determined from the definition of admittance as the inverse of impedance:

$$A_j = \frac{1}{Z_j} = \frac{\sigma_j}{Z_{0j}}\cdot\frac{\Theta_{0j}-i\chi_{0j}}{\Theta_{0j}^2+\chi_{0j}^2}. \tag{13}$$

5. The influence of flow on the specific acoustic resistance of perforation orifices

On the basis of INGARD's and ISING's papers [10] GARRISON et al. [15] formulated a mathematical model of the specific acoustic resistance of perforation orifices at flow conditions of the medium

$$\Theta_0 = K_0\frac{\bar{v}_0}{c},$$

where: $\bar{v}_0$ – average velocity at laminar flow of medium in the orifice, [m/s],

K_0 – numerical constant.

The above formula is valid for average flow velocities in the perforation orifice which exceed half the value of the vibration velocity amplitude of an acoustic particle in this orifice

$$\bar{v}_0 > \frac{1}{2}\cdot\hat{u}_0,$$

where $\hat{u}_0$ is the vibration velocity amplitude of an acoustic element in the perforation.

SULLIVAN [15] proposed the value of the numerical constant to be equal $K_0 = 2.57$. Hence, the acoustic resistance of perforations determined by the flow of the medium can be noted as

$$\Theta_0 = 2.57\cdot M_{00} = 2.57\cdot M_0/\sigma, \tag{14}$$

where: M_{00} – Mach number with the consideration of the average flow velocity in the orifice; $M_{00} = \bar{v}_0/c$, M_0 – Mach number with the consideration of the average flow velocity related to the perforated surface S_0 (as it is accepted in equations of energy and mass balances and as it is denoted in Figs. 1 and 2).

Given above expressions for the specific acoustic resistance of perforations, (12) and (14), do not include flows with small velocities in the interval

$$\bar{v}_0 \in (0, \tfrac{1}{2}\cdot\hat{u}_0).$$

The author of this paper suggests that the following approximation of the specific acoustic resistance of the perforation related to the j-row of perforations should be used in practical calculations:

$$\Theta_{0j} = \frac{4\sqrt{\pi f\nu}}{c}\left[\frac{h}{d}+(1-\sigma_j)\right]+2.57\frac{M_{0j}}{\sigma_j}. \tag{15}$$

Formula (15) exhibits good conformity with calculation results obtained from formula (12) for a medium at rest ($\bar{v}_0 = 0$) and from formula (14) for flow velocities in perforation orifices: $v_0 > 5$m/s. In this last case the first term in formula (15) is by an order of magnitude smaller than the second term. The mentioned above formula gives good conformity of calculation and measurement results of insertion loss at flow velocities of the medium in perforation orifices $v_0 < 5$m/s (discrepancies did not exceed 4 dB).

It should be noted that presented above calculation formulae for a case of a medium in motion ($\bar{v}_0 > 0$) are valid for small orifices which satisfy the laminar flow condition

$$\mathrm{Re} = \frac{\bar{v}_0\cdot d}{\nu} < 10^3.$$

Additional experimental verification is necessary for the turbulent flow range. As for a medium at rest or for small flow velocities in perforation orifices $\bar{v}_0 < 0.5$m/s the

condition stated for formula (11) is valid. It can be expressed as the limitation of the frequency range in terms of the diameter of the perforation orifices

$$f < 0.06c/d.$$

6. The determination of the transmission matrix for detailed solutions of filters

Table 3 presents three basic possibility of flows in the studied filter and corresponding to them special solutions of filters with a part of their channels closed with rigid acoustically impermeable baffles. In every case considered systems have only one inlet channel and one outlet channel. The impedance of a segment from the

Table 3. Transformation matrices determining the relations between external (extrinsic) parameters of model elements

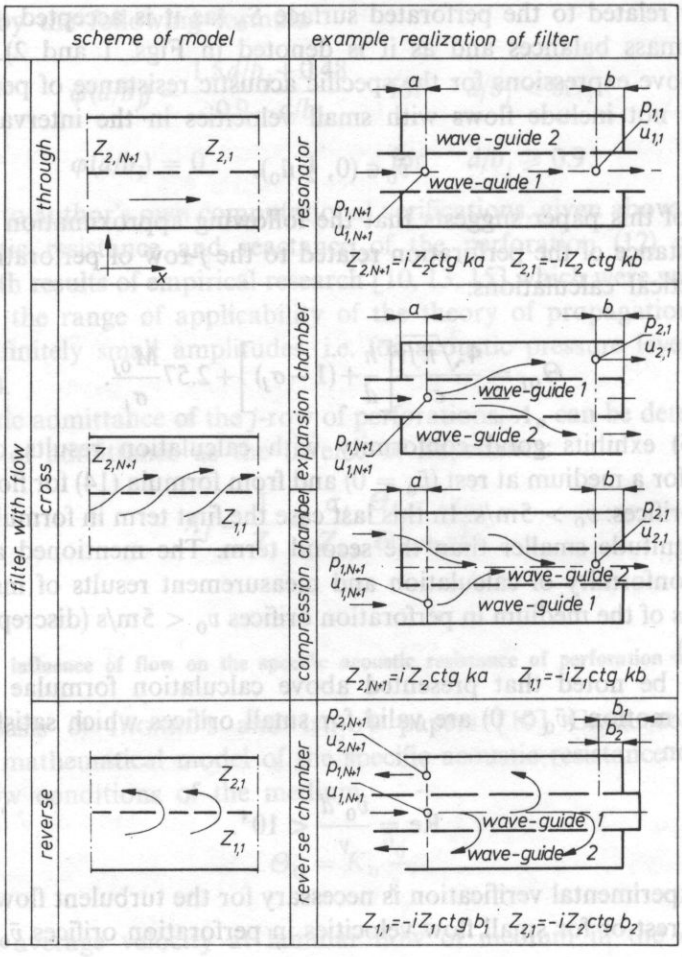

baffle to the axis of the nearest row of perforation orifices can be determined in segments of closed channels.

The relationship between acoustic parameters at the inlet of the acoustic wave to the investigated muffler model and the outlet from this model can be presented in the form of a four-element transmission matrix. The conversion of the general form of the transmission matrix [T] for extreme rows of perforations in the channel, into the mentioned four-element matrix is also interesting. This problem will be considered separately for individual cases of filter solutions presented in Table 3.

6.1. *Filter with through flow*

This case can be characterised by the following form of the transmission matrix:

$$\begin{bmatrix} p_{1,N+1} \\ U_{1,N+1} \end{bmatrix} = [\mathbf{T}'] \begin{bmatrix} p_{1,1} \\ U_{1,1} \end{bmatrix}.$$

Besides, relationships

$$p_{2,N+1} = Z_{2,N+1} \cdot U_{2,N+1},$$
$$p_{2,1} = Z_{2,1} \cdot U_{2,1}. \tag{17}$$

are valid. When these formulae are included in expressions for elements of the (4×4) transmission matrix [T] and parameters $p_{2,1}$ and $U_{2,1}$ are eliminated from equations, then we reach the following formulae which describe elements of a (2×2) transmission matrix [T']

$$T'_{11} = T_{11} + \frac{a \cdot b}{e}, \quad T'_{12} = T_{12} + \frac{a \cdot c}{e},$$
$$T'_{21} = T_{21} + \frac{b \cdot d}{e}, \quad T'_{22} = T_{22} + \frac{c \cdot d}{e}, \tag{18}$$

where:

$$a = T_{14} + Z_{2,1} \cdot T_{13}, \quad b = T_{31} - Z_{2,N} \cdot T_{41},$$
$$c = T_{32} - Z_{2,N} \cdot T_{42}, \quad d = T_{24} + Z_{2,1} \cdot T_{23},^{(2)} \tag{19}$$
$$e = (T_{44} + Z_{2,1} \cdot T_{43}) Z_{2,N} - (T_{34} + Z_{2,1}\ T_{33}).$$

6.2. *Filter with cross flow*

The relation between parameters at the entry of an acoustic wave to the muffler model under consideration and at its exit from this model is

$$\begin{bmatrix} p_{1,N+1} \\ U_{1,N+1} \end{bmatrix} = [\mathbf{T}'] \begin{bmatrix} p_{2,1} \\ U_{2,1} \end{bmatrix}. \tag{20}$$

(2) The transmission matrix element T_{24} was mistakenly given instead of T_{23} in SULLIVAN'S paper [14].

Formulae for closed segments of the channel can be written in the following form:

$$p_{2,N+1} = Z_{2,N+1} \cdot U_{2,N+1},$$
$$p_{1,1} = Z_{1,1} \cdot U_{1,1}. \tag{21}$$

The following expressions for elements of matrix [T'] are achieved as a result of transformations similar to those performed previously:

$$T'_{11} = T_{13} + \frac{ab}{e}, \quad T'_{12} = T_{14} + \frac{ac}{e},$$
$$T'_{21} = T_{23} + \frac{bd}{e}, \quad T'_{22} = T_{24} + \frac{cd}{e}, \tag{22}$$

where:

$$a = T_{12} + Z_{1,1}\, T_{11}, \quad b = T_{33} - Z_{2,N}\, T_{43},$$
$$c = T_{34} - Z_{2,N}\, T_{44}, \quad d = T_{22} + Z_{1,1}\, T_{21}, \tag{23}$$
$$e = (T_{42} + Z_{1,1}\, T_{41}) Z_{2,N} - (T_{32} + Z_{1,1}\, T_{31}).$$

6.3. *Filter with reverse flow*

In this case the transmission matrix has the following form:

$$\begin{bmatrix} p_{1,N+1} \\ U_{1,N+1} \end{bmatrix} = [\mathbf{T}'] \begin{bmatrix} p_{2,N+1} \\ U_{2,N+1} \end{bmatrix}. \tag{24}$$

and formulae for closed channels are:

$$p_{1,1} = Z_{1,1}\, U_{1,1},$$
$$p_{2,1} = Z_{2,1}\, U_{2,1}. \tag{25}$$

As a result of certain transformations, elements of the matrix [T'] can be noted as

$$T'_{11} = \frac{de - cf}{ad - bc}, \quad T'_{12} = \frac{af - be}{ad - bc},$$
$$T'_{21} = \frac{dg - ch}{ad - bc}, \quad T'_{22} = \frac{ah - bg}{ad - bc}, \tag{26}$$

where:

$$a = T_{32} + Z_{1,1}\, T_{31}, \quad b = T_{34} + Z_{2,1}\, T_{33},$$
$$c = T_{42} + Z_{1,1}\, T_{41}, \quad d = T_{44} + Z_{2,1}\, T_{43},$$
$$e = T_{12} + Z_{1,1}\, T_{11}, \quad f = T_{14} + Z_{2,1}\, T_{13}, \tag{27}$$
$$g = T_{22} + Z_{1,1}\, T_{21}, \quad h = T_{24} + Z_{2,1}\, T_{23}.$$

7. The determination of values of basic filter loss measures

Transmission loss TL and insertion loss IL are generally applied attenuation measures in acoustic filters. Properties, significant differences and inaccuracies of these attenuation measures are discussed in WYRZYKOWSKI's, PUCH's and SNAKOWSKI's papers [12, 16], and papers written by the author [3, 5].

7.1. *Insertion loss*

Figure 3 presents two diagrams of electric analogues which consist of substitute four-terminal networks. Their acoustic properties are described with a transmission matrix for a case before and after the insertion of the investigated filter (acoustic element or system) for which the insertion loss is to be determined. The studied filter is represented by a four-terminal network determined by a transmission matrix [**T**]. A four-terminal network with transmission matrix [**A**] substitutes the inlet system

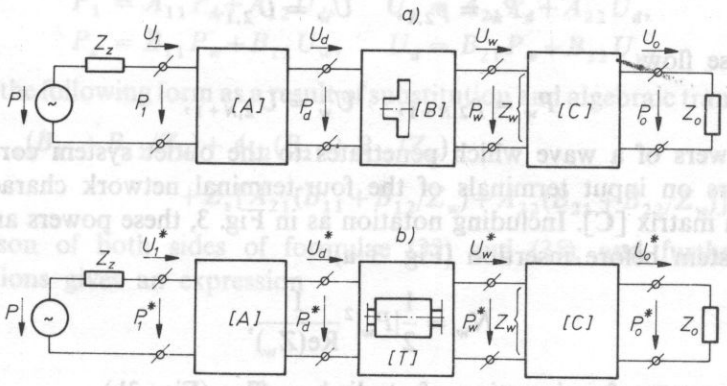

Fig. 3. Diagrams of analogue systems reflecting conditions corresponding to the definition of insertion loss a – system before insertion of filter (element of acoustic system), b – system after insertion of filter

through which the acoustic wave is supplied to the studied filter and a four-terminal network with transmission matrix [**C**] and outlet load impedance Z_0 represent the outlet system which carried away the acoustic wave. According to the definition of insertion loss, in both considered cases the inlet system and outlet system are identical. They are denoted by the same matrices, [**A**] and [**C**], and by impedance Z_0 in both diagrams (Fig. 3a and 3b).

Also a frequently encountered case of diversified cross-sections of the inlet and outlet wave-guide is included in the diagram. It is modelled in Fig. 3a by a four-terminal network. Its transmission matrix [**B**] describes the relationship for a sudden change of the cross-section, typical for expansion chamber mufflers [4].

Acoustic pressure P is the equivalent of voltage and volume acoustic velocity U is the equivalent of current in mentioned diagrams. It was also accepted that in both

cases under consideration an acoustic wave with amplitude P is supplied to the inlet system and the impedance of the source of this wave is equal to Z_z. Except for special cases, it can be expected that values of other acoustic parameters on terminals of individual four-terminal networks in both diagrams will vary. Parameters of a system with an inserted filter are denoted by a star (Fig. 3b). Furthermore, parameters on input terminals of the four-terminal network which represents the studied muffler are denoted P_d, U_d, and on the outlet terminals – P_w, U_w.

With respect to the previously applied notation, the following substitution has to be taken into consideration at the entry:

$$P_d = p_{1,N+1}, \qquad U_d = U_{1,N+1},$$

and on the outlet – in terms of flow direction of the acoustic wave

– through flow

$$P_w = p_{1,1}, \qquad U_w = U_{1,1},$$

– cross flow

$$P_w = p_{2,1}, \qquad U_w = U_{2,1},$$

– reverse flow

$$P_w = p_{2,N+1}, \qquad U_w = U_{2,N+1},$$

Acoustic powers of a wave which penetrates to the outlet system correspond to active powers on input terminals of the four-terminal network characterised by transmission matrix [C]. Including notation as in Fig. 3, these powers are equal to:

– in system before insertion (Fig. 3 a)

$$N_w = \frac{1}{2}|P_w|^2 \frac{1}{\mathrm{Re}(Z_w)},$$

– in a system after insertion of studied muffler (Fig. 3b)

$$N_w^* = \frac{1}{2}|P_w^*|^2 \frac{1}{\mathrm{Re}(Z_w)}.$$

Outlet systems in both considered cases are identical, so their resistances are equal (real parts of impedance). Including above formulae in the definition of insertion loss, we have

$$IL = 10\lg\frac{Nw}{N_w^*} = 20\lg\left|\frac{P_w}{P_w^*}\right|. \tag{30}$$

Relationships between acoustic parameters for a case of an inserted filter (Fig. 3b) can be noted by following formulae

$$\begin{aligned} P_w^* &= Z_w U_w^*, & P &= P_1^* + Z_z U_1^*, \\ P_d^* &= T_{11} P_w^* + T_{12} U_w^*, & U_d^* &= T_{21} P_w^* + T_{22} U_w^*, \\ P_1^* &= A_{11} P_d^* + A_{12} U_d^*, & U_1^* &= A_{21} P_d^* + A_{22} U_d^*. \end{aligned} \tag{31}$$

where acoustic impedance of the outlet system is described by expression

$$Z_w = \frac{p_w}{U_w} = \frac{p_w^*}{U_w^*} = \frac{Z_0 C_{11} + C_{12}}{Z_0 C_{21} + C_{22}}. \tag{32}$$

The value of this impedance determines the value of the outlet load impedance Z_0 and the values of elements of the transmission matrix [C] of the outlet system. Substituting expressions (31) and performing several algebraic transformations, a formula for the amplitude of an acoustic wave emitted by the source after a studied filter was inserted is achieved

$$P = \{A_{11}(T_{11} + T_{12}/Z_w) + A_{12}(T_{21} + T_{22}/Z_w) + Z_z[A_{21}(T_{11} + T_{12}/Z_w) + A_{22}(T_{21} + T_{22}/Z_w)]\} P_w^*. \tag{33}$$

Similarly, expressions for a case before the insertion (Fig. 3a) can be noted

$$\begin{aligned} P_w &= Z_w U_w, & P &= P_1 + Z_z U_1, \\ P_1 &= A_{11} P_d + A_{12} U_d, & U_1 &= A_{21} P_d + A_{22} U_d, \\ P_d &= B_{11} P_w + B_{12} U_w, & U_d &= B_{21} P_w + B_{22} U_w, \end{aligned} \tag{34}$$

which have the following form as a result of substitution and algebraic transformations

$$P = \{A_{11}(B_{11} + B_{12}/Z_w) + A_{12}(B_{21} + B_{22}/Z_w) + Z_z[A_{21}(B_{11} + B_{12}/Z_w) + A_{22}(B_{21} + B_{22}/Z_w)]\} P_w. \tag{35}$$

A comparison of both sides of formulae (33) and (35), and further algebraic transformations gives an expression

$$\left|\frac{P_w}{P_w^*}\right| = \left| \frac{A_{11}\left(T_{11} + \frac{T_{12}}{Z_w}\right) + A_{12}\left(T_{21} + \frac{T_{22}}{Z_w}\right) + Z_z\left[A_{12}\left(T_{11} + \frac{T_{12}}{Z_w}\right) + A_{22}\left(T_{21} + \frac{T_{22}}{Z_w}\right)\right]}{A_{11}\left(B_{11} + \frac{B_{12}}{Z_w}\right) + A_{12}\left(B_{21} + \frac{B_{22}}{Z_w}\right) + Z_z\left[A_{12}\left(B_{11} + \frac{B_{12}}{Z_w}\right) + A_{22}\left(B_{21} + \frac{B_{22}}{Z_w}\right)\right]} \right| \tag{36}$$

According to author's derivations [4] elements of the transmission matrix for a sudden change of the cross-section, [**B**], are equal to

$$\begin{aligned} B_{11} &= 1, & B_{12} &= Z_{FC} M_C - \frac{1 - M_C^2}{1 - M_A^2} M_A Z_{FA}, \\ B_{21} &= 0, & B_{22} &= \frac{1 - M_C^2}{1 - M_A^2}, \end{aligned} \tag{37}$$

where: Z_{FA}, Z_{FC} – characteristic impedance of wave-guides at the entry and at the

outlet of the investigated filter, [Pa·s/m^3], M_A, M_C – Mach numbers in waveguides at the entry and outlet of the studied filter.

As a result of the substitution of (36) and (37) in (30), an expression for insertion loss is achieved

$$IL = 20\lg\left|\frac{A_{11}\left(T_{11}+\frac{T_{12}}{Z_w}\right)+A_{12}\left(T_{21}+\frac{T_{22}}{Z_w}\right)+Z_z\left[A_{21}\left(T_{11}+\frac{T_{12}}{Z_w}\right)+A_{22}\left(T_{21}+\frac{T_{22}}{Z_w}\right)\right]}{A_{11}\left(1+\frac{B_{12}}{Z_w}\right)+A_{12}\frac{B_{22}}{Z_w}+Z_z\left[A_{21}\left(1+\frac{B_{12}}{Z_w}\right)+A_{22}\frac{B_{22}}{Z_w}\right]}\right|. \tag{38}$$

Expressions for insertion loss for chosen special cases are presented in Table 4.

Table 4

	description of model	assumptions	mathematical model of insertion loss IL
1	wave-guides identical at the entry and outlet of the muffler	$Z_{FA}=Z_{FC}$ $B_{12}=0$ $B_{22}=1$	$IL=20\lg\left\|\frac{A_{11}(T_{11}+T_{12}/Z_W)+A_{12}(T_{21}+T_{22}/Z_W)+Z_z[A_{21}(T_{11}+T_{12}/Z_W)+A_{22}(T_{21}+T_{22}/Z_W)]}{A_{11}+A_{12}/Z_W+Z_z(A_{21}+A_{22}/Z_W)}\right\|$
2	a reflectionless entry of an acoustic wave to the muffler	$Z_z=Z_{FA}$ [A] - transmission matrix of wave-guide with wave impedance Z_{FA}	$IL=20\lg\left\|\frac{T_{11}+T_{12}/Z_W+Z_{FA}T_{21}+Z_{FA}T_{22}/Z_W}{1+(B_{12}+Z_{FA}B_{22})/Z_W}\right\|$
3	source with constant pressure	$Z_z=0$	$IL=20\lg\left\|\frac{A_{11}(T_{11}+T_{12}/Z_W)+A_{12}(T_{21}+T_{22}/Z_W)}{A_{11}(1+B_{12}/Z_W)+A_{12}B_{22}/Z_W}\right\|$
4	source with constant velocity	$Z_z\to\infty$	$IL=20\lg\left\|\frac{A_{21}(T_{11}+T_{12}/Z_W)+A_{22}(T_{21}+T_{22}/Z_W)}{A_{21}(1+B_{12}/Z_W)+A_{22}B_{22}/Z_W}\right\|$
5	reflectionless entry and outlet of an acoustic wave to and from the muffler	$Z_z=Z_{FA}$ $Z_W=Z_{FC}$ [A], [B] - transmission matrices of wave-guides with wave impedances Z_{FA} and Z_{FC} respectively	$IL=20\lg\left\|\frac{T_{11}+T_{12}/Z_W+Z_{FA}T_{21}+Z_{FA}T_{22}/Z_{FC}}{1+(B_{12}+Z_{FA}B_{22})/Z_{FC}}\right\|$
6	reflectionless entry and outlet of anacoustic wave to and from the muffler at identical wave impedance	as in 5 and $Z_{FC}=Z_{FA}$	$IL=20\lg\left\|\frac{T_{11}+T_{12}/Z_F+Z_FT_{21}+T_{22}}{2}\right\|$

7.2. *Transmission loss*

The model presented in Fig. 3b can be applied in calculations of this loss measure on the assumption that the output of the acoustic wave from the four-terminal network representing the studied filter is reflexionless. This condition can be noted as

$$Z_w = Z_{FC}$$

Acoustic powers necessary in further calculations are derived from the following expressions:

– for a wave inciding onto studied filter

$$ {}^{+}N_d^* = \frac{1}{2} \cdot \frac{|{}^{+}P_d^*|^2}{Z_{FA}} $$

– for a wave trasmitted from the filter to the outlet system (to a reflexionless outlet wave-guide)

$$ N_w^* = \frac{1}{2} \cdot \frac{|P_w^*|^2}{Z_{FC}} $$

where ${}^{+}P_d$ denotes the pressure of an acoustic wave which incides into the studied filter.

When given above expressions are substituted in the formula for transmission loss, the following formula is obtained

$$ TL = 10\lg \frac{{}^{+}N_d^*}{N_w^*} = 20\lg \frac{|{}^{+}P_d^*|}{|P_w^*|} + 10\lg \frac{Z_{FC}}{Z_{FA}}. \tag{39} $$

Using formulae (31) and following relationships between parameters at the entry to the four-terminal network representing the studied filter

$$ P_d^* = {}^{+}P_d^* + {}^{-}P_d^*, \quad U_d^* = \frac{{}^{+}P_d^* - P_d^*}{Z_{FA}}, \tag{40} $$

where ${}^{+}P_d$, ${}^{-}P_d$ – acoustic pressures at progressive and reflected wave, respectively, at the entry of the four-terminal network representing the studied filter, the following expression is reached

$$ \frac{|{}^{+}P_d^*|}{|P_w^*|} = \left| \frac{T_{11} + \frac{1}{Z_{FC}} T_{12} + Z_{FA} T_{21} + \frac{Z_{FA}}{Z_{FC}} T_{22}}{2} \right| $$

as a result of substitutions and algebraic transformations. Substituting the above expression in formula (40) we achieve the following expression for transmission loss

$$ TL = 20\lg \left| \frac{T_{11} + \frac{1}{Z_{FC}} T_{12} + Z_{FA} T_{21} + \frac{Z_{FA}}{Z_{FC}} T_{22}}{2} \right| + 10\lg \frac{Z_{FC}}{Z_{FA}}. \tag{41} $$

8. Conclusions

This paper presents a calculation model of a low-pass acoustic filter with a perforated baffle which separates two channels with constant cross-sections at the

assumptions for the propagation conditions of a plane wave with infinitely small amplitude. The model was built on the basis of the segmentation principle for repeated segments of channels between individual rows of perforations. Acoustic properties of these segments were described with a transmission matrix on the basis of a discrete parameter model of the perforation orifice, on the assumption of a laminar flow through these orifices. A distributed parameter model describes wave-guide segments.

Properties of the whole filter can be described with a transmission matrix as a result of successive multiplications of transmission matrices of individual segments. Properties of the chain matrix were utilized as well as detailed mathematical model of the basic flow directions of an acoustic wave through the filter.

The presented above description of properties of discussed filters is very convenient for further computer processing and determination of acoustic characteristics of these filters. Also numerical values of both generally applied measures – transmission loss TL and insertion loss IL – can be calculated when entry and source impedances are known. Calculations can be performed on widely applied personal computers.

Unfortunately the application of presented calculation models is limited to small orifices of the perforation, e.g. orifices which satisfy conditions of a discrete parameter model and laminar flow of the medium through these orifices. Further studies are aimed at the elimination of these restrictions.

The condition of plane wave propagation is another limitation. Much more complicated calculation methods which would include spatial propagation of an acoustic wave (such as the method of finite elements) are necessary in order to remove this limitation.

References

[1] G. BRZÓZKA, *Taking the influence of medium motion into consideration in the description of an acoustic filter with perforated baffles* (in Polish), Proc. XXXI Open Seminar on Acoustics OSA-84, Warsaw, 1984, 99–101.

[2] G. BRZÓZKA, *On calculations of acoustic filters with a perforated channel* (in Polish), Proc. XXXI Open Seminar on Acoustics OSA-84, Warsaw, 1984, 102–106.

[3] G. BRZÓZKA, *A proposition of a specification of parameters of acoustic filters used in suction and exhaust systems of combustion engines* (in Polish), Sc. Report of the Institute of Machine Construction and Operation of the Technical University of Wrocław, N° 43, Wrocław 1984, 29–37.

[4] G. BRZÓZKA, *A description of properties of expansion chamber mufflers with the application of transmission matrices* (in Polish), Proc. Conf. NOISE Control '85, Cracow 1985, 173–177.

[5] G. BRZÓZKA, *On a certain problem of experimental verification of acoustic muffler effectiveness in flow systems of combustion engines* (in Polish), KONES '85, Poznań-Błażejewko 1985, 173–177.

[6] G. BRZÓZKA, *A transmission matrix of a wave-guide segment with a constant cross-section, during flow of medium* (in Polish), Report of the Institute of Machine Construction and Operation of the Engineering College in Zielona Góra, GB/1985/06, Zielona Góra 1985.

[7] D. DAVIS Jr., *Acoustical filters and mufflers*, Chapter 21 Handbook of Noise Control, Mc Graw-Hill Book Company, 1957.

[8] D. D. DAVIS, G. M. STOKES, D. MOORS, G. L. STEVENS, *Theoretical and experimental investigation of mufflers with comments of engine-exhaust muffler design*, NACA Rep. TN 1192 (1953).
[9] R. D. FAY, *Attenuation of sound in tubes*, JASA **12**, 62–63 (1967).
[10] U. INGARD, H. ISING *Acoustic nonlineary of an orifice*, JASA, **13**, 6–17 (1967).
[11] M. KRUKOWSKI, *Theoretical electroacoustics*, vol.I: *Linear and non-linear circuits* (in Polish), PWN, Warszawa-Poznań 1980.
[12] A. PUCH, *Chain matrix of a low-pass acoustic filter* (in Polish), Archiwum Akustyki, **13**, 3, 333–343, (1978).
[13] J. W. SULLIVAN, J. M. CROCKER, *Analysis of concentric-tube resonators having unpartitional cavities*, JASA, **64**, 207–215 (1978).
[14] J. W. SULLIVAN, *A method for modelling perforated tube muffler components, I. Theory*, JASA, **66**, 772–778 (1979).
[15] J. W. SULLIVAN, *A method for modelling perforated tube muffler components*, II. *Applications*, JASA **66**, 779–788 (1979).
[16] R. WYRZYKOWSKI, A. PUCH, J. SNAKOWSKI, *Acoustic filters* (in Polish), WSP, Rzeszów 1977.
[17] J. ZALEWSKI, M. RABIEGA, B. MYŚLECKA, *Insertion loss of a filter with coupled resonance chambers operating in conditions of an input-output misfit* (in Polish), Proc. XX Open Seminar on Acoustics, Poznań-Mierzyn 1973, part II, 164–168.
[18] Z. ŻYSZKOWSKI, *Fundamentals of electroacoustics* (in Polish) WNT, Warszawa 1984.

Received June 23, 1987.

ARCHIVES OF ACOUSTICS
12, 3–4, 199–214 (1987)

THE AEROSOL PARTICLE DRIFT IN A STANDING WAVE FIELD

HENRYKA CZYŻ

Institute of Physics, Pedagogical University
(35–311 Rzeszów, ul. Rejtana 16a)

This study considers the equation of motion of an aerosol particle in a standing wave field under the influence of drift and resistance forces in the Stokes and Oseen approximation. It evaluates the possibility of simplifying the equation of motion, taking into account the drift related to the radiation pressure, periodic viscosity changes and the asymmetry of motion of particle vibrating in a standing wave field. It gives the general properties of the solutions of motion equations for considerable attenuation and formulates the applicability of approximation which consists in neglecting the inertia of a particle.

1. Introduction

Although the method of cleaning gases acoustically has long been known, its use in the industry still remains limited. The main reason for this are the high investment and exploitation costs of the proper technical installations. Despite this, the acoustical cleaning remains a method which is irreplaceable in some special cases, such as the clearing gases with high temperatures and chemically active. The aerosol of particles which are difficult to electrify or explosive can also be cleaned acoustically, excluding the use of electrofilters. Recently, this method has been applied in the nuclear technology [1].

The organizations engaged in the protection of the natural environment point out that the aerosols and suspensions of fine-particle dust, with diameters smaller than a few micrometers [2], are particularly dangerous for Nature and man's health. In this case, acoustic methods appear to be very useful; the forces which act in a standing wave field are most effective for exactly such particle sizes. Moreover, in the process of acoustic coagulation the mean particle size increases, decreasing the toxicity of the aerosol and facilitating its further cleaning by traditional method.

To lower the costs of applying the acoustic method to clean gases, research efforts were undertaken in the following main directions:

1) the investigation of new, highly efficient sources of acoustic energy;

2) the development of acoustic field configuration, e.g., the superposition of a standing wave and a nonsinusoidal travelling wave [3];

3) the search for the optimum parameters of the acoustic field depending on the type of aerosol, in particular on its dispersion.

This study is a contribution to research in the second and third of fields mentioned above. It considers the motion of aerosol particles caused by the drift forces in a standing acoustic wave field. These forces, a consequence of interaction between the particle and the vibrating medium, result from such phenomena as the radiation pressures, the asymmetric vibration motion of the particle or periodic changes in the viscosity of the gas. On the other hand, different kinds of drift have a common property: the forces applied on the particle depend in the same way on its position with respect to the loops and nodes of the standing wave and are proportional to the density of the wave energy. However, the drift forces depend very strongly on the particle size. So far, the problem of the contributions of the different drift forces in the complex process of aerosol coagulation has not been investigated. Studies on the drift-driven transport mostly considered the radiation drift, which a detailed analysis found to be weakest. No study was also carried out on the character of the trajectory of a particle moving under the effect of the drift forces, or on the role of the friction forces in the general equation of motion.

This paper is devoted to the problem of the equation of motion of a particle, considering the drift and resistance forces caused by viscosity. It evaluates the effect of the drift forces of different types depending on the particle size. It also defines the applicability range of the approximation consisting in neglecting the nonlinear term in the friction force. It also analyzes the general properties of the equation of motion of the aerosol particle in the case of large attenuation constants, corresponding for typical values of the drift forces to particles with radii less than 10^{-5}m. Finally, it defines the applicability criterion of the so-called King–St. Clair approximation, most widely applied in the literature to describe the motion, consisting in the assumption of equilibrium between the drift and the Stokes viscosity forces, neglecting the term representing inertia. This approximation is of particular significance, since it makes possible analytical estimation of the time constants of the particle transport to points of stable equilibrium in a standing wave field. Methods for determining these constants will be presented in another study [4].

Below, consideration is given only to the problem of the motion of a single aerosol particle. This means that the effect of interaction of particles is neglected, i.e., the process leading to coagulation itself, namely the fact that smaller particles link to form larger aggregates. Causing particles to gather near points of stable equilibrium (minima of the potential of the drift forces), the phenomena caused by the drift forces assist in a way the elementary acts of coagulation by increasing the concentration of particles near the nodes or loops of the standing wave. The ultimate coagulation can then occur through an orthokinetic process if the standing wave is combined with the saw-tooth travelling wave moving along the planes of the loops and nodes. With such a configuration of the field, proposed by SCOTT [3] and so far the most efficient, the transport under the effect of the drift forces determines the rate of the cleaning process.

2. The drift forces in a standing wave field

If the acoustic potential of the standing wave is described by the function

$$\Phi(x, t) = \Phi_0 \cos kx \cos \omega t, \tag{1}$$

the deflection x_g of particles of the gaseous medium, as a function of the position x and the time t, is given by the equation

$$x_g = x_0 \sin kx \sin \omega t. \tag{2}$$

In the planes $kx = n\pi$, $n = 0, \pm 1, \pm 2, \ldots$, these deflections are permanently equal to zero; therefore, they are nodes of the standing wave. The planes with equations $kx = (n+\frac{1}{2}\pi), n = 0, \pm 1, \pm 2, \ldots$, correspond to the nodes. In an acoustic field of this type aerosol particles are acted upon by forces which do not decay on average in time, directing these particles to the closest planes of nodes of loops. It appears that, irrespective of the mechanism of the occurrence of such forces, they can be described by the formula

$$F_D(x) = F_0 \sin 2kx. \tag{3}$$

The forces of this type are called the drift forces. Therefore the potential related to their action has the form

$$U_D(x) = F_0(2k)^{-1} \cos 2kx. \tag{4}$$

The position of the potential minima depends on the sign of the constant F_0, describing the maximum value of the drift force. For $F_0 > 0$ the minima of potential (4) coincide with the value $2kx = (2n+1)\pi$, giving the equation of the planes of loops. In turn, for $F_D < 0$ the drift forces gather aerosol particles at the nodes of the standing wave. It is clear, however, that the sign of the constant F_0 has no effect on the kinetics of the process of particle transport.

The review of the drift forces should begin with the so-called radiation drift related to the radiation pressure. Calculating the difference between the momentum of the incident wave and that of a wave scattered on a sphere, WESTERVELT [5] gave for the drift of this type an expression of the force in the form

$$F_{DR} = \frac{8}{3}\pi k r^3 \mu_g^2 \bar{E} \sin 2kx, \tag{5}$$

where $\bar{E}$ denotes the density of the acoustic wave energy and μ_g is the so-called coefficient of the particle flow,

$$\mu_g^2 = \omega^2 \tau^2 (1+\omega^2 \tau^2)^{-1}, \tag{6}$$

the value of which, very strongly dependent on the frequency ω, describes the degree of participation of an aerosol particle in the oscillation motion of the medium and plays a fundamental in the theory of coagulation microprocesses. In turn,

$$\tau = m_p (6\pi r \eta)^{-1}, \tag{7}$$

called the relaxation time, which is the quotient of the particle mass m_p and the coefficient of the Stokes resistance connected to the viscosity of the medium η, characterizes the effect of the resistance on the motion.

The radiation drift was studied earlier by KING [6] and later also by GORKOV [7]. In each of the cases the theoretical considerations led the authors to slightly different numerical coefficients characterizing the intensity of the radiation drift. The validity of formula (5) given above was finally established by experimental research [8].

Over many years, even in relatively recent studies [9], [10] the radiation drift was regarded as the fundamental effect which concentrates particles in a standing wave field. However, as early as 1950, WESTERVELT [11] predicted theoretically the existence of another type of drift. It is connected with periodic changes in the viscosity of the medium, which result in turn from periodic changes in temperature in a standing wave field. The averaging in time of the Stokes force gives a non vanishing component which causes a drift which will be called the viscosity drift below, and the L-type drift in short. The force of the viscosity drift is expressed by the formula [11]

$$F_{DL} = 3\pi(\varkappa-3)\eta r(\varrho_g c)^{-1}\mu_g^2 \bar{E}\sin 2kx. \tag{8}$$

The constant $\varkappa$ is here the exponent of the adiabate whose value for air can be assumed as 1.4, and ϱ_g is the density of the gas. In this case, the constant F_0, which characterizes in the general formula (5) the amplitude of the drift force, is negative, therefore, the L-type drift concentrates particles at the loops of a standing wave. It will be shown below that its action on particles can be considerably stronger than the radiation drift.

Another type of drift is characteristics only of a standing wave. It results from the fact that in such a wave the vibration amplitude of the gaseous medium depends on position being greater in the area of loops. In view of their inertia, aerosol particles do not keep pace with the motion of the medium and are affected by variable forces over the time of their oscillation. Thus, their motion is asymmetrical, causing a constant motion towards the loops. The component of this motion which does not decay after averaging in time is called the asymmetric drift, and will be called the A-type drift below. The expression of the force of the asymmetric drift was given for the first time by DUCHIN [12]; however, his original study contained certain faults, including probably printers' errors which were partly removed in the monograph work [13]. A detailed analysis of the problem indicates that the correct expression of the force of the asymmetric drift has the form

$$F_{DA} = \frac{\pi}{3}kr^3\mu_p[(3+\frac{9}{2}b)\mu_p - \frac{9}{2}b(b+1)\mu_g]\bar{E}\sin 2kx, \tag{9}$$

where $b = r^{-1}(2\eta/\omega\varrho_g)^{\frac{1}{2}}$ and μ_p is the coefficient of particle entrainment known from orthokinetic theory [13]

$$\mu_p = (1+\omega^2\tau^2)^{-\frac{1}{2}}, \tag{10}$$

which is the coefficient of proportionality between the vibration amplitudes of the medium and the aerosol particle. Along with the flow coefficient introduced in formula (6), it satisfies the relation $\mu_p^2+\mu_g^2=1$.

Apart from those mentioned above, one should mention a drift connected with distortions of a sinusoidal acoustic wave. WESTERVELT [15] derived an expression of the drift force of this type, taking into account the amplitude and phase of the first harmonic in a travelling wave. The estimation of the magnitude of the action of this drift on aerosol particles, carried out in study [4], indicates that for the amplitude of the first harmonic equal to half the amplitude of the fundamental wave, this drift acts a force of the same order of magnitude, as was discussed above. Since, however, the possibility of constructing a device applying a distorted standing wave does not seem real, this problem will be neglected here, to concentrate instead on phenomena typical for a sinusoidal standing wave.

3. Analysis of the equation of motion

Considering the motion of an aerosol particle effected by the drift forces, let us now write the equation of motion of this particle, taking into account the resistance forces on the part of the medium,

$$m_p\frac{d^2x}{dt^2}=-6\pi\eta r\frac{dx}{dt}-\frac{9}{4}\pi r^2\varrho_g\frac{dx}{dt}\left|\frac{dx}{dt}\right|+F_0\sin 2kx. \tag{11}$$

The first term on the right side of the equation represents the Stokes force related to the viscosity of the medium, whereas the second one represents the nonlinear Oseen correction which is significant for large Reynolds numbers. The above simple differential equation, which is nonlinear in view of the last two terms, has no elementary solution. Therefore, further attempts will be made to investigate the general properties of solutions of this equation, taking into account such values of its coefficients as result from the practice of acoustic coagulation of aerosols.

By dividing both sides by the particle mass, equation (11) can be rewritten in the form

$$\frac{d^2x}{dt^2}+\frac{1}{\tau}\frac{dx}{dt}+\frac{27\varrho_g}{16r\varrho_p}\frac{dx}{dt}\left|\frac{dx}{dt}\right|-\frac{F_0}{m_p}\sin 2kx=0. \tag{12}$$

Now, the effect of the Stokes force is characterized by the relaxation time τ, which was earlier introduced by equation (7). The term representing the drift force is accompanied by the coefficient F_0/m_p denoting the acceleration of the particle in the absence of the friction forces at points of the maximum drift force. Depending on the value of this coefficient, the other terms of the equation of motion, namely the first (inertial) the linear and nonlinear terms representing friction, would affect the particle motion to a lesser or greater extent. Therefore, it is purposeful to introduce

the quantity

$$A_D = \frac{F_0}{m_p}, \tag{13}$$

which by analogy to other interactions, can be called the intensity of the drift force field. The calculation of the value of this quantity will make possible above all to compare the efficiency of particular kinds of drift discussed in the previous chapter. To compare the efficiency of various types of drift, previous studies usually applied the comparison of the values of the force amplitudes [13]. It can be seen from (12) that the effect of a force causing motion of a particle on the trajectory is rather represented by the constant A_D. An additional aspect of the problem is the complex dependence of the drift forces on the particle radius. Expressions (5), (8) and (9) depend explicitly on r in the form of power functions and by the coefficients of entrainment and flow, which are strongly dependent on the relaxation time, which is in turn a function of the particle radius. So one should expect the strong variation of the drift forces as a function of r, and, in particular, distinct maxima. Maxima of the quantity A_D which is the coefficient of the principal equation (12) usually occur somewhere else as a function of the radius, since the particle mass varies as r^3. Moreover, by calculating the quantity A_D, with the dimension of acceleration, it is possible to evaluate the part of the Earth's acceleration in the motion of aerosol particles. It is essential in problems where the drift and fall of particles in the gravitational field are considered simultaneously [6], [9].

Applying the expressions of the drift forces of different kinds as given in the previous point, it is now possible to write the corresponding field intensities

radiation drift

$$A_{DR} = 2k\varrho_p^{-1}\mu_g^2\bar{E}, \tag{14}$$

viscosity drift

$$A_{DL} = \frac{9}{4}(\varkappa-3)\eta r^{-2}(\varrho_p\varrho_g c)^{-1}\mu_g^2\bar{E}, \tag{15}$$

asymmetric drift

$$A_{DA} = 4k\varrho_p^{-1}\mu_p\left[\left(3+\frac{9}{2}b\right)\mu_p-\frac{9}{2}b\left(b+1\right)\mu_g\right]\bar{E}. \tag{16}$$

In calculating the numerical values it is assumed that $\bar{E} = 100 J/m^3$, $\varrho_p = 10^3$ kg/m^3, $\varrho_g = 1.2$ kg/m^3, $\eta = 1.85\cdot10^{-5}$ Ns/m^2 and $c = 340$m/s. The plots of the maximum intensities of the field of force of different types of drift are shown in Figs. 1 and 2, where the respective frequencies of 1 KHz and 10 KHz were assumed. The plots made for particle radii within the interval 10^{-7}–10^{-4} m on a double logarithmic scale. This makes it easy to read the values of intensity for a density of the wave energy other than the given one, since the quantities represented in plots

depend on E in a linear way and an increase or decrease in this value by one order of magnitude causes the same change in the value of the intensity drift fields.

Analysis of the plots indicates that particular kinds of drift dominate various intervals of variation of the particle radius. Thus, for the largest particles, with radii of the order of 10^{-4} m, the radiation drift is the strongest, whereas the smallest

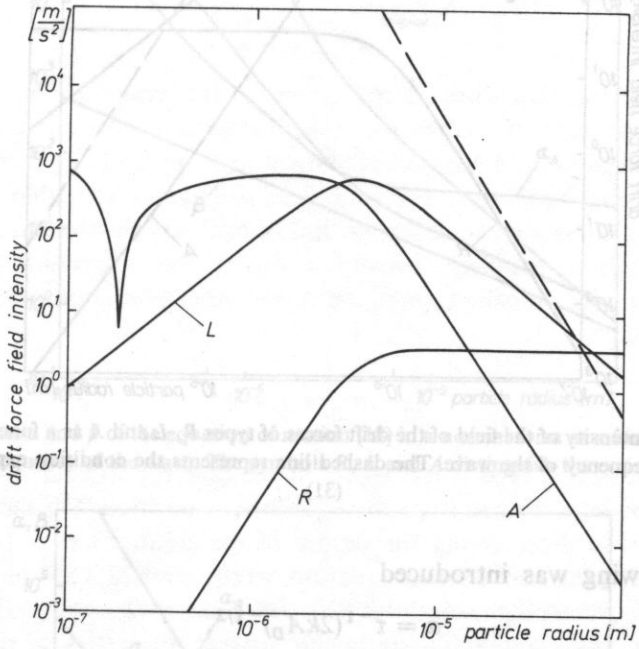

Fig. 1. Plots of the intensity of the field of the drift forces of types R, L and A as a function of the particle radius at 1 KHz frequency of the wave. The dashed line represents the condition represented by formula (31)

particles, $r < 10^{-6}$ m, move under the effect of the A-type drift. In the intermediate interval, the L-type drift dominates.

Let us now evaluate the other components of the basic equation of motion (12). To estimate their effect on the character of the solution, let us reduce to a minimum the number of constants in the equation by replacing the position and time by the nondimensional variables

$$y = \pi - 2kx, \qquad \theta = (2kA_D)^{\frac{1}{2}}t. \tag{17}$$

For the new variables the equation of motion becomes

$$\frac{d^2y}{d\theta} + \alpha\frac{dy}{d\theta} + \beta\frac{dy}{d\theta}\left|\frac{dy}{d\theta}\right| + \sin y = 0, \tag{18}$$

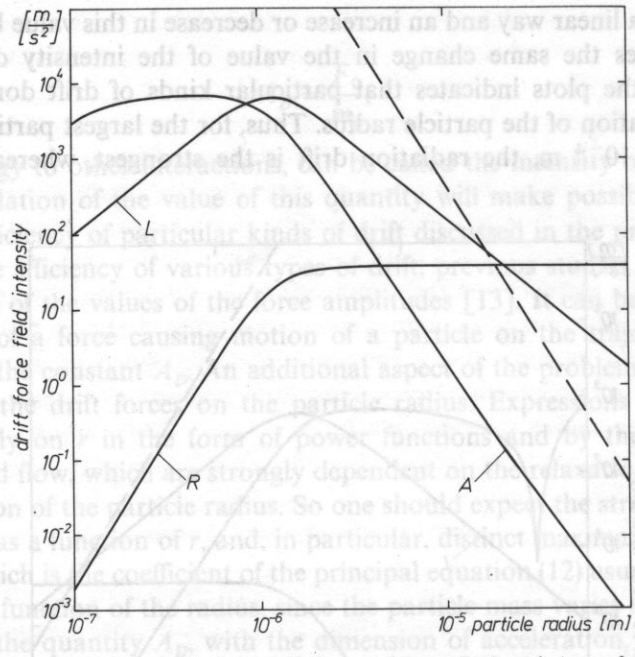

Fig. 2. Plots of the intensity of the field of the drift forces of types R, L and A as a function of the particle radius at 10KHz frequency of the wave. The dashed line represents the condition expressed by formula (31)

where the following was introduced

$$\alpha = \tau^{-1}(2kA_D)^{-1/2}, \tag{19}$$

$$\beta = 27\varrho_g/(32kr\varrho_p). \tag{20}$$

The equation of motion in this form, which in the theory of differential equations is called the normal form, contains only two constants, whereas the initial equation (12) contained four of them (including the wave number k in last term). The constant represents the contribution of Stokes resistance force to the particle motion, and the constant β describes the Oseen correction to this force. The particle mass and the drift force, and also the wavelength, are normalized in a way in this equation making it easier to analyze the effect of the two dissipation terms on the solution.

In general, the constants α and β depend on the parameters characterizing the particle and the wave; moreover, the constant α depends on the intensity of the drift force field, and, therefore, on the kind of drift. Assuming that same numerical values which were used in calculating the quantity A_D, one can estimate the constants α and β, and, thus, evaluate the two terms representing friction in the equation of motion.

Figs. 3 and 4 show plots of the constants of equation (18) as a functions of the particle radius for the respective frequencies of 1 KHz and 10 KHz. Analysis of these plots justifies one to state that the nonlinear friction term, represented by the

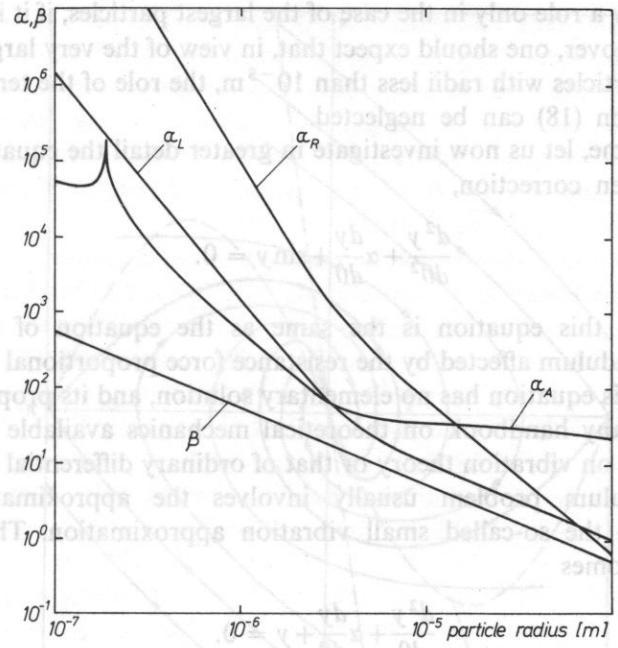

Fig. 3. The constants α and β of the equation of motion (18) in a normal form as a function of the particle radius at 1 KHz frequency of the wave. The symbols R, L and A distinguish the considered types of drift

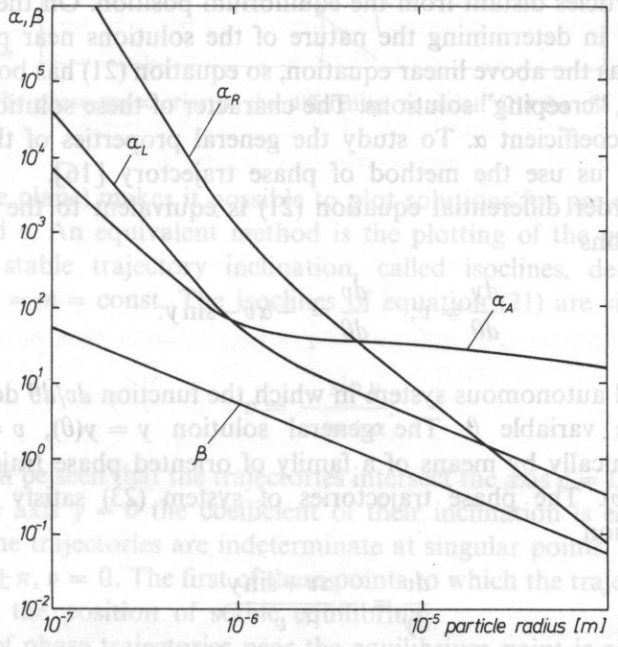

Fig. 4. The constants α and β of the equation of motion (18) in a normal form as a function of the particle radius at 10 KHz frequency of the wave. The symbols R, L and A distinguish the considered types of the drift

constant, can play a role only in the case of the largest particles, if it is assumed that $|dy/d\theta| < 1$. Moreover, one should expect that, in view of the very large values of the constant α for particles with radii less than 10^{-5} m, the role of the term representing inertia in equation (18) can be neglected.

In the meantime, let us now investigate in greater detail the equation of motion, refusing the Oseen correction,

$$\frac{d^2y}{d\theta^2}+\alpha\frac{dy}{d\theta}+\sin y = 0. \tag{21}$$

In formal terms, this equation is the same as the equation of motion of the mathematical pendulum affected by the resistance force proportional to the velocity. However, even this equation has no elementary solution, and its properties have not been studied in any handbook on theoretical mechanics available to the present author, nor those on vibration theory or that of ordinary differential equations. The analogous pendulum problem usually involves the approximation $\sin y = y$, corresponding to the so-called small vibration approximation. The equation of motion then becomes

$$\frac{d^2y}{d\theta}+\alpha\frac{dy}{d\theta}+y = 0. \tag{22}$$

The linearization of this type is not useful in the case if particular interest is in the trajectories of particles distant from the equilibrium position. On the other hand, it may prove useful in determining the nature of the solutions near points of stable equilibrium. Just as the above linear equation, so equation (21) has both quasi-periodic and aperiodic, "creeping" solutions. The character of these solutions depends on the value of the coefficient α. To study the general properties of the solutions of equation (21), let us use the method of phase trajectory [16].

The second-order differential equation (21) is equivalent to the system of two first-order equations

$$\frac{dy}{d\theta} = v; \quad \frac{dv}{d\theta} = -\alpha v-\sin y. \tag{23}$$

This is a so-called autonomous system in which the function $dv/d\theta$ does not depend explicitly on the variable θ. The general solution $y = y(\theta)$, $v = v(\theta)$ can be represented graphically by means of a family of oriented phase trajectories on the phase plane (y, v). The phase trajectories of system (23) satisfy the first-order differential equation

$$\frac{dv}{dy} = -\frac{\alpha v+\sin y}{v}, \tag{24}$$

which subordinates the inclination of the differential curve crossing this point to each point (y, v). The field of directions thus obtained (the "image" of the differential

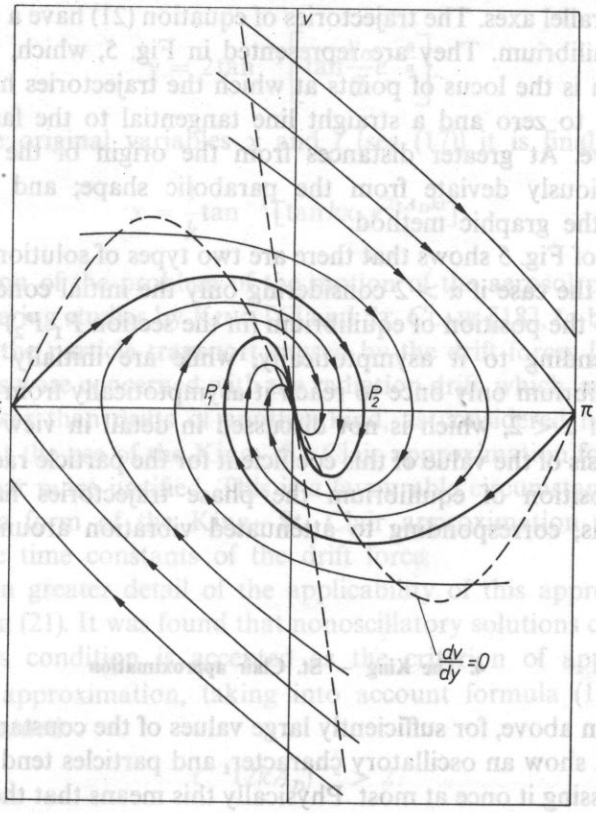

Fig. 5. The phase trajectories of the differential equation (21) for the case $\alpha > 2$

equation on the plane) makes it possible to plot solutions for pre-determined initial values of y and v. An equivalent method is the plotting of the geometric locus of points of the stable trajectory inclination, called isoclines, determined by the equation $dv/dy = m = \text{const}$. The isoclines of equation (21) are sinusoids with the equation

$$v = -\frac{\sin y}{m+\alpha}. \tag{25}$$

In general, it can be seen that the trajectories intersect the axis $v = 0$ perpendicularly, whereas on the axis $y = 0$ the coefficient of their inclination is equal to $-\alpha$. The inclination of the trajectories are indeterminate at singular points, which are $y = 0$, $v = 0$ and $y = \pm\pi$, $v = 0$. The first of these points to which the trajectories converge, corresponds to the position of stable equilibrium.

The shape of phase trajectories near the equilibrium point is approximately the same as for the linear equation (22). About this elementary equation, it is known [17] that for $\alpha > 2$ its trajectories are parabolic in shape, tangential to a common straight

line and with parallel axes. The trajectories of equation (21) have a similar shape near the point of equilibrium. They are represented in Fig. 5, which, in addition, mark a sinusoid which is the locus of points at which the trajectories have an inclination coefficient equal to zero and a straight line tangential to the family of parabolas mentioned above. At greater distances from the origin of the phase plane, the trajectories obviously deviate from the parabolic shape; and their course was determined by the graphic method.

The analysis of Fig. 5 shows that there are two types of solutions of the nonlinear equation (21) in the case if $\alpha > 2$ considering only the initial condition $y_0 = 0$. The particles close to the position of equilibrium (in the section $P_1 P_2$) do not go beyond this position, tending to it asymptotically, while are initially further cross the position of equilibrium only once to reach it asymptotically from the opposite side.

In the case if $\alpha < 2$, which is not discussed in detail in view of the previously performed analysis of the value of this coefficient for the particle radii of interest here, close to the position of equilibrium the phase trajectories have the shape of tightening spirals, corresponding to attenuated vibration around the position of equilibrium.

4. The King – St. Clair approximation

As was shown above, for sufficiently large values of the constant in equation (21), solutions do not show an oscillatory character, and particles tend to the position of equilibrium, crossing it once at most. Physically this means that the force of inertia is negligible compared with other forces: of friction and that of drift, leading the particle to the position of equilibrium. For large α, in equation (21) it is possible to neglect the second derivative representing the inertia force, therefore it is obtained that

$$\alpha \frac{dy}{d\theta} + \sin y = 0. \tag{26}$$

It is a nonlinear differential equation of the first order with separating variables,

$$\frac{dy}{\sin y} = -\frac{d\theta}{\alpha}. \tag{27}$$

The indeterminate integral on the left side of the equation is elementary,

$$\int \frac{dy}{\sin y} = \ln \tan \frac{y}{2} + \text{const}, \tag{28}$$

therefore, with the initial condition $y(0) = y_0$, the solution is in the form

$$\ln \tan \frac{y}{2} = -\frac{\theta}{\alpha} + \ln \tan \frac{y_0}{2},$$

or

$$y = 2\tan^{-1}\left[\tan\frac{y_0}{2}e^{-\frac{\theta}{\alpha}}\right]. \tag{29}$$

Returning to the original variables x and t (see (17)) it is finally obtained that

$$x = \frac{1}{k}\tan^{-1}[\tan kx_0 e^{2\tau A_D kt}]. \tag{30}$$

The above solution of the problem of the motion of the aerosol particle was given even in the pioneering studies by KING [6] and ST. CLAIR [18], to be applied later in other studies on the particle transport caused by the drift forces [9], [10]. In each case, those studies were concerned with the radiation drift, which, as could be seen, is significantly weaker than drifts of another kind, as considered here. It should be experted then that the use of the King–St. Clair approximation for the other types of drift may appear more justified. This is a favourable circumstance in view of the fact that analytic form of the King–St. Clair approximation permits accurate estimation of the time constants of the drift force.

To evaluate in greater detail of the applicability of this approximation, let us return to equation (21). It was found that nonoscillatory solutions could be obtained for $\alpha > 2$. If this condition is accepted as the criterion of applicability of the King–St. Clair approximation, taking into account formula (19), the following inequality is obtained:

$$\tau^{-1}(2kA_D)^{-\frac{1}{2}} > 2.$$

To connect mutually the more fundamental parameters of the particle and medium, let us also make use of formula (7), representing the relaxation time, and also the relation $k = 2\pi f/c$. Appropriate transformations give the condition

$$A_D < \frac{81\eta^2 c}{64\pi r^4 \varrho_p^2 f}. \tag{31}$$

The above inequality defines for what accelerations of the drift forces the particle motions do not have an oscillatory character and the King–St. Clair approximation can be used. In Figs. 1 and 2, representing the dependence $A_D(r)$ for different drift forces, condition (31) determines an area beneath the straight line marked by dashed line. It can be seen that it is satisfied for almost the whole considered range of particle radii and all drifts except for the radiation drift for $r > 10^{-5}$m.

5. Conclusions

The criterion of applicability of the King–St. Clair approximation derived above can be confronted with the results of numerical calculations. It is most convenient to consider the equation of motion in the normal form (21), since the character of its

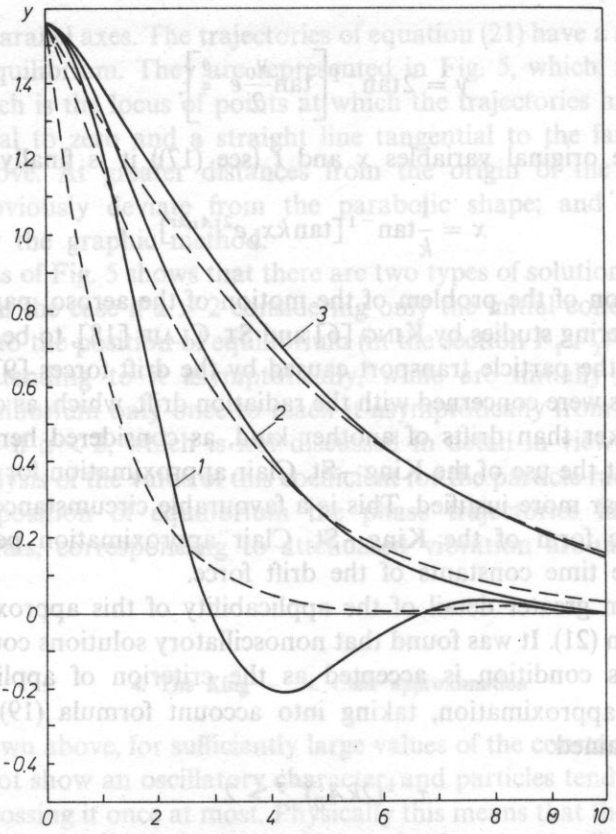

Fig. 6. A comparison of the exact solutions (solid line) and the approximate solutions of the King-St. Clair (dashed line) type for chosen attenuation coefficients: 1) $\alpha = 1.0$; 2) $\alpha = 2.5$; 3) $\alpha = 4.0$

solutions depends only on one constant. Fig. 6 shows the numerically obtained solutions of this equation for three different values of α and the courses of the respective approximate solutions given by formula (29). In both cases it was assumed that $y(0) = \pi/2$, where, moreover, for equation (21) it was put that $y(0) = c$ (solution (29) does not depend on the initial velocity, as the first-order integral of the equation). It can be seen that for $\alpha > 2$ approximate solutions are close to the accurate ones. What is, however, more important is that, in each of the presented cases, even for $\alpha = 1$, a particle moving along the trajectory given by the accurate equation, reaches the position of equilibrium earlier than expected by the King–St. Clair formula. Because of this it is possible to predict that the application of the approximate solution gives a beforehand estimation of the constants of the transport phenomenon.

In summing up the earlier considerations, it can be stated moreover, that:

1) the drift forces directing aerosol particles to nodes or loops of the standing

wave, act in the most efficient way on particles with radii of the order of 10^{-5} m and less; with the radiation drift appearing to be the weakest;

2) for particles smaller than 10^{-5} m, it is possible to neglect the nonlinear correction for friction; on the other hand, it does not apply to the region where the radiation drift dominates;

3) within the same interval of the aerosol particle size, in investigating the motion, it is useful to apply the King – St. Clair approximation, making it possible to study the motion analytically. In this case, too, the region of domination of the radiation drift is outside the applicability range of the approximation.

Therefore, the radiation drift, which has been best investigated and most frequently indicated as the reason for the local concentration of aerosol particles acts only on relatively large particles, and the approximations presented here are hardly useful in studies on the motion which it causes. The drift plays, on the other hand, as a mechanism facilitating coagulation, a large role for particles with radii of the order of micrometers when the L-type and A-type forces dominate.

References

[1] D. T. SHAW, *Application of acoustic agglomerators for emergency use in liquid-metal fast breeder reactor plant*, Nucl. Sci. Eng., 70, 2, 127–134 (1979).

[2] *Proceedings of the Symposium on Control of Fine-Particle Emissions from Industrial Sources*, San Francisco 1974.

[3] D. S. SCOTT, A *new approach to the acoustic conditioning of industrial aerosol emissions*, J. Sound Vib., **43**, 4, 607–619 (1975).

[4] H. CZYŻ, *Kinetics of the transport of aerosol particles under the influence of drift forces in the standing wave field*, Archiv. of Acoustics, **12**, 3–4 (1987).

[5] P. J. WESTERVELT, *The theory of steady forces caused by sound waves*, J. Acoust. Soc. Am., **23**, 3, 312–315 (1951).

[6] L. V. KING, *On the acoustic radiation pressure on spheres*, Proc. Roy. Soc. A **147**, 861, 212–240 (1934).

[7] Л. П. ГОРКОВ, *О силах, действующих на малую частицу в акустическом поле в идеальной жидкости*, Доклады АНССР, **140**, 1, 88–91 (1961).

[8] J. RUDNICK, *Measurements of the acoustic radiation pressure on a sphere in a standing wave field*, J. Acoust. Soc. Am., **23**, 5, 633–634 (1951).

[9] F. FITTIPALDI, *Particle coagulation by means of ultrasonics*, Acustica **41**, 4, 263–266 (1979).

[10] T. HIGASHITANI, *Migration of suspended particles in plane stationary ultrasonic field*, Chem. Eng. Sci., **36**, 12, 1877–1882 (1981),

[11] P. J. WESTERVELT, *The mean pressure and velocity in a plane acoustic wave in a gas*, J. Acoust. Soc. Am., **22**, 3, 319–327 (1950).

[12] С. С. ДУХИН, *Теория дрейфа аэрозольной частицы в стоящей звуковой волне*, Коллодный Журнал **22**, 1, 128–130 (1960).

[13] Е. П. МЕДНИКОВ, *Акустическая коагуляция и осаждение аэрозолей*, Изд. АНССР Москва 1963.

[14] H. CZYŻ, *The aerosol particle drift in a standing wave field*, (in Polish), Instytut Telekomunikacji i Akustyki Politechniki Wrocławskiej, Wrocław 1982.

[15] P. J. WESTERVELT, *Acoustic radiation pressure*, J. Acoust. Soc. Am., **29**, 1, 26–29 (1957).

[16] G. A. KORN, T. M. KORN, *Mathematical handbook for scientists and engineers*, § 9.5, McGraw-Hill, New York-Toronto-London 1961.

[17] Н. Н. Боголюбов, Ю. А. Митровский, *Асимптотические методы в теории нелинейных колебаний*, Гос. Изд. Техн.-Теор. Лит., Москва 1955.

[18] H. W. ST. CLAIR, *Agglomeration of smoke, fog or dust particles by sonic waves*, Indust. Engng. Chem., **41**, 11, 2434–2438 (1949).

Received May 15, 1987.

ARCHIVES OF ACOUSTICS
12, 3–4, 215–224 (1987)

KINETICS OF THE TRANSPORT OF AEROSOL PARTICLES UNDER THE INFLUENCE OF DRIFT FORCES IN THE STANDING WAVE FIELD

HENRYKA CZYŻ

Institute of Physics, Pedagogical University
(35–311 Rzeszów, ul. Rejtana 16 a)

In the paper the time constants of the aerosol particles transport process under the influence of drift forces appearing in the standing wave field have been estimated. The transport phenomenon which causes particle concentration in the neighbourhood of the minimum of drift force potential significantly supports the coagulation microprocesses by reducing the distances between particles. It has been demonstrated that the growth of particle concentration around the points of stable equilibrium is exponential. The time constant of this growth was estimated and the formulae which precisely determine the time needed to obtain the assumed concentration increase have been derived. Parameters of spatial particle distribution in the equilibrium state and time necessary for reaching such distribution have been estimated under an assumption of lack of interactions between particles.

Basic notation

x spatial coordinate in the direction of wave propagation
t time,
f frequency,
ω angular frequency,
λ wave-length,
k wave-number,
ϱ_g gas density,
ϱ_p density of the aerosol particle,
r radius of the particle,
m particle mass,
η gas viscosity,
k_B Boltzmann constant,
T temperature.

1. Introduction

In the field a standing wave defined by the deflection function of particles of the medium

$$\xi = \xi_0 \sin kx \sin \omega t, \tag{1.1}$$

the particles of aerosol, in the first approximation, exhibit a harmonic motion with amplitude and phase depending on the particle magnitude, frequency and other quantities characteristic for the particle, the medium and the acoustic wave. If the second order effects are taken into consideration, such as radiation pressure, asymmetry of medium oscillations resulting from the standing wave amplitude dependence on the position or periodical changes of viscosity then it can be concluded that the real motion of a particle is a superposition of the oscillating and translatory motion [1]. Averaging of the second-order-approximation solutions of the equations of motion indicates that the motion of instantaneous equilibrium position of a particle is induced by the resistance force and a certain force F_D which depends on the position according to the formula [1]

$$F_D(x) = F_0 \sin 2kx. \tag{1.2}$$

irrespectively of the considered mechanism of the phenomenon.

Such forces are called the drift forces. Depending on the sign of the constant F_0 which denotes the maximum value of the force, these forces cause the constant movement of aerosol particles towards the nodes (given by an equation $kx = n\pi$ or loops $kx = \left(n+\frac{1}{2}\right)\pi$, $n = 0, \pm 1, \pm 2, \ldots$) of the standing wave. In the case $F_0 > 0$ the minimum of the force potential given with the formula

$$U_D(x) = F_0(2k)^{-1}\cos 2kx + \text{const}, \tag{1.3}$$

are in the loops of the wave. On the contrary, if $F_0 < 0$, the drift forces make the aerosol particles move towards the nodes.

In approximation which is valid for small Reynolds numbers the equation of motion of the average position of the particle is [1]

$$m_p \frac{d^2x}{dt^2} + 6\pi\eta r \frac{dx}{dt} - F_0 \sin 2kx = 0, \tag{1.4}$$

where the second summand represents the resistance force in the Stokes approximation. By dividing this equation by the particle mass we obtain

$$\frac{d^2x}{dt^2} + \frac{1}{\tau}\frac{dx}{dt} - A_D \sin 2kx = 0, \tag{1.5}$$

where $\tau = m_p/(6\pi\eta r) = 2r^2\varrho_p/(9\eta)$ is the relaxation time and $A_D = F_0/m_p$ denotes the maximum value of acceleration induced by the drift force. This value which, by analogy to other force fields can be considered as the intensity of the drift force field, depends strongly on the particle size and the nature of drift. In our previous paper [2] we have presented the qualitative analysis of the intensity of several drift types. We have demonstrated that the drift connected with the radiation pressure called the radiation drift (abbrev.: R drift) dominates in the case of relatively large particles with radii about 10^{-4}m. The order of magnitude of the value of field intensity for this drift

is $10 m/s^2$ and decreases rapidly with the decrease of radius of particles. Because this value is near to the value of gravity acceleration, the motion of large particles under the influence of R drift forces with simultaneous settling is frequently investigated [3, 4]. The L drift concerned with periodical temperature changes and appropriate viscosity changes in the standing wave dominates in the range of radii between 10^{-5} and 10^{-6}m, where it attains maximum of intensity. For the frequency 10 kHz and wave energy density $100 J/m^3$ this maximum is greater than $10^3 m/s^2$. Similar values characterize the A drift, concerned with the phenomenon of asymmetry of the particle motion in the standing wave field, when the influence of the wave on the particle changes according to the decrease of vibration amplitude of particles of the medium together with the decrease of distance to the wave node. Maximum of intensity of this drift appears for the particles of radii slightly smaller than 10^{-6}m.

Equation (1.5) is analogical to the equation of motion of a pendulum in a viscous medium. Despite the simplicity of the phenomenon it represents, this equation does not have an elementary solution. The small displacements approximation which is applied in the case of a pendulum can not be applied, because here the motion of particles at the points far from equilibrium position is of special interest. Analogy with the pendulum allows to expect the quasiperiodical solutions with amplitude damping and the monotonic (aperiodical) solutions, if the damping is large enough, the driving force is small, and the particle inertia is negligible. Analysis of the solution type, carried out by means of graphical and numerical methods in the paper [2], allowed for finding the relation between the constants of Eq. (1.5) (i.e. relaxation time τ, drift forces field intensity A_D and wavenumber k), which constitutes the monotonicity criterion of solutions. This relation is

$$\tau^{-1}(2kA_D)^{-1/2} > 2, \tag{1.6}$$

what, after some transformations and after substituting the equation parameters expressed by basic quantities characterising the particle and the wave gives the conditions

$$A_D < 81\eta^2 c/(64\pi r^4 \varrho_p^2 f). \tag{1.7}$$

For fixed values of viscosity, wave velocity and frequency and density of a particle, the above condition relates the drift force field intensity to the particle radius. As it has been demonstrated in the paper [2], this condition is fulfilled for all drift types, if the particles radii are restricted to the values smaller than 10^{-5}m.

The motion of aerosol particles consists then in monotonically approaching the stable equilibrium point. From the physical viewpoint this is the evidence of the negligible inertia of a particle. Hence, in the analysis of the motion in the range of applicability of the condition (1.7), we shall consider the differential equation

$$\frac{1}{\tau}\frac{dx}{dt} = A_D \sin 2kx, \tag{1.8}$$

obtained from eq. (1.5) by neglecting the inertial component. This equation, called the King–St. Claire equation for the names of the scientists who for the first time applied it in the theory of drift (cf. [4], [5]), can be integrated by separation of variables. Simple calculations lead to the solution

$$\operatorname{tg} kx = \operatorname{tg} kx_0 \exp(2\tau A_D kt), \tag{1.9}$$

where $x = x_0$ is put for $t = 0$. The solution (1.9) does not depend on the initial velocity of particles, being integral of a first order equation. Usefulness of this approximation in the range of drift force intensities and particle radii defined by the condition (1.7) has been confirmed by numerical calculations [1].

2. Estimation of the time constants of the motion

The solution (1.9) anticipates that for positive values of constant A_D which represents the drift forces field intensity the aerosol particles will move towards the points in which $kx = (n+\frac{1}{2})\pi$, i.e. to the standing wave loops. On the other hand, the wave nodes are the points of unstable equilibrium and particles which initial positions satisfy the equation $kx_0 = n\pi$ will remain in the nodes infinitely long, putting aside the random forces which can throw them off such points. For the negative values of the constant A_D the roles of loops and modes exchange; anyway, this does not change the kinematics of the transport process, because the change of sign of the exponent in Eq. (1.9) is equivalent to the linear change of variables $kx \to kx - \frac{\pi}{2}$. In practice the sign of the constant A_D is positive only in the case of radiation drift, and only for relatively heavy particles, for which $\varrho_p/\varrho_g > 5/2$ [4]. For lighter particles the sign of A_D for the R drift, as well as for the L and A drifts, is negative in the whole range of particle density. Hence as a rule aerosols are concentrated around the nodes.

A particle, the motion of which is described by Eq. (1.9), tends to the equilibrium position asymptotically and reaches if after a theoretically infinite period. The concentration of particles increases then around such a point and decreases in the region between a loop and a node. Hence, calculation of the period needed for attaining the equilibrium position is aimless. Instead of this, we shall investigate the changes of particle concentration as a function of time and position.

Let us assume that at instant $t = 0$ all the particles are in rest and that their distribution along the x axis perpendicular to the nodes and loops plane is uniform. Let us denote the number of particles present in a unit interval of this axis at the point x and at the time t as $N(x, t)$. We have then

$$N(x, t)|_{t=0} = N_0 = \text{const}. \tag{2.1}$$

The type of the approximation of the equation of motion as well as the form of the solution indicate that particles tending to a loop or a mode do not overtake each

other (it could have been so in the case when, in contradiction to our assumption, particles were placed farther from the points of balance had and larger initial velocity). If all particles start their motion at the time $t = 0$, then those from a point x_0 will be at a point x, at the time t and those from a point $x_0 + dx_0$ at the same time will be at a point $x + dx$ (cf. Fig. 1). It can be seen at once that if the velocity of

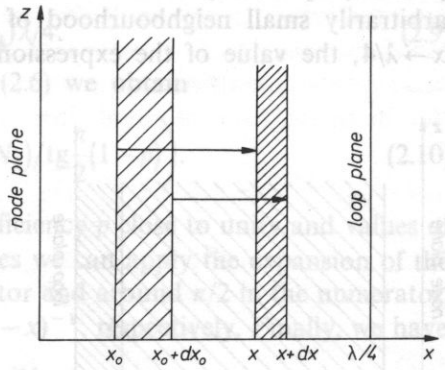

Fig. 1. Concentration of aerosol as the effect of an asymptotic travel of aerosol particles towards the loop planes

particles drops while approaching the equilibrium point, then their concentration grows. Relative concentration (with respect to the initial one) is then equal to

$$\frac{N(x, t)}{N_0} = \frac{dx_0}{dx}. \tag{2.2}$$

The value of the derivative in the above equation can be found by taking differential of both sides of (1.9):

$$\sec^2 kx dx = \sec^2 kx_0 \exp(2\tau A_D k t) dx_0. \tag{2.3}$$

Eliminating x_0 by means of eq. (1.9) we obtain

$$N(x, t) = N_0(\cos^2 kx \exp(\alpha t) + \sin^2 kx \exp(-\alpha t))^{-1}, \tag{2.4}$$

where $\alpha = 2\tau A_D k$.

As it can be easily seen at the standing wave nodes ($kx = n\pi$) the concentration decreases exponentially as $N_0 \exp(-\alpha t)$ and at the loops it grows as $N_0 \exp(\alpha t)$. Time constant of this process, equal to α^{-1}, depends on relaxation time, wavenumber and drift force intensity, thus on the drift type. From the formula (2.4) one can calculate the time after which the particle concentration in a given point x achieves a specified value. However, because the solution of Eq. (2.4) leads to a complex solution which is not very useful, we shall pass to other methods of estimating the rate of the process of concentrating particles by the drift forces.

If we fix a time period during which the concentration of particles in a specific neighbourhood of a stable equilibrium point should take place, then this time will always occur to be insufficient for a certain number of particles, initially distributed near the unstable equilibrium points. The form of the approximate solution (1.9)

indicates that particles travel to the wave loop during an arbitrarily long period. It is clear when we solve Eq. (1.9) with respect to time:

$$t = \alpha^{-1}\ln(\mathrm{tg}kx/\mathrm{tg}kx_0). \tag{2.5}$$

If $x_0 \to 0$ then $t \to \infty$. On the other hand, particles move towards an equilibrium point asymptotically. Hence, one can not speak about their complete clustering in an arbitrarily small neighbourhood of a wave loop after a finite time. Indeed, for $x \to \lambda/4$, the value of the expression (2.5) also tends to infinity.

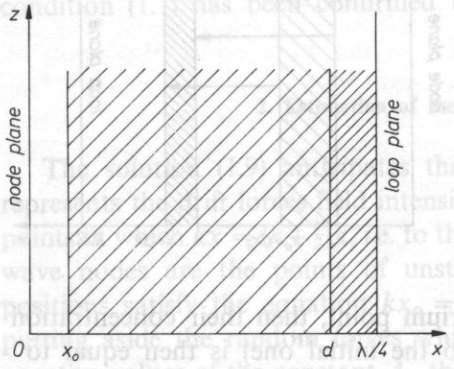

Fig. 2. Cleared zone (interval $[x_0, \lambda/4)$ and intensive coagulation zone (interval $[d, \lambda/4]$)

Let us denote by d the coordinate of a point which a particle should surpass to enter a "zone of intense coagulation", where the inter-particle processes reach the intensity high enough for an "almost immediate aggregation" (such concepts, which are useful in considerations where the nature of microcoagulation processes is neglected, were introduced in the paper [6]). Other particles which were initially displaced in the range $[x_0, d]$ will reach the point d earlier (cf. Fig. 2). This means that after the period

$$t_k = \alpha^{-1}\ln(\mathrm{tg}kd/\mathrm{tg}kx_0), \tag{2.6}$$

the zone defined by dx will be reached by the fraction $(\lambda/4 - x_0)/(\lambda/4)$ of all particles, provided that their distribution along the x axis was uniform at $t = 0$. Then, the quantity

$$p = (\lambda/4 - x_0)/(\lambda/4) = 1 - 4x_0/\lambda, \tag{2.7}$$

denotes the relative number of particles which would reach the zone defined by d in time t_k, with respect to the number of all particles. This value can be called the efficiency of the mechanism of transport of particles by the drift forces to the zone of intense coagulation. If it is assumed that particles in this zone will undergo coagulation for certain then p can be called simply the efficiency of coagulation. The latter formula makes it possible to express the value x_0 from the initial condition of Eq. (1.9) by this useful parameter

$$x_0 = (1-p)\lambda/4. \tag{2.8}$$

After the period found from Eq. (2.6) almost all the particles of aerosol will be in the zone defined by d (except for those which at $t = 0$ were in the interval $[0, x_0]$). It can be assumed then that the average concentration of particles in this zone grew as many times as the distance from point d to the loop is smaller than a quarter of wave-length. Hence, we have $N_0/N_k = (\lambda/4-d)/(\lambda/4) = 1-4d/\lambda$, from which it follows

$$d = (1-N_0/N_k)\lambda/4. \tag{2.9}$$

Substituting the two latter formulae to Eq. (2.6) we obtain

$$t_k = \alpha^{-1}\ln\left(\operatorname{tg}\frac{\pi}{2}(1-N_0/N_k)/\operatorname{tg}\frac{\pi}{2}(1-p)\right). \tag{2.10}$$

What interests us the most are the values of efficiency p close to unity and values of the quotient N_0/N_k close to zero. In these cases we can apply the expansion of the function tangent around zero in the denominator and around $\pi/2$ in the numerator, using approximations $\operatorname{tg}x \approx x$ and $\operatorname{tg}x = (\pi/2-x)^{-1}$, respectively. Finally, we have

$$t_k = \alpha^{-1}\ln\frac{4N_k/N_0}{\pi^2(1-p)}. \tag{2.11}$$

It should be reminded that the value

$$\alpha^{-1} = (2\tau A_D k)^{-1} = 9\eta c/(8\pi r^2 \varrho_p f A_D), \tag{2.12}$$

is a time constant, characteristic for the process of exponential concentration variations (cf. Eq. (2.4)). Expression (2.11) introduces a significant amount of precision into the notion of coagulation time for given efficiency of the process and specified concentration increase. In agreement with our expectations this time grows if both these parameters increase. Note that this growth is logarithmic, so in the estimations only the order of magnitude of the parameters $1 - p$ and N_k/N_0 is important. For example if we put $1 - p = 10^{-2}$, then the value of coagulation time given by the expression (2.11) will be $8.30\cdot\alpha^{-1}$ for $N_k/N_0 = 10^2$ and $17.52\alpha^{-1}$ for $N_k/N_0 = 10^6$. So, the growth of assumed concentration by four orders of magnitude gives only the doubling of time needed to obtain it. In addition, for average wave-lengths and typical particle dimensions, the concentration growth larger than 10^4 is unrealistic.

For the quantitative estimation of the speed of process of gathering the particles in the regions of around wave loops or nodes let us assume now in the formula (2.11) some numerical values of parameters characterizing the particle, the acoustic field and the transport process. Similarly as in the estimation of drift forces field intensities for various types of drifts in the paper [2], we shall put: $\varrho_p = 10^3$ kg/m^3, $\varrho_g = 1.2$ kg/m^3, $\eta = 1.85\cdot10^{-5}$ Ns/m^2 and $c = 340$ m/s, what corresponds with an acoustic wave in the air. If we also fix the frequency and energy of the wave (f = 10 kHz and $\bar{E} = 100$ J/m^3 in our example), then, according to formula (2.11), the equation $t_k = \text{const}$ will provide a relation between the drift force field intensity A_D and the aerosol particle radius. In the Fig. 3, where the graphs of A_D for various drift types

taken from paper [2] are also shown, equation $t_k = \text{const}$ is represented by a straight line. For the concentration process the following values were assumed: $1 - p = 10^{-2}$, what corresponds to the efficiency equal to 99%, and $N_k/N_0 = 10^3$. The dashed line delimits the range of applicability of the King–St. Claire approximation and represents the condition (1.7). As it can be seen, for the above listed values of wave parameters, the L type drift effectively gathers the particles around the equilibrium positions in the time about 0,1 s. The R type drift induces the concentration of particles with radii larger than 10^{-5}m in the time shorter than 1 s, while the A type drift can provide for concentration of particles with radii about 10^{-6}m in the time of equal order of magnitude.

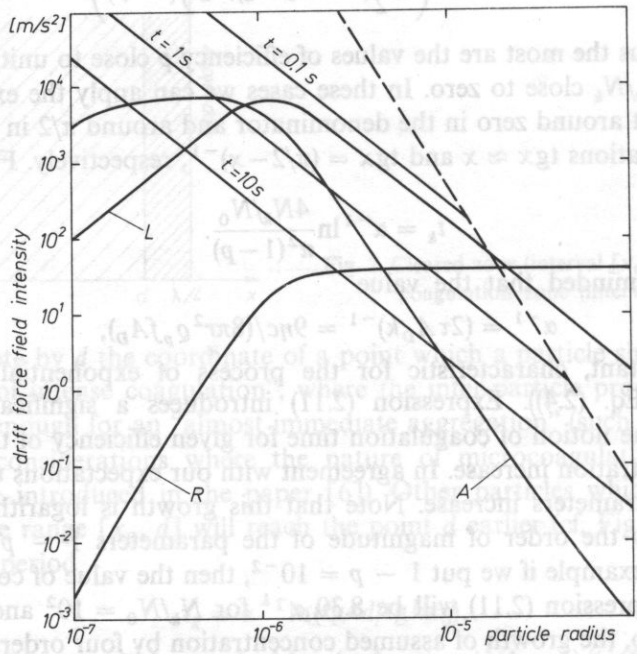

Fig. 3. Plots of intensity of the drifts type R, L and A vs particle radius and lines of constant values of coagulation times. The straight dashed line defines the region of application of the King-St. Claire approximation

3. Spatial distribution of particles around the equilibrium points

While discussing the phenomenon of transport of the aerosol particles under the influence of drift forces we have not taken into account the processes responsible for the coagulation of particles. We have assumed however that the appropriate growth of concentration, corresponding to the reduction of mutual distances between particles, will cause quick coagulation in concentration zones. In the two-particle problem a similar approach was applied by JESSEL and TIMOSHENKO [6], by

introducing the concept of the „coagulation parameter" as a dimension of the zone in which particles coagulate „automatically and almost immediately". The constant of all exponential function of time which describes the decrease of concentration of aerosol particles was expressed by them with the use of the dimensions of such a zone, assumed to be an ellipsoid of revolution, elongated in the direction of wave propagation.

Theoretical approach which consists in neglecting the interactions between particles makes it possible to estimate statistically the dimensions of a zone in which the particles will gather. The distribution of equilibrium of the particles is described by the Boltzmann distribution

$$\mathcal{N}(x) = \text{const} \cdot \exp\left(-\frac{U(x)}{k_B T}\right), \tag{3.1}$$

while potential is given by Eq. (1.3). In the neighbourhood of a minimum, e.g. near the point $x = \lambda/4$, the function $U_D(x)$ has approximately the following form

$$U_D(x) \approx \text{const} + m_p A_D k \left(x - \frac{\lambda}{4}\right)^2, \tag{3.2}$$

where the terms of order $(x - \lambda/4)^{-4}$ are rejected. Then, in this approximation, the spatial distribution is of gaussian type

$$\mathcal{N}(x) = \text{const} \cdot \exp\left(-\frac{m_p A_D k \left(x - \frac{\lambda}{4}\right)^2}{k_B T}\right). \tag{3.3}$$

Dimension of a zone of particle concentration is then of the order of magnitude

$$\sigma = \left(\frac{k_B T}{2 m_p A_D k}\right)^{\frac{1}{2}} \tag{3.4}$$

The above value can be considered as the dimension of the zone of concentration of particles, if the particle interactions are neglected and the particle dimensions are not taken into account. Such estimation can be useful if the coagulation itself is caused by additional factors which are independent of the standing wave. A technical arrangement proposed by SCOTT [7] can be an example here. In this arrangement the particles are concentrated in the loop or node planes with the use of an intensive standing wave, and the coagulation is due mainly to the ortokinetical effect caused by a perpendicular, sawtooth progressive wave.

The time required to obtain an equilibrium distribution of particles near the stable equilibrium points can be estimated more precisely with the use of Eq. (2.6) which describes the time of travel of a particle from an initial point to a point of coordinate d, i.e. to the border of a given concentration zone. Putting $x_0 = d = \sigma$ we shall estimate the time necessary for establishing an equilibrium distribution of nearly all the particles, excluding those which initially were placed at the distance

from the ustable equilibrium point smaller than σ. Here we shall use the same expansion of the tangent function as previously:

$$t_k = \alpha^{-1}\ln(k\sigma)^{-2} = (2\tau A_D k)^{-1}\ln\frac{2m_p A_D}{k k_B T}. \tag{3.5}$$

For the numerical values assumed in the quantitative discussion at the end of the previous paragraph and for $T = 300$ K we get $t_k \approx 14\alpha^{-1}$. This is the value of the same order of magnitude as the coagulation times obtained above.

References

[1] Е. П. Медников, *Акустическая коагуляция и осаждение аэрозолей, Издательство Наук СССР, Москва 1963.*

[2] H. Czyż, *The aerosol particle drift in a standing wave field, Archiwum Akustyki,* **22**, 3, (1987).

[3] F. Fittipaldi, *Particle coagulation by means of ultrasonics, Acoustica,* **41**, 4, 263–266 (1979).

[4] L. V. King, *On the acoustic radiation pressure on spheres,* Proc. Roy. Soc., A 147, 861, 212–240 (1934).

[5] H. W. St. Clair, *Agglomeration of smoke, fog or dust particles by sonic waves,* Indust. Engng. Chem., **41**, 11, 2434–2438 (1949).

[6] M. Jessel, V. Timochenko, *Sur la dynamique des processus de coagulation acoustique,* C. R. Acad. Sc. Paris, **272**, 1457–1460, (1971).

[7] D. S. Scott, *A new approach to the acoustic conditioning of industrial aerosol emissions,* J. Sound Vib., **34**, 4, 607–619.

Received October 2, 1986.

ARCHIVES OF ACOUSTICS
12, 3–4, 225–242 (1987)

THE ACOUSTIC WAVE GENERATION BY A THIN LAYER WITH VARIABLE TEMPERATURE

ROMAN DYBA, BRONISŁAW ŻÓŁTOGÓRSKI

Telecommunications and Acoustics Institute,
Wrocław Technical University
(Wybrzeże Wyspiańskiego 27, 50–370 Wrocław)

This study considers the problem of the thermal sound generation in the air by an unmoving solid body with a time-variable temperature. Applying the linear relations between the thermal energy stream supplied to a thin layer of a solid body in touch with a gaseous medium and an energy stream of the acoustic wave, and then taking advantage of electrothermo-acoustic analogies, the phenomena of the energy transport were represented in the form of an equivalent linear electric circuit with lumped constants. On the basis of the equivalent circuit, both the properties of the considered thermal source of the acoustic wave were investigated and the problem of thermo-acoustic cooling of the solid body was discussed. It was shown that, in view of the low efficiency of the temperature–pressure conversion, it is necessary to generate large layer temperature changes to obtain the mean values of sound intensity, whereas the maximum of the modulus of the transmittance function of the source occurs even for very thin layers. It was also shown that in the course of cooling of thin layers the amounts of energy: that carried by the acoustic wave and that supplied to the environment as a result of external conduction are comparable, so that in the energy balance of a thin layer with varying temperature, it is necessary to take into account the two factors which bring about an energy loss.

Notation

c_0 sound velocity, $c_0^2 = \gamma P_0/\varrho_0$
c_p specific heat of gas at constant pressure
c_v specific heat of gas at constant volume
c_w specific heat of a solid body layer
C_1 thermal capacity of a solid body layer $C_1 = dgc_w$
d thickness of a solid body layer
g density of a solid body layer
h enthalpy of unit volume of the gaseous medium, the coefficient of the external conduction of a solid body
H transmittance of the thermal source of the acoustic wave $H = \hat{p}/\hat{I}_z$
I efficiency of energy flux in acoustic field
I_z efficiency of the controlled heat flux source
$j = \sqrt{-1}$
k heat conduction coefficient of the solid body

N_p pressure level in $2 \cdot 10^{-5}$ Pa [dB]
p acoustic pressure
P_0 pressure in unperturbed gas
P_r Prandtl number, $P_r = c_p v \varrho \varkappa^{-1}$
R gas constant, $R/\mu = c_p - c_v$
R_1 heat resistance of a solid layer, $R_1 = d/k$
R_2 heat resistance corresponding to external conduction $R_2 = 1/h$
t time
T variable component of the gas temperature
T_0 temperature in unperturbed gas
T_p initial temperature of the cooling solid body
v acoustic velocity
x spatial coordinate distance in the gas from the solid body surface
Z_{ta} thermal-acoustic impedance in the harmonic excitation method, $Z_{ta} = \hat{\theta}/\hat{I}$
$\mathcal{L}\{\cdot\}$, $\mathcal{L}^{-1}\{\cdot\}$ operators of the simple and inverse Laplace transformations
γ adiabate exponent, $\gamma = c_p/c_v$
θ amplitude of the sinusoidally variable temperature of the boundary layer of the gas medium
$\varkappa$ heat conduction coefficient of the gas
Λ $-(d/dt)\ln(T(t)/T_p)$
μ molar mass
ν kinematic viscosity coefficient
ϱ variable component of the total density of the gas medium
ϱ_0 density of the gas medium in an unperturbed state
φ velocity potential $v = \varphi_x$
$\phi(z)$ probability integral, $\phi(z) = \frac{2}{\sqrt{\pi}} \int_0^z e^{-x^2} dx$
ω angular frequency
$(\cdot)' = d/dx(\cdot)$
$(\hat{\cdot})$ complex amplitude in the harmonic excitation method
$(\bar{\cdot})$ Laplace transform of a given time function

1. Introduction

A stationary solid body with the time variable external surface temperature generates an acoustic wave in the surrounding gas medium. The present study carries out a quantitative analysis of the relation between a constant heat flux fed to the body (causing changes in its temperature) and a pressure level, of the generated acoustic wave. The results of this analysis made it possible to determine the fundamental properties of the thermal source of the acoustic wave.

Another problem discussed in the study is related to the above effect – namely that a solid body at a temperature higher than that of the ambient gaseous medium cools faster than results from the classical external conduction, since it gives away part of the energy to the generated acoustic wave (the thermo-acoustic cooling effect). It is justified to neglect the component energy carried out by the acoustic wave for thick layers whose temperature varies slowly in the course of cooling. On the other

hand, the situation changes essentially for thin layers, and the time course of the temperature of such a layer deviates from that expected by the classical analysis of the problem.

To determine the fundamental relations characterizing the thermal source of an acoustic wave, an idealized case was considered, in which a flat layer of a solid body is in contact with a gaseous medium. A time variable heat flux with constant density is supplied to the whole Surface of the layer (Fig. 1). Moreover, the notion of

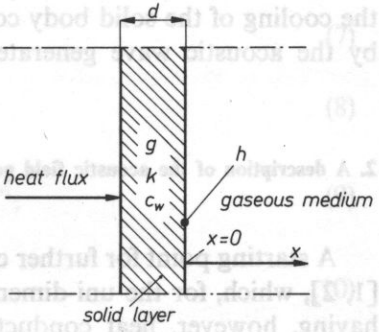

Fig. 1. The cross-section of the thermal source of a plane acoustic wave: d – solid layer thickness, g – solid body density, k – conduction coefficient, c_w – specific heat, h – external conduction coefficient

supplied heat flux denotes a flux penetrating into the solid body, neglecting the problem of the reflection of part of the incident flux (if such a way of energy supply were applied). As a result of temperature changes, the solid layer becomes a source of a plane acoustic wave propagating in the gaseous medium.

The first stage of solving the above problem is to determine the dependence between the time variable temperature on the border of the gaseous medium and the pressure in the generated acoustic wave. This dependence was obtained by solving the hydrodynamics equations with the following boundary condition

$$T(x = 0, t) = f(t), \tag{1}$$

$$v(x = 0, t) = 0, \tag{2}$$

where all these quantities describing the state of the medium are functions of the spatial variable x and the time t, v denotes the particle velocity, T is the temperature and $f(t)$ a function describing temperature changes in the boundary layer of the medium. In analysis of wave phenomena in a gas, a frequently assumed model of the medium, is an ideal gas undergoing no dissipation processes. In the considered problem, such a model is not appropriate, since the assumed boundary conditions (1) and (2) would then be mutually contradictory: they can be satisfied only if one takes into account the heat conduction of the gas and the resultant fact that all the quantities characterizing the acoustic field are expressed by the sums of two components. The two components are the solutions of auxiliary second-order equations, corresponding to the so-called pressure and temperature modes of vibration in the medium (see solutions (12) and (13)).

The value of temperature changes in the surface in contact with the gas depends on the quantity of the supplied heat flux, on the heat capacity of the solid layer, on the value of the external conduction and on the quantity of the load generated by the gaseous medium as a result of energy convection in the generated acoustic wave. Applying electro-thermo-acoustic analogies, the considered processes of energy transport wave represented in the form of a linear component electric circuit with lumped constants. On the basis of the above circuit, both the properties of the considered thermal source of the acoustic wave were investigated and the problem of the cooling of the solid body considered, taking into account the energy convection by the acoustic wave generated in the medium.

2. A description of the acoustic field generated by temperature changes in the stationary boundary layer of the medium

A starting point for further considerations are linearized Navier-Stokes equations [1, 2], which, for the uni-dimensional problem of the thermodynamically ideal gas, having, however, heat conductions and viscosity, are in the form

$$\varrho_t + \varrho_p \cdot v_x = 0, \tag{3}$$

$$v_t + \frac{1}{\varrho_0} \cdot p_x = \frac{4}{3} v_{xx}, \tag{4}$$

$$\varrho_0 c_v T_t - T_0 \frac{R}{\mu} \varrho_t = \varkappa T_{xx}, \tag{5}$$

$$\frac{\mu}{R} p = \varrho_0 T + T_0 \varrho, \tag{6}$$

where ϱ, p and T denote variable components of the total quantities of the density, of pressure and temperature; ϱ_0, P_0 and T_0 are the constant components of these quantities, R is the gas constant ($R/\mu = c_p - c_v$ where c_p and c_v denote respectively the specific heats for constant pressure and constant volume, μ is the molar mass, v is the velocity, $\varkappa$ is the heat conduction coefficient, ν is the kinematic viscosity coefficient. Along with the boundary conditions (1) and (2), the system of equations (3)–(6) makes it possible to determine the relation between temperature changes in the boundary layer of the medium and the quantities describing the generated acoustic field.

A similarly formulated problem was considered by TRILLING [3]. Since the final results of the Trilling study were obtained by the method of approximate determination of the inverse Laplace transformation, there occurs a difference between these results and those obtained by the authors of the present study. Because of the above fact and since the present authors were aware that the problems of the tempeature boundary conditions have quite seldom occurred in the

acoustic literature, it was decided that the solution of the hydrodynamic equations (3)–(6) along with the temperature boundary conditions (1)–(2), should be cited in brief form.

Therefore, let all the quantities characterizing the state of the gas have the form: $a(x, t) = \hat{a}(x)\exp(j\omega t)$, where $\hat{a}(x)$ denotes the complex amplitude of a given quantity, while ω is the angular frequency. After this substitution differential equations with partial derivatives transform into the corresponding simple differential equations connecting complex amplitudes, namely:

$$j\omega\hat{\varrho} + \varrho_0\hat{v}' = 0, \tag{7}$$

$$j\omega\hat{v} + \frac{1}{\varrho_0}\hat{p}' = \frac{4}{3}\nu\hat{v}'', \tag{8}$$

$$j\omega\varrho_0 c_v\hat{T} - j\omega T_0\frac{R}{\mu}\hat{\varrho} = \varkappa\hat{T}'', \tag{9}$$

$$\frac{\mu}{R}\hat{p} = T_0\hat{\varrho} + \varrho_0\hat{T}, \tag{10}$$

where these equations introduced the denotation $(\cdot)' = d/dx(\cdot)$ The above system of equations can be reduced to an equivalent fourth-order differential equation. As $\hat{\varphi}$ denotes the complex amplitude of the velocity potential ($\hat{v} = \hat{\varphi}$), this equation is in the form

$$\frac{\omega^2}{c_0^2}\hat{\varphi} + \left[1 + j\omega\left(\frac{\varkappa}{\varrho_0 c_v c_0^2} + \frac{4}{3}\frac{\nu}{c_0^2}\right)\right]\hat{\varphi}'' - \left(\frac{4}{3}\frac{\varkappa\nu}{\varrho_0 c_v c_0^2} + \frac{\varkappa}{j\omega\varrho_0 c_p}\right)\hat{\varphi}'''' = 0, \tag{11}$$

where $c_0 = \sqrt{\gamma P_0/\varrho_0}$ denotes the sound velocity and $\gamma = c_p/c_v$ is the adiabate exponent.

The characteristic equation corresponding to the differential equation (11) has the form of an algebraic biquadratic equation. The solution of equation (11) can be represented as the sum of the solutions of two second-order equations, each of which corresponds to the pair of roots of the characteristic equation. In determining these roots, simplifications were carried out, taking into account the real values of c_0, $\varkappa$, ν, ϱ_0, P_0 and T_0 for the air in normal conditions and neglecting very low-value components. Despite these simplifications, the obtained final dependencies ensure sufficient accuracy over a very broad frequency range ($\omega < 10^6$). The seconed-order equations obtained by this way and the relations between the complex amplitude of the velocity potential and the complex amplitude of the other quantities characterizing the acoustic field are as follows:

$$\hat{\varphi}'' + \frac{\omega^2}{c_0^2}\hat{\varphi} = -j\frac{4}{3}\omega\nu\frac{\gamma}{c_0^2}\hat{\varphi}'', \tag{12a}$$

$$\hat{v} = \hat{\varrho}', \tag{12b}$$

$$\hat{p} = -j\omega\varrho_0\hat{\varphi}, \tag{12c}$$

$$\hat{\varrho} = -j\omega\varrho_0\frac{1}{c_0^2}\hat{\varphi}, \tag{12d}$$

$$T = -j\omega\frac{1}{c_p}\hat{\varphi}, \tag{12e}$$

and

$$\hat{\varphi}'' - \frac{j\omega\varrho_0 c_p}{\varkappa}\hat{\varphi} = 0, \tag{13a}$$

$$\hat{v} = \hat{\varphi}' \tag{13b}$$

$$\hat{p} = j\omega\varrho_0\left(\frac{4}{3}\varrho_0 v\frac{c_p}{\varkappa} - 1\right)\hat{\varphi}, \tag{13c}$$

$$\hat{\varrho} = -\varrho_0^2\frac{c_p}{\varkappa}\hat{\varphi}, \tag{13d}$$

$$\hat{T} = T_0\varrho_0\frac{c_p}{\varkappa}\hat{\varphi}. \tag{13e}$$

The values of the parameters v and $\varkappa$ are not independent for the medium, and even for numerical studies, it is necessary to take into account their interdependencies. In particular, this interdependence is strong for gases, so that the dimensionless Prandtl number $P_r = c_p v\varrho\varkappa^{-1}$ takes for the most real gases values close to unity. For the air, in normal conditions, $P_r \cong 3/4$, hence, it follows that $\hat{p}$ in equation (13c) is 0 irrespective of the boundary condition and the value of the velocity potential amplitude.

Therefore, the two systems of equations (12) and (13) correspond to two different modes of the medium vibrations – namely, equation (12) corresponds to the pressure mode, equation 13 to the temperature mode.

Limiting below the considerations to the analysis of waves travelling from the source and assuming that $f(t)$ in equation (1) has the form: $f(t) = \theta\exp(j\omega t)$, it is obtained that (see [4])

$$\varphi_{\text{pressure}}(x) = A\exp\left(-j\frac{\omega}{c_0}x\right)\exp\left(-\frac{2}{3}v\gamma\omega^2 c_0^{-3}x\right), \tag{14}$$

$$\varphi_{\text{temp}}(x) = B\exp\left[-\sqrt{\frac{\omega\varrho_0 c_p}{2\varkappa}}\cdot(1+j)\cdot x\right], \tag{15}$$

where the constants A and B determined from the boundary conditions (1)–(2), have

the form

$$A = \frac{\theta}{-j\dfrac{\omega}{c_p} - \dfrac{T_0}{c_0}\sqrt{\dfrac{j\omega\varrho_0 c_p}{\varkappa}}} = -\theta\frac{c_0}{T_0}\sqrt{\frac{\varkappa}{j\omega\varrho_0 c_p}}, \tag{16}$$

$$B = \theta\frac{\varkappa}{T_0\varrho_0 c_p}. \tag{17}$$

From (16), (14), (12b), the pressure wave generated in the medium as a result of forced temperature, is described by the following relation:

$$\frac{\hat{p}}{p_0} = \frac{\theta}{T_0}\cdot\frac{2\gamma}{c_0}\sqrt{\frac{\omega\nu}{3}}\cdot\exp\left[-j\left(\frac{\omega}{c_0}x - \frac{\pi}{4}\right)\right]\cdot\exp\left(-\frac{2}{3}\nu\gamma\omega^2 c_0^{-3}x\right). \tag{18}$$

In dependence (18), the occurring factor $\exp\left[(-2/3)\nu\gamma\omega^2 c_0^3 x\right]$ and the related dissipation coefficient $\alpha = (2/3)\nu\omega^2 c_0^{-3}$ correspond to wave attenuation caused by the presence of dissipation effects in the medium, namely heat conduction and viscosity. In the literature, these two causes of wave energy dissipation were discussed separately (see [14, 15]). Two solutions of the problem of propagation in a viscous medium lead to the Stokes absorption coefficient $\alpha_1 = (2/3)\nu\omega^2 c_0^{-3}$, and in a heat-conducting medium, to the Kirchhoff absorption coefficient $\alpha_2 = \omega^2\varkappa(\gamma-1)/2c_0^3 c_v\varrho_0\gamma$. The total dissipation coefficient is the sum of the above factors: $\alpha_c = \alpha_1 + \alpha_2$. If one considers the relation between ν and $\varkappa$ resulting from $P_r = c_p\nu\varrho\varkappa^{-1} \doteq 3/4$ it can readily be verified that α_c is the same as α gained here by another way.

It follows from dependencies (14) and (15) that velocity potentials, both in the pressure and temperature modes, contain exponential factors corresponding to the decay of both these quantities with increasing distance from the source. In both these modes the dissipation coefficients are given by the dependencies: $\alpha_{\text{pressure}} = \alpha = \frac{2}{3}\nu\gamma\omega^2 c_0^{-3}$, $\alpha_{\text{temperature}} = \sqrt{\dfrac{\omega\varrho_0 c_p}{2\varkappa}}$. Considering the values of the parameters occurring in these two expressions (see the Appendix) it appears that $\alpha_{\text{pressure}} = 3.5\cdot 10^{-13}\omega^2[\text{m}^{-1}]$, while $\alpha_{\text{temperature}} = 155\sqrt{\omega}\,[\text{m}^{-1}]$, therefore, for a very wide temperature frequency range $\alpha_{\text{temp}} \geqslant \alpha_{\text{pres}}$. Hence, the components of particular quantities characterizing the acoustic field related to the temperature mode rapidly decay and are essential only in a region in direct contact with the source, namely in an area where the two modes interact; where the acoustic wave is generated. The above remarks emphasize in addition the difference between these two vibration modes of the medium.

Example 1: The dependence of the the pressure level in the wave in the air on the temperature change amplitude on the boundary

Substitution in formula (18) of the values of the constants characteristic of the air in normal conditions (see the juxtaposition of the constants in the Appendix) gives

$$\hat{p} = 6.38 \cdot 10^{-3}\, \theta \sqrt{\omega} \exp\left[-j\left(\frac{\omega}{c_0}x - \frac{\pi}{4}\right)\right] \exp(-3.5\ 10^{-13}\omega^2 x)\ [\mathrm{Pa}]. \tag{19}$$

It can be seen that the pressure wave is weakly attenuated, and even for $x = 0$ it is shifted in phase by $\pi/4$ with respect to the temperature on the boundary. Neglecting the attenuation and expressing the pressure in decibels with espect to $2 \cdot 10^{-5}$ Pa, it follows directly from dependence (19) that

$$N_p = 58 + 20\log(\sqrt{f}\theta)\mathrm{dB}. \tag{20}$$

To illustrate the value of the pressure level for a given amplitude of temperature changes it was assumed that for $f = 1000$ Hz and $\theta = 1$K. Then, $N_p = 88$dB.

3. The thermo-acoustic impedance

In the case of negligible dissipation effects, the energy flux density in the acoustic field, is given by the dependence [1]:

$$I = \varrho v\left(\frac{v^2}{2} + h\right), \tag{21}$$

where h is the enthalpy of unit volume of the medium. The dissipation effects in a gas with properties close to those of the air are small (see (19)). Because of this, use will be made of dependence (21) and the relation between the pressure and enthalpy of a gas unit volume subject to adiabatic transformation, and also the relation between the pressure and the acoustic velocity of an ordinary plane wave [1, 2], namely

$$h = \frac{c_0}{\gamma - 1}\left(1 + \frac{p}{p_0}\right)^{(\gamma-1)/\gamma}, \tag{22}$$

$$v = \frac{2c_0}{\gamma - 1}\left[\left(1 + \frac{p}{p_0}\right)^{(\gamma-1)/2\gamma} - 1\right]. \tag{23}$$

From relations (21), (22) and (23), with an accuracy up to components of the second order of smallness, it is obtained that

$$I = \frac{c_0}{\gamma - 1}p + \frac{(3\gamma - 1)}{4(\gamma - 1)\varrho_0 c_0}p^2. \tag{24}$$

Considering the $p/P_0 \ll 1$ and applying (18) it is possible to determine the ratio between the complex amplitude of the boundary layer temperature of the gaseous

medium and the complex amplitude of the flux energy in the acoustic wave, namely the thermo-acoustic impedance, i.e.,

$$Z_{ta} \stackrel{df}{=} \frac{\theta}{\hat{I}} = \frac{\gamma-1}{2\gamma}\frac{T_0}{P_0}\sqrt{\frac{3}{\nu}}\frac{1}{\sqrt{\omega}}e^{-j\frac{\pi}{4}} = \frac{Z_0}{\sqrt{\omega}}e^{-j\frac{\pi}{4}}, \tag{25}$$

where

$$Z_0 = [(\gamma-1)/(2\gamma)]\,(T_0/P_0)\sqrt{3/\nu}.$$

The determination of the impedance as a ratio between the temperature amplitude temperature surplus and the energy flux is typical of an electric modelling of heat transport processes. The impedance determined in this way has all the properties of the complex electric impedance; in particular, it is subject to the same rules of series and parallel connections.

It can be seen from the obtained dependence that as the frequency increases, the impedance Z_{ta} decreases, therefore, for a given amplitude of temperature changes at the solid body surface, for increasing frequency, there is an increase in the energy flux carried by the acoustic wave.

4. The electric equivalent circuit of the thermal source of the acoustic wave. The frequency properties of the thermal wave source

The following assignments were made:

– a difference in the potentials in the electric equivalent circuit corresponds to the increase in temperature (i.e., the variable component T of the total temperature), and – the heat flux density corresponds to the electric voltage intensity.

Assuming that the thickness of the solid layer is much thinner than the temperature wavelength in this layer, the electric equivalent circuit of the thermal wave source has the form shown in Fig. 2.

The lumped elements of the circuit are connected with the physical parameters of a solid body and the gaseous medium in the following way:

$R_1 = d/k$ is the heat resistance of a solid layer, where k is the heat conduction coefficient of the solid body, and d is the layer thickness; $C_1 = dgc_w$ is the thermal capacity of the solid body, g is the density of the solid body, c_w is the specific heat of

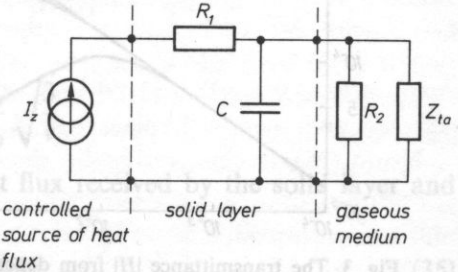

Fig. 2. An electric equivalent circuit of a thermal source working in a steady state at harmonic forcing

the solid body; $R_2 = 1/h$ is a resistance corresponding to the external conduction, and h is the external conduction coefficient; Z_{ta} is the thermo-acoustic impedance, given by dependence (25); I_z is the efficiency of the controlled heat flux source.

The above lumped elements were determined for a solid layer with unit surface.

It can be noted that a consequence of the assumption of the small thickness of the solid layer is the lack of the influence of the heat resistance R_1 on the properties of the considered wave source.

On the basis of the equivalent circuit and dependences (18) and (25), it is easy to determine the transmittance $H = p/I_z$, namely

$$H = \frac{\hat{p}}{\hat{I}_z} = \frac{\gamma/c_0}{1+(h+j\omega dgc_w)Z_{ta}}. \tag{26}$$

Example 2: The frequency properties of the thermal source working in the air

After including in dependencies (25) and (26) the values of the constants (see the Apppendix), the dependence of $|H|$ on the frequency and thickness of the layer is given by the expression

$$|H| = \frac{1.51\cdot 10^{-3}\omega^{0.5}}{\sqrt{10^{10}d^2\omega^2+5.2\cdot 10^4 d\omega^{1.5}+0.135\omega+0.52\omega^{0.5}+1}}. \tag{27}$$

The following conclusions follow from dependence (27):

– for low values of $|H| \sim \sqrt{\omega}$ (H increases proportionally to $\sqrt{\omega}$),

– for large values of $\omega|H| \sim 1/\sqrt{\omega}$ (H decreases proportionally to $1/\sqrt{\omega}$);

– the maximum value $|H|_{\max}$ is proportional to $1/\sqrt{d}$, and – $\omega_{\max} \sim 1/d$, namely the frequency for which there occurs a maximum modulus of the transmittance function, increases in proportion to the inverse of the layer thickness.

Fig. 3 represents the plot of $|H|$ against frequency for a few thickness of the solid layer d.

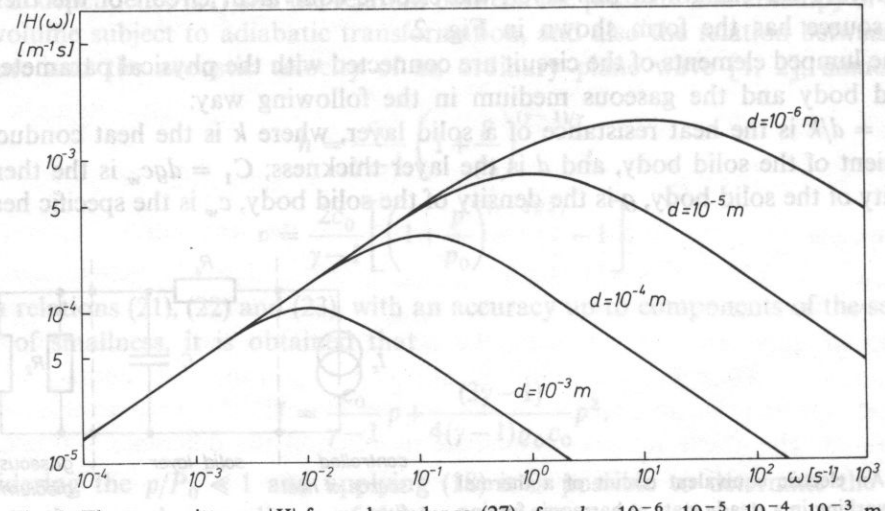

Fig. 3. The transmittance $|H|$ from dependence (27) for $d = 10^{-6}$, 10^{-5}, 10^{-4}, 10^{-3} m.

5. The thermoacoustic cooling effect

Let the heated solid body be in contact with an unbounded gaseous medium, and let the loss of thermal energy be compensated by the external source of energy, so that the temperature of the solid body may be constant at the time of the observation. From the energy balance, it is possible to determine directly the power carried off to the ambient medium by unit surface area for the temperature difference between the solid body and the gaseous medium, namely 1K, i.e. the thermal coefficient of external conduction. If at a certain moment there is a break in the energy supply to the solid body, its temperature begins to decrease. A classical analysis of the phenomenon leads to the conclusion that the surplus of the temperature over the ambient temperature T depends on time in the following way:

$$T(t) = T_1 \exp\left(-\frac{S}{Vgc_w} ht\right),$$

where Vgc_w is the thermal capacity of the solid body, while S is the surface area of the contact with the gaseous medium; moreover, this analysis neglects the thermo-acoustic effect.

Below, the time course of the temperature of the cooling body will be determined, including the effect of energy convection in the form of an acoustic wave. For this purpose, it is more convenient to apply the solutions of the system of equations (3)-(6) obtained by the Laplace transformation method.

If zero-value initial conditions are assumed in the gaseous medium, without any changes it is possible to apply the solutions gained by the method of harmonic input signal; moreover, $j\omega$ will be now replaced by the complex variable s. To distinguish between the operator quantities and the complex amplitudes of quantities which are functions of time, two types of overhead indexes were introduced: ($\hat{\cdot}$) denotes the complex amplitude occurring in the harmonic excitation method, and ($\bar{\cdot}$) represents the Laplace transform of a given quantity.

Connecting equations (24), (28) and (32) it is possible to determine the operator thermo-acoustic impedance an equivalent to the impedance given by formula (25), namely

$$Z_{ta}(s) = \frac{\bar{\theta}(s)}{\bar{I}(s)} = Z_0 \frac{1}{\sqrt{s}}, \tag{34}$$

where

$$Z_0 = \frac{\gamma - 1}{2\gamma} \frac{T_0}{P_0} \sqrt{\frac{3}{\nu}}.$$

Considering the dependence between the heat flux received by the solid layer and changes in its temperature

$$I_{sc} = gdc_w \, dT/dt, \tag{35}$$

where I_{sc} denotes a heat flux assimilated by unit surface area of the solid body, while the operator equivalent circuit for energy transport processes in the thermal source has the form shown in Fig. 4. The additional current source in this diagram with the efficiency $gdc_w T_p$ corresponds to the initial condition related to the initial temperature T_p of the solid body at the time $t = 0$.

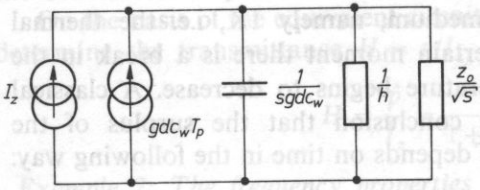

Fig. 4. The operator equivalent circuit of the thermal source of an acoustic wave

An analysis of the electric diagram shown in Fig. 4 makes it possible to determine the operator dependence corresponding to the time course of the temperature of the solid body during cooling after switching off the external source of the heat flux ($I_z = 0$), namely

$$\bar{T}(s) = \frac{T_p}{s + \sqrt{s}/(Z_0 gdc_w) + h/(gdc_w)}. \tag{36}$$

The irrational form of the right side of dependence (36) causes the fact that the methods applied to determine the inverse transform which are usually used in the analysis of electric circuits are here useless.

Certainly, neglecting the energy transport in the form of an acoustic wave (corresponding to the impedance Z_0 taking an infinitely large value), the problem becomes simplified, leading to the well-known solution

$$T(t) = T_p \exp\left(-\frac{h}{gdc_w}t\right). \tag{37}$$

The calculation of the inverse Laplace transform from (36) is made easier by a certain conclusion from Efros theorem [5] which can be written in the following form:

$$\mathscr{L}^{-1}\left\{\frac{1}{\sqrt{s}}A(\sqrt{s})\right\} = \frac{1}{\sqrt{\pi t}}\int_0^\infty a(\tau)\exp\left(-\frac{\tau^2}{4t}\right)d\tau, \tag{38}$$

where $A(s) = \mathscr{L}\{a(t)\}$ and $\mathscr{L}$ and $\mathscr{L}^{-1}$ denote respectively the operators of the ordinary and inverse Laplace transformations.

Using (38), it can readily be shown that

$$\mathscr{L}^{-1}\left\{\frac{1}{\sqrt{s}+a}\right\} = \frac{1}{\sqrt{\pi t}} + a\exp(a^2 t)\,[\phi(a\cdot\sqrt{t}) - 1], \tag{39}$$

where

$$\phi(z) = \frac{2}{\sqrt{\pi}} \int_0^z e^{-x^2} dx,$$

is the so-called probability integral.

Therefore, representing (36) in the form

$$\bar{T}(s)/T_p = 1/[(\sqrt{s}+a_1)(\sqrt{s}+a_2)] = \\ = 1/[(a_2-a_1)(\sqrt{s}+a_1)] - 1/[(a_2-a_1)(\sqrt{s}+a_2)] \tag{40}$$

and applying formula (39), the following formula of $T(t)/T_p$ is obtained:

$$\frac{T(t)}{T_p} = \frac{1}{a_2-a_1}\{a_1 \cdot \exp(a_1^2 t) \cdot [\phi(a_1\sqrt{t})-1] - a_2 \exp(a_2^2 t)[\phi(a_2\sqrt{t})-1]\} \tag{41}$$

in a special case if

$$\Delta = [1/(Z_0 g d c_w)]^2 - 4h/(g d c_w) = 0, \tag{42}$$

the equivalent of dependence (40) becomes

$$\bar{T}(s)/T_p = 1/(\sqrt{s}+a)^2, \tag{43}$$

and the time course is as follows:

$$T(t)/T_p = 2a\sqrt{t}/\sqrt{\pi} + (2a^2 t+1)\exp(a^2 t)[1-\Phi(a\sqrt{t})]. \tag{44}$$

The time course $T(t)$ essentially depends on the layer thickness d; for a certain characteristic thickness $d = d_0$ the discriminent Δ given by dependence (42) takes a zero value and $T(t)$ is given by formula (44). For greater thickness, a_1 and a_2 occurring in (40) and (41) are complex conjugate quantities, and for smaller thickness, a_1 and a_2, are real.

Example 3. The temperature of the solid layer during cooling in the air

Substitution in dependences (41) or (44) of parameters characterizing the air and the solid layer (see the Appendix) gives dependences describing the analyzed relation. For these parameters, the characteristic thickness is $d_0 = 3.35 \cdot 10^{-7}$m. Figs. 5 and 6 represent the temperature $T(t)$ for two layer thicknesses. Each of these figures shows three curves: $T(t)$ from dependence (41) or (44), $T_{cl}(t)$ from dependence (37) and the logarithmic decrement of attenuation $\Lambda = -(d/dt) \ln (T(t)/T_p)$. In the case of the exponential decrease of the temperature takes a constant value independent of time. Therefore, the respective curves obtained from dependences taking into account the thermo-acoustic effect illustrate the quantity of deviation of the temperature of a thin layer on the curve resulting from the classical analysis.

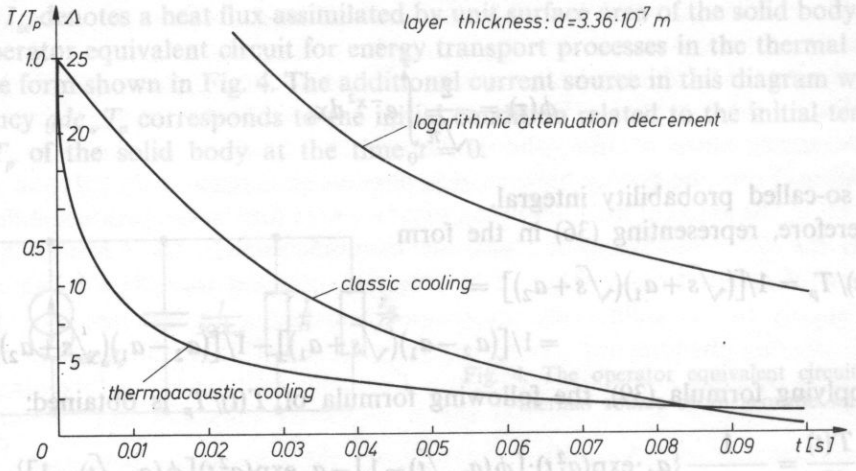

Fig. 5. The plots of $T(t)$ from (41), of T_{cl} from (37) and of Λ for $d = 3.36 \cdot 10^{-6}$m

The following conclusions can be drawn from the results obtained in this case:

(i) $$\bigvee t_c > 0, \text{ that } \bigwedge t \in (0, t_c),\ T(t) < T_{cl}(t),$$

and $$\bigwedge t > t_c,\ T(t) > T_{cl}(t),$$

meaning that initially the thermo-acoustic cooling is faster than classical in view of the convection of part of the energy in the form of an acoustic wave, and then, as a result of heating the medium, and at the same time, of a considerable decrease in the velocity of temperature changes and, hence, a considerable decrease in the

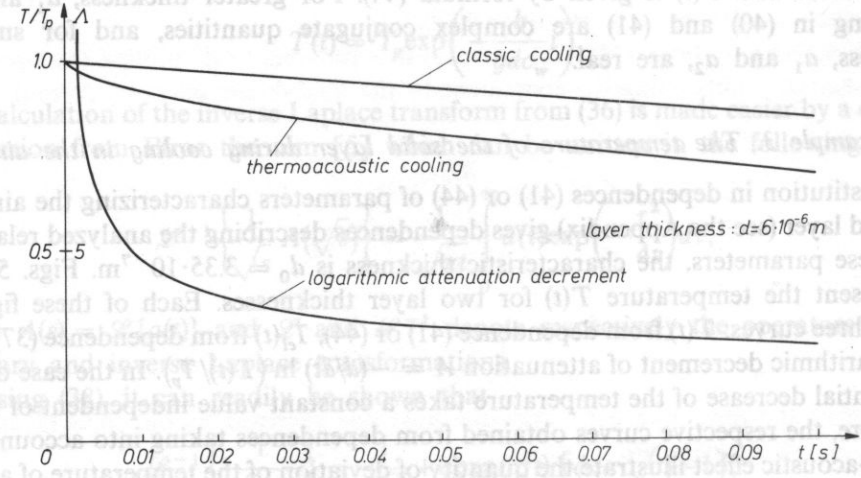

Fig. 6. The plots of $T(t)$, $T_{cl}(t)$ and Λ for $d = 6 \cdot 10^{-6}$m

pressure component in the wave, the thermo-acoustic cooling, from a certain time moment t_c, proceeds more slowly than the classical cooling;

(ii) $$T(0) = T_{cl}(0) = T_p, \lim_{t\to\infty} T(t) = \lim_{t\to\infty} T_{cl}(t) = 0$$

(iii) $$\lim_{t\to\infty} \Lambda = \infty, \lim_{t\to\infty} \Lambda = 0$$

(iv) for greater layer thicknesses $T(t)$ and $T_{cl}(t)$ decrease more slowly and so does the difference between these curves

(v) for $d \gg 1$ $a_{1,2} \cong \sqrt{\dfrac{h}{gdc_w}}$, and dependence (41) becomes (37).

The theory of cooling presented in this chapter is an extention of the classical theory and, as follows from quantitative analysis, the introduced complementation (i.e., considering the energy convection by the acoustic wave) must be included in the analysis of cooling of thin layers. Certainly, the presented problem is not only concerned with the question of cooling of bodies. Additional energy load should be considered for all processes in which the temperature of a solid body immersed in a gaseous medium varies in time.

6. Final conclusions

An inspiration to undertake the analysis presented in this study was an interest in the problem of sound generation by means of nonmechanical methods, i.e., by sources which do not contain moving mechanical elements (see [1, 6, 7, 8]).

One of the possibilities of nonmechanical sound generation is thermal generation. The idea of thermal generation has repeatedly been discussed in the literature [2, 3, 6], and practical examples of the implementation of this method can be: e.g., the pistophone, and the parametric source of the acoustic wave using coherent light absorption ([9], see also [10, 11]).

One of the imaginable models of thermal source of the acoustic wave in a gaseous medium is a solid layer immersed in this medium in which the temperature is a function of time. A separate problem is the question of the implementation of temperature changes. As an example, control of temperature can be performed by using absorption in this layer of light with variable intensity, or the emission of Joule heat by electric current with variable intensity (analogously to the pistophone). In these two cases, energy is supplied by an external source, while cooling is effected by removing energy to the ambient medium.

Another possibility is ensured by the use of the Peltier effect in the metal-semiconductor junction (see, e.g. [12]). Since in this effect, depending on the direction of the flowing currents, the thermal energy is absorbed or emitted, the metal-semiconductor junction is a practical implementation of the source of a heat flux with a variable sign, and the metal layer which forms a connection of two semiconductor

elements of types n and p is heated and cooled in an active way. Moreover, the quantity of the heat flux emitted or absorbed is linearly dependent on the density of the current flowing through the junction for a relatively wide range of this density.

The detailed analysis of the operation of the thermal source, presented in the first part of this study, led to the conclusion that the transmission band of such a transducer was limited by two factors: for low frequencies – by the low efficiency of the temperature-pressure conversion, and for high frequencies – by the heat capacity of the layer. As a consequence of the common effect of these two factors, even for thin layers with thickness of about 10^{-6}m, the transmittance function modulus of the transducer has a maximum for $\omega = 10\text{s}^{-1}$, decreasing for both increasing and decreasing frequencies.

It is difficult to implement practically the electro-thermo-acoustic using the thermo-acoustic effect described above, for the following reasons:

– the unfavourable course of the transmittance of the transducer:

– the necessity of causing large temperature changes of the layer, to gain the mean levels of sound intensity (the low efficiency of the temperature-pressure conversion, resulting from the effect of the stationary boundary condition) and

– the limitation of the current density range for which it is possible to observe the Peltier cooling effect, and also the necessity of using a thin metal cramp linking two semiconductor elements, for which there arises the problem of the surface nonuniformity of the current density distribution in the p-n junction.

The essential result of this study is the construction of a model of the phenomenon of the thermal energy transport in a metal layer, considering the energy carried by the acoustic wave generated in the gaseous medium. In the form of an electric equivalent circuit for harmonic cases, such a model is shown in Fig. 2, and that for pulsed courses and for initial problems, in Fig. 4. In these diagrams, the introduced thermo-acoustic impedance Z_{ta} connects the surplus layer temperature exceeding the ambient temperature with the energy carried by the acoustic wave.

The layer thickness range which can be analyzed within the presented theory is limited. Over the range of greater thickness, this limitation results from the assumed model of the solid body for the heat transport phenomenon in the form of the lumped elements of capacity and resistance. Such a model is valid if the temperature wavelength in the body is much greater than the layer thickness. For pulsed excitation, this limits the maximum variability rate for the analyzed courses. There are no principal barriers against which one could not generalize the results by assuming a solid body model in the form of an adequate system with distributed constants. The low-thickness range is limited by the possibility of applying a macroscopic description of the heat transport in thin layers with atomic thickness.

The above model made it possible to carry out analysis both for the thermal source of the acoustic wave and the other problem discussed in this study, namely the thermo-acoustic cooling effect. The obtained results show that as the thin layer cools the amount of energy carried by the acoustic wave and given away to the ambient medium, as a result of external conduction, are comparable, so that in the

energy balance of a thin layer with variable temperature, it is necessary to include the two factors causing the loss of energy.

The topical nature of the problems verging on thermal studies and acoustics was recently confirmed by a study of GERVAIS [13]. This author concentrated on the problems of the solution of the fundamental Navier-Stokes equations by the harmonic input signal method for plane and cylindrical waves.

The model of the thermal source of the acoustic wave assumed in this study does not always coincide with a real situation. E.g., a solid body can be contact with a gaseous medium on both sides, or energy can be supplied to the solid body in different ways etc. It is, therefore, necessary to modify correspondingly the substitute circuit for the energy processes in the source where, moreover, the basic elements of this basic remain uncharged. Therefore, if one were to consider the cooling of a thin layer by energy radiation to both sides, in the circuit and the respective dependencies, it is sufficient to replace the layer thickness by $d/2$ to obtain a correct description of the phenomenon.

Appendix

In numerical examples illustrating the obtained results, the following values of the constants characteristic of the air in normal conditions were applied:

$$P_0 = 1.018 \cdot 10^5 \mathrm{Nm}^{-2},\ T_0 = 293\mathrm{K},\ \varrho_0 = 1.205\mathrm{kgm}^{-3}$$

$$c_0 = 344\mathrm{ms}^{-1},\ \gamma = 1.4,\ \frac{R}{\mu} = \frac{P_0}{\varrho_0 T_0} = 288.33 = c_p - c_v$$

$$c_p = 1009.16\mathrm{Jkg}^{-1}\mathrm{K}^{-1},\ c_v = 720.83\mathrm{Jkg}^{-1}\mathrm{K}^{-1},\ R = 8.36\mathrm{JK}^{-1}$$

$$\mu = 0.029\ \mathrm{kg\ mol}^{-1},\ \varkappa = 0.049\mathrm{mkgK}^{-1}s^{-3},\ \nu = 1.53 \cdot 10^{-5}\mathrm{m}^2\mathrm{s}^{-1}$$

In turn for the solid body, constants close to the parameters of a metal were assumed, namely

$$g = 5 \cdot 10^3 \mathrm{kgm}^{-3},\ k = 10^2 \mathrm{Jm}^{-1}\mathrm{s}^{-1}\mathrm{K}^{-1},\ c_w = 3 \cdot 10^2 \mathrm{Jkg}^{-1}\mathrm{K}^{-1},\ h = 15\ \mathrm{Wm}^{-2}\mathrm{K}^{-1}.$$

References

[1] L. K. ZAREMBO, V. A. KRASILNIKOV, *Vvedenie v nielinejnuju akustiku*, Izd. Nauka, Moskva 1966.

[2] P. M. MORSE, K. U. INGARD, *Theoretical acoustics*, Mc Graw Hill Book Co. New York 1968.

[3] L. TRILLING, *On thermally induced sound fields*, Journ. of the Acoustic Soc. of America, **27**, 3, 425–431 (1955).

[4] R. DYBA, B. ŻÓŁTOGÓRSKI, *Thermal boundary condition for linearized Navier-Stokes equations*, 11th ICA, Paris 1983, vol. 2, 27–30.

[5] J. OSIOWSKI, *An outline of operator calculus* (in Polish), WNT, Warsaw 1972, p. 165.

[6] H. M. MERKLINGER, *On nonlinear and thermal acoustic sources*, Abstract of the 7th International Symp. on Nonlinear Acoust., Backsburg 1976.

[7] K. RATHMAN, *Influence of velocity slip and temperature jump in rarefied gas acoustic oscillations in cylindrical tubes*, Journ. of Sound and Vibr., **103** 3, 448–452 (1985).

[8] J. S. TOMAR, A. K. GUPTA, *Effect of thermal gradient on frequencies of an orthotropic rectangular plate whose thickness varies in two directions*, Journ. of Sound and Vibr., **98**, 2, 257–262 (1985).

[9] T. G. MUIR, C. R. GULBERTSON, J. R. CLYNCH, *Experiments on thermoacoustic array with laser excitation*, Journ. of the Acoustic Soc. of America, **59**, 4, 735–742 (1976).

[10] A. M. AINDROW, R. J. DEWHURST, D. A. HUTCHINS, S. B. PALMER, *Laser-generated pluses at free metal surfaces*, J. Acoust. Soc. Am., **69**, 449–455 (1981).

[11] R. J. DEWHURST, D. A. HUTCHINS, S. B. PALMER, C. B. SCRUBY, *Quantitative measurements of laser-generated acoustic wave forms*, J. Appl. Phys., **53**, 4064–4071 (1982).

[12] A. F. IOFFE, *Semiconductor thermoelements and thermoelectric cooling*. Infosearch Ltd., London 1975.

[13] Y. GERVAIS, *Le generation de bruit par conduction thermique*, Acustica, **59**, 3, 199–205 (1986).

[14] I. MALECKI, *Physical foundations of technical Acoustics*, Pergamon Press, PWN, Warszawa 1969.

[15] R. WYRZYKOWSKI, *Linear theory of acoustic field of gaseous media* (in Polish), Rzeszów Society of the Friends of Sciences, Rzeszów 1972.

Received December 17, 1986.

ARCHIVES OF ACOUSTICS
12, 3-4, 243-250 (1987)

MEASUREMENTS OF THE RAYLEIGH WAVE PROPAGATION VELOCITY IN THE POLYMER LAYERS

ZENOBIA KRZEŚNIAK, JERZY RANACHOWSKI, JADWIGA RZESZOTARSKA

Institute of Fundamental Technological Research Polish Academy of Sciences
(00-049 Warszawa, Świętokrzyska 21)

ZDZISŁAW JAKUBCZYK

Institute of Physics, Silesian Univ. of Technology
(44-100 Gliwice, Bolesława Krzywoustego 2)

In the paper are presented the results of measurements of the Rayleigh wave propagation velocity in the polyvinyl carbazole (PCV), polyvinyl carbazole with trinitrofluorenon (PVC-TNF) and their halogen derivatives. The correlation relationship between the activation energy of the investigated compounds and the linear combination of the squares of longitudinal and transverse ultrasonic wave velocity was found to be linear.

1. Introduction

The paper deals with the measurements of surface wave propagation velocity in the layers of PVC, PVC-TNF and their halogen derivatives.

Because of the interesting and promising properties of the polymers from the point of view of electronical applications, they are the object of interest of numerous scientific centres [2, 4, 9, 12, 13, 14]. Although a lot of information about polymers has been gathered, the trials to construct their theoretical model which would be capable of describing their experimentally observed electrical properties failed. Attempts are made of describing the mechanisms of carriers generation and transport in polymers with the models worked out for inorganic semiconductors. The assumption that lies in the basis of many such concepts, as the band or excitation model, is the existence of long range interactions. In numerous polymers which are amorphous or exhibit low level of crystallization the long range is found only in one direction. Nevertheless, the examples are known in which the band structure can be present in amorphic solids and where the exciton concept is also

valid for polymers [13, 14]. It is understood that such application of notions which were introduced for crystalline materials is only the first approximation and it can not be applied without criticism. It is an experimentally verified fact that in semiconducting polymers the electron type, and not ionic type conduction takes place [12].

The phenomena, observed in polymers, concerned with the mechanisms of carrier generation and transport are similar to those observed in amorphous semiconductors [2, 3, 4] and perhaps will be described by the same relationships. Elaboration of a uniform model for polymers which would fully explain these phenomena is difficult for several reasons. Organic polymer semiconductors form a large group of materials. Most generally they can be divided into activated and nonactivated polymers, while further distinction can be made into optically activated (by adding a dye) and chemically activated (by forming donor-acceptor complexes also named charge-transfer complexes) [13]. Experimental data obtained by various authors differ what is probably caused by technologically different preparation of samples. As it has been found, not only the chemical modification impurities or structural defects influence the result, but also physical conditions (e.g. atmospheric conditions) during the preparation of samples and measurements [12, 4].

In spite of the above mentioned significant influence of many factors on the results of electrical experiments on polymers, decision has been made to introduce acoustic methods into the investigations of electrical properties of these materials. An encouraging circumstance was that in the case of inorganic semiconductors in which an electron type conduction is observed a linear relationship occurs between the energetic gap width and the acoustic field parameters [5, 11]. The aim of the present paper is an attempt to find out if similar relationship hold for inorganic semiconductors. The experimental investigations indicated that such linear correlation relationship exists for the tested polymers.

2. Experiment

2.1. Measurement samples

Experiments were carried out on polyvinyl carbazole (PVC) – Fig. 1 and its compounds. The halogen derivatives of PVC were obtained with two methods. The first method was to introduce a halogen to the monomer ring and then to polymerize it. The second consisted in introducing a substituent to the PVC available in the market. The substitution reaction and the radical polimerization was carried out in solutions. The 1:1 molar ratio charge transfer complexes (CT) were obtained by mixing the equimolar volumes of the solutions of the donor (PVC and it's halogen derivatives) and the acceptor (trinitrofluorenon TNF).

Acoustical methods gained a number of applications in testing of the properties of media, with the use of these methods also the electrical properties correlated with

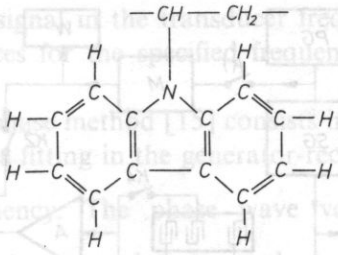

Fig. 1. Chemical formula of the polyvinyl carbazole PVC

the elastic waves propagation constants were investigated [1]. The condition for using the volumetric wave in the experiments is obtaining the samples of dimensions 15mm × 5mm × 5mm, adequately homogeneous and free from porosity and cracks. This condition turned out to be unsatisfiable, because the samples were obtained by pouring out the solution of the compound and letting the solver evaporate slowly. Hence the necessity arose to restrict the measurements to thin layers and to apply the surface waves in the tests [1, 8].

Accounting for the fact that the investigated polymers (PVC compounds) do not exhibit piezoelectric properties, it has been necessary to choose the substrate in which generation, propagation and receiving surface waves would be possible. The quartz slabs of Y cut have been applied. The system of transducers was formed with the photolithographical method. Nine interdigital transducers were used (three for each frequency), which generated the surface waves of basic frequencies: 27 MHz, 52 MHz and 63 MHz. The polymer layer was poured out on the substrate prepared in this way. After measuring surface wave velocity for a given layer thickness the next layer was applied. Every time the polymer was applied and the solver evaporated, the assembly was held at a temperature of about 423K to remove the solver. Thicknesses of the layers ranged between 1 μm and 25 μm.

2.2. Measuring technique

Rayleigh wave propagation velocity in the samples was measured with the following methods:

- pulse method,
- phase-interference method,
- zero phase method.

Measurement of using pulse method allows for measuring group velocity. The block diagram of the measuring set has been displayed in Fig. 2. The value of the surface wave velocity has been calculated as a ratio of distance and pulse propagation time between transducers. The time was found by comparison with the period of a rectangular pulse generator. The distance between transducers was measured with the toolroom microscope, with the accuracy of ± 1μm.

The phase interference method [6, 15] consists in measuring the frequencies of

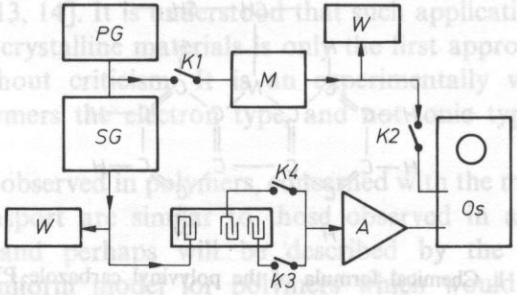

Fig. 2. The block of the measuring set. *SG* – signal generator, *PG* – pulse generator, *M* – modulator, *W* – wavemeter, *A* – amplifier, *Os* – oscilloscope

phase coincidencies in the transmitted frequency band of the interdigital transducers. The frequency band of a symmetrical interdigital transducer is:

$$\Delta f = \frac{f_0}{N_0},$$

where N_0 – number of pairs of electrodes, f_0 – resonance frequency.
The highest frequency of the band equals

$$f_g = f_0 + \frac{\Delta f}{2} = f_0 \frac{2N_0 + 1}{2N_0},$$

If the distance between the centres of the transducers is L, then at resonance the number of wave lengths fitting into this distance is $L/\lambda_m = m_0$. The lowest frequency of the band will be:

$$m_0 + \Delta m = \frac{L}{\lambda_0} + \Delta m.$$

Wave length for this frequency equals:

$$\lambda = \frac{L}{m_0 + \Delta m} = \frac{V_f}{f_g} \frac{2N_0}{2N_0 + 1}.$$

After elementary transformations we obtain:

$$\Delta m = \frac{L}{2N_0 \cdot \lambda_0}.$$

Because $N_0 \lambda_0$ is the transducer width, and under the assumption that L is equal to the doubled width, we have $\Delta m = 1$.

Generally speaking, if

$$N < \Delta m < N + 1$$

where N is a natural number, then there can be $2N + 1$ phase coincidence between

the generated and received signal in the transducer frequency band. Knowing the number of phase coincidences for the specified frequency, we can find the phase velocity for this frequency.

The concept of the zero phase method [15] consists in finding the changes of the complete surface wavelengths fitting in the generator-receiver distance for changing the excitation signal frequency. The phase wave velocity is $v = \frac{L\Delta f}{nL}$, where L – distance between transducers, and n – number of phase changes by 2π for frequency change of Δf.

2.3. Results of the measurements and their discussion

The investigated layer system consists of two materials with different elastic properties; therefore the velocity dispersion phenomenon takes place in this system. For a change in wave frequency or layer thickness the phase and group velocity changes can be observed then. From the theory of layer systems [1, 14] it follows that of the layer „loads" the substrate, i.e. if the elasticity coefficients of the layer are smaller than those of the substrate, then for growing frequency f and layer thickness h the value of the surface wave velocity v_R decreases from its value in the substrate to the value in the layer. It follows from the fact that the acoustic surface wave is a wave which vanishes in the distance of several wave lengths from the free surface of the material in which it propagates. If the layer is thick enough, the major part of the acoustic field energy is transmitted by the layer, which then determines the properties of the field.

The phase and group velocity dispersion has been measured for the two first modes of a surface wave for six polymer compounds (PVC and it's derivatives). The results are shown in the Table 1.

Table 1. Acoustic wave velocities for the investigated compounds [11]

Compound	C_R [m/s]	C_t	C_l
PVK	2600	2810	5135
PVK-Br_2	2890	3120	5763
PVK-Cl_2	2850	3065	5906
PVK-TNF	2535	2890	4120
PVKBr_2-TNF	2730	3020	4746
PVKCl_2-TNF	2645	2900	4767

The example dispersion characteristic for the first mode of the surface wave for a PVC-TNF compound is shown in Fig. 3.

It is known from the literature [1, 8] that in the case where the layer „loads" the

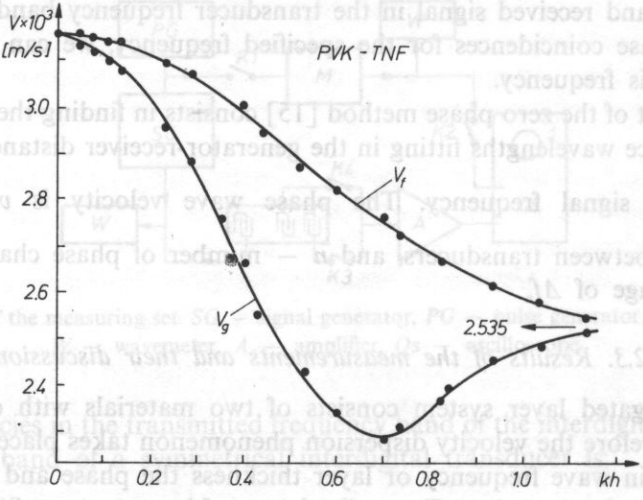

Fig. 3. Dispersion characteristic of the tested layer systems

substrate, for $kh \to \infty \left(k = \frac{2\pi f}{v_R} \right)$ the velocity of higher order modes of the surface wave tends asymptotically to the transverse wave velocity in the material of the layer. Furthermore it is known that together with the frequency growth, the displacement amplitudes of particles vanish slower for higher modes, what for the given layer thickness gives slower decay of the amplitudes of signals resulting from these modes. This makes it possible to measure the dispersion of higher modes for large layer thicknesses and to measure the transverse wave velocity for the materials of layers.

If the Rayleigh wave velocity v_R and transverse wave velocity v_t is known for the given compound, the logitudinal wave velocity v_l can be found from the known Rayleigh formula

$$\left[2-\left(\frac{V_R}{V_t}\right)^2\right]^2 = 4\left[1-\left(\frac{V_R}{V_1}\right)^2\right]^{1/2}\left[1-\left(\frac{V_R}{V_t}\right)^2\right]^{1/2}.$$

The velocity values found for the compounds under investigation are listed in the last column of Table 1.

In the papers [5, 10] it has been demonstrated that exists a relation between the width of the energetic gap E_g and the ultrasound wave velocity in the inorganic semiconductors of various types. Such relation has also been demonstrated for the conducting glasses. In the case of inorganic semiconductors the linear relation between the energetic gap width and the linear combination of the squares of propagation velocities has been obtained for the compounds having one type of bondings [10].

Conducting polymers characterize themselves by a far more complex structure and more diverse conduction mechanisms. The electrical properties of the investiga-

Table 2. Activation energies of the investigated compounds [7]

Compound	Voltage [V]	Activation energy [eV]
PVK	50	0.2
PVK-TNF	50	0.66 ± 0.04 0.17 ± 0.06
$PVKBr_2$-TNF	50	0.92 ± 0.04 0.31 ± 0.06
$PVKCl_2$-TNF	50	0.64 ± 0.05 0.63 ± 0.05
$PVKBr_2$	50	0.32
$PVKCl_2$	50	0.2 0.65 0.12

ted compounds have been presented in the paper [7]. The common feature of the majority of polymers is the activated character of conduction. This is concerned with the necessity of providing sufficient energy for releasing the charge carrying complex. On the basis of the results of activation energy measurements with the use of electrical methods [7] (Table 2) and ultrasonic waves propagation velocity, it has been demonstrated that there exists a linear correlation relationship between the activation energy and the propagation velocity for the investigated group of polymers (Fig. 4), similarly as in the case of inorganic semiconductors [5, 10].

The inorganic compounds exhibited the electron type conduction. It has been stated then, that the compounds of similar ionity of bondings formed straight lines in the plane $(V_L^2 - 4/3V_t^2) \times 10^6 [m^2/s^2]$, E_g while the compounds with different bonding ionity formed different lines. Nevertheless, the type of the relation was always linear. As it has been mentioned previously, the above described polymer

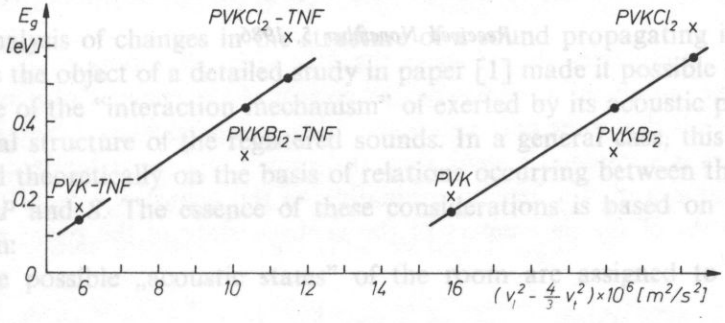

Fig. 4. Relationship between the activation energy and ultrasound wave velocities for the investigated compounds. The mapping of the abscissa into the ordinate shown in the figure with the three points has been linearly approximated with the least squares method

compounds have had the similar properties: PVC and it's halogen derivatives form one straight line in the plane $(V_l^2 - 4/3\,V_t^2) \times 10^6 [m^2/s^2]$, E_g while the PVC-TNF and it's halogen derivatives form another line.

The question arises, if a conclusion about the electron type conduction in the investigated polymers made on the basis of the observed linear correlation relationships is justified, similarly to the case of inorganic semiconductors. The presented results do not allow to answer this question in a unique way, without carrying out some further studies.

References

[1] G. W. FARNELL, E. L. ADLER, *Physical Acoustics*, [ed] W. P. Mason vol. IX, Academic Press 1972.

[2] H. FRITSCHE, *Electronic and structural properties of Amorphous Semiconductors*, Academic Press 1973.

[3] C. H. GRIFFITHS, A. van LACKEN, J. Polym. Sci., **14**, 1433 (1976).

[4] C. H. GRIFFITHS, K. OKUMARA, A. van LACKEN, J. Polym. Sci., **15**, 1627 (1977).

[5] V. L. GUREWICZ, I. V. POGORELSKIJ, Z. Eksp. Teor. Fiz., **25**, 566 (1977).

[6] Z. JAKUBCZYK, Ph. D. thesis, (in Polish), IFTR PAS (1984).

[7] Z. KRZEŚNIAK, J. RANACHOWSKI, J. RZESZOTARSKA, Electric conduction of the chosen PVC compounds, (in Polish), IFTR Reports, (1978).

[8] W. P. MASON, Physical acoustics, vol. VI, Academic Press 1967.

[9] R. M. MEHRA, P. C. MATHUR, A. K. KATHURICA, R. SHYAN, J. Phys. Chem., **39**, 295 (1978).

[10] L. OPILSKA, A. OPILSKI, Physica Status Solidii, **35**, K138 (1976).

[11] A. OPILSKI, *Influence of the surface states on the ultra and hypersound wave in semiconductors*, (in Polish), Habilitation thesis, Silesian University of Technology, (1974).

[12] K. PIGOŃ, K. GUMIŃSKI, J. VETULANI, *Organic Semiconductors* (in Polish), WNT, Warsaw 1964, pp. 47, 49, 70–71.

[13] P. J. REUCROFT, *Photoconduction mechanisms in polymeric solids*, Photocond. Polym. [ed] Patsis, Westport Conn. 1976.

[14] P. J. REUCROFT, *Photocurvier generation mechanisms in polymers*, Photocond. Polym. [ed] Patsis, Westport Conn. 1978.

[15] J. WEHR, *Measurement of velocity and damping of ultrasound waves*, (in Polish), PWN, Warsaw 1972.

Received November 5, 1986.

ARCHIVES OF ACOUSTICS
12, 3–4, 251–272 (1987)

THE PROBLEM OF CHANGES IN THE STRUCTURE OF A SOUND PROPAGATING IN A ROOM IN THE ASPECT OF MULTIDIMENSIONAL SPACE

EDWARD OZIMEK

The Acoustics Institute of A. Mickiewicz University
(ul. Matejki 48/49, 60–769 Poznań)

A change in the amplitude-frequency structure of sound in a room is a complex physical phenomenon depending on a number of acoustic properties of the interior. The essence of this change consists in the influence of the acoustic parameters of the room on the spectral-temporal course of the sound propagating in it.

The starting point of the undertaken studies was to represent the changes in the sound structure in the room based on the relations occurring between the elements of two sets, P and S. All the possible acoustic states of the room were subordinated to the elements of the set P, thus gaining the so-called space of states. On the other hand, all the possible changes in the sound structure were subordinated to the elements of the set S, thus achieving the so-called space of the signal structure. Analysis of the relation occurring between these two spaces showed that physical changes in the sound structure in a room could be mapped in a space of subjective sensations with coordinates being the corresponding psychoacoustic quantities. Such a mapping can be an important step towards the determination of the common plane of objective and subjective evaluations of the acoustic quality of a room, which is still looked for in the problems of room acoustics.

1. Introduction

The analysis of changes in the structure of a sound propagating in a room (1), which was the object of a detailed study in paper [1] made it possible to gain better knowledge of the "interaction mechanism" of exerted by its acoustic parameters on the spectral structure of the registered sounds. In a general case, this effect can be considered theoretically on the basis of relations occurring between the elements of two sets, P and S. The essence of these considerations is based on the following conception:

All the possible „acoustic states" of the room are assigned to the elements

(1) The notion of changes in the sound structure in a room is understood to be a change of the value of the physical parameters of this sound caused by the acoustic properties of the interior.

$p_1, p_2, \ldots, p_r$ of the set P [2]. The notion of the acoustic state of a given room is understood to mean a set of real numbers $x_1, x_2, \ldots, x_n$ (namely, the values of the parameters of the state) describing its acoustic properties.

All the possible changes in the sound structure related to particular acoustic states of the room can be assigned to the elements $s_1, s_2, \ldots, s_r$ of the set S. Let the character and the form of these changes be determined by the set of real numbers $y_1, y_2, \ldots, y_n$. On the other hand, the function F connecting each element of the set S with an element of the set P describes in quantitative terms changes in the signal structure which occur for a given acoustic state of the room. If it were possible to assume that these sets are equivalent, it would then be possible to predict, on the one hand, the character of changes in the sound structure for known values of the parameters of an acoustic state, or, also, on the other hand, to evaluate its acoustic properties on the basis of measurements of the quantity of changes in the sound structure registered in this room. However, in practice this problem is a very complex one, above all because of the difficulties in determining the set of all possible acoustic states of the room and the set of the occurring changes in the signal, and in determining the one-to-one and only one-to-one relation between these sets. So far it has not been considered in this approach in the literature.

Considering this problem, the present study consists of two principal parts. The first contains theoretical considerations, involving a certain conception of the representation of changes in the sound structure in a room in the aspect of a multidimensional space. An attempt was made to use this conception in the other part of this study, representing the results of initial experimental studies in a simplified three-dimensional space of changes in the spectral structure of the transient courses of chosen speech sounds propagating in the room.

2. The space of the acoustic states of the room

As was mentioned above, the acoustic state of a room can be defined by giving a set of the values of certain parameters $x_i (i = 1, 2, \ldots, n)$, describing its acoustic properties.

This set of parameters should meet the following assumptions.

An arbitrary parameter x_i can vary irrespective of the changes of parameter x_k $(i \neq k)$. This means that these parameters should be independent variables. The set of such parameters is a minimal system, since it does not contain redundant elements, which are insignificant in a general evaluation of the acoustic state of the room. Moreover, the set of the parameters of the acoustic state of the room should be complete.

---

[2] In this study it is assumed that a given room can take different so-called "acoustic states", as a result, e.g., of applying appropriate acoustic adaptations, various ways of its being filled by the audience etc.

As the set of the three numbers x_1, x_2, x_3 can be considered as a vector given in a three-dimensional space, so, analogously, the set of n numbers $x_1, x_2, \ldots, x_n$, can be considered a vector in a n-dimensional space ([3]). This means that the acoustic state of the room can be regarded as a vector quantity pre-determined in a n-dimensional space of states, namely that a certain point in this space corresponds to each acoustic state of the room. Let us now consider what relations occur between the elements of this space. Let us consider the two acoustic states of the room, p_l and p_m, and determine the difference between them. Since two points in a n-dimensional space correspond to these states, the determination of the difference between these states is reduced to the estimation of the distance $d(p_l, p_m)$ between these points, which, in a n-dimensional space, is expressed by the following formula

$$d(p_l, p_m) = \sqrt{\sum_{i=1}^{n} (x_i^{(l)} - x_i^{(m)})^2}. \tag{1}$$

Thus, this gives a distance which is a function which subordinates to each pair of elements (states) p_l and p_m of the set P a certain positive number $d(p_l/p_m)$. This set is called the metric space, while the function $d(p_l, p_m)$ defines the metric of this space.

Formula (1) can also be written in a more general form, in the following form:

$$d_k(p_l, p_m) = \sqrt[k]{\sum_{i=1}^{n} |x_i^{(l)} - x_i^{(m)}|^k}, \tag{2}$$

where $k = 1, 2, 3, \ldots$

If $k = 2$, formula (2) is obtained for, on the other hand, , $k = 1$

$$d(p_l, p_m) = \sum_{i=1}^{n} |x_i^{(l)} - x_i^{(m)}|.$$

Assuming that the value of the coefficient $k \to \infty$, it can be seen that the estimation of the distance between the points (acoustic states of the room) is basically reduced to the determination of the difference between the coordinates of just one, with axis of the n-dimensional space, along which these points are farthest each other, namely

$$d_\infty(p_l, p_m) \to \max |x_i^{(l)} - x_i^{(m)}|, \tag{3}$$

where $i = 1, 2, \ldots, n$.

The difference between two acoustic states of a room can also be evaluated on the basis of the value of the angle between the state vectors $\boldsymbol{p}_l$ and $\boldsymbol{p}_m$.

Since the scalar product of two state vectors is equal to

$$\boldsymbol{p}_l \cdot \boldsymbol{p}_m = x_1^{(l)} \cdot x_1^{(m)} + x_2^{(l)} \cdot x_2^{(m)} + \ldots + x_n^{(l)} \cdot x_n^{(m)} = |\boldsymbol{p}_l||\boldsymbol{p}_m| \cos\varphi,$$

([3]) The notion of space is understood to be a set of arbitrary elements between which certain geometrical relations were established.

hence

$$\cos\varphi = \frac{x_1^{(l)} \cdot x_1^{(m)} + x_2^{(l)} \cdot x_2^{(m)} + \ldots + x_n^{(l)} \cdot x_n^{(m)}}{\sqrt{\sum_{i=1}^{n} (x_i^{(l)})^2} \sqrt{\sum_{i=1}^{n} (x_i^{(m)})^2}}. \tag{4}$$

According to formula (4), the greater the value of $\cos\varphi$, the smaller the difference between two acoustic states of the room. The extension of the set of points (the acoustic state of the room) in the considered the n-dimensional space can be expressed by means of the variance σ_d^2 in the following form

$$\sigma_d^2 = \sum_{i=1}^{n} \frac{1}{z} \sum_{i=1}^{z} (x_i^{(l)} - \overline{x_i^{(l)}})^2 = \sum_{i=1}^{n} \delta_i^2,$$

where δ_i – is the standard deviation.

It can be seen that for a pre-determined i, this variance is the sum of the squares of the distances of all points from their common "centre of gravity", determined by an average divided by the number of points, from the n-dimensional space.

The set of acoustic states of a room, expressed by points in a n-dimensional space, can be arranged in a certain way by introducing the notion of the state vector length and the angle between these vectors. As was mentioned previously, each vector of the state $\boldsymbol{p}$, with the coordinates $(x_1, x_2, \ldots, x_n)$, defines the position of the point P in a n-dimensional space with respect to the initial point P_0 with the coordinates $(0, 0, \ldots)$, to which, e.g., the standard acoustic state of the room can be assigned. Therefore, the length of the vector $\boldsymbol{p}$ is, e.g., the number $p \geqslant 0$ determining the distance between the points P_0 and P_m. According to formula (1), this distance can be expressed in the form:

$$d(p_0, p_m) = |\boldsymbol{p}_m| = \sqrt{\sum_{i=1}^{n} (x_i^{(m)})^2}. \tag{5}$$

Applying in turn formulae (2) and (3), one can obtain formula (6), from which it follows that the measure of the length of this vector is its projection with the highest value

$$d_k(p_0, p_m) = |\boldsymbol{p}_m| = \sqrt[k]{\sum_{i=1}^{n} (x_i^{(m)})^k} = \max|x_i^{(m)}|, \tag{6}$$

for $k \to \infty$

3. The space of the acoustic signal structure

In a general case, it can be assumed that the set of resultant changes in the acoustic signal structure is a mapping of the set of acoustic states of the room. It was already mentioned previously that a point in a n-dimensional space of the structure can be subordinated to each change in the signal structure, and it is

possible to subordinate each point in a n-dimensional space of states to each acoustic state of the room. To determine exactly the „interaction mechanism" of acoustic parameters of the room and the form of the signal, the mapping of the space of the acoustic states of the room and the space of the structure of the signal must be on a one-to-one basis, i.e., only one point in the space of the signal structure should correspond to each point in the space of states. Assuming the similarity between the features of the space of states and that of the signal structure, in analyzing the features of the space of the signal structure, it is possible to apply the formulae given in chapter 1, changing only the physical sense of some of the notation. On the other hand, it should be borne in mind that then these formulae would describe changes in the sound structure only for the steady state, where it can be assumed that these changes are only static in nature. For this state

$$ds_l/dt = 0 \quad \text{where} \quad s_l = [y_1^{(l)}(x_i^{(l)}),\ y_2^{(l)}(x_i^{(l)}),\ \ldots,\ y_n^{(l)}(x_i^{(l)})]$$
$$ds_l = \frac{\partial s_l}{\partial y_1^{(l)}} dy_1^{(l)} + \frac{\partial s_l}{\partial y_2^{(l)}} dy_2^{(l)} + \ldots + \frac{\partial s_l}{\partial y_n^{(l)}} dy_n^{(l)}; \quad l = 1, 2, \ldots, r, \tag{7}$$

where

$$dy_i^{(l)} = \frac{\partial y_i^{(l)}}{\partial x_1^{(l)}} dx_1^{(l)} + \frac{\partial y_i^{(l)}}{\partial x_2^{(l)}} dx_2^{(l)} + \ldots + \frac{\partial y_i^{(l)}}{\partial x_n^{(l)}} dx_n^{(l)}; \quad i = 1, 2, \ldots, n.$$

On the other hand, in transient states of sound, namely in their growths or decays, the representation of changes in the signal structure in a n-dimensional space becomes much more complex in view of the nonstationary character of this process. It is then that it is necessary to assume the dynamic character of these variations, related to the time-continuous change in the position of the vector s_l in a n-dimensional space. In a mathematical approach, this could be expressed in the following way,

$$\frac{ds_l}{dt} = \frac{\partial s_l}{\partial t} + \frac{\partial s_l}{\partial y_1^{(l)}} \frac{\partial y_1^{(l)}}{\partial t} + \frac{\partial s_l}{\partial y_2^{(1)}} \frac{\partial y_2^{(l)}}{\partial t} + \ldots + \frac{\partial s_l}{\partial y_n^{(l)}} \frac{\partial y_l^{(n)}}{\partial t}, \tag{8}$$

Therefore to determine the rate of change in signal structure in its transient state, it is necessary to known the already present change at the moment t and the change at the moment $t+dt$ expressed by the vector $s+ds$, with the coordinates $(y_1+dy_1,\ y_2+dy_2,\ \ldots,\ y_n+dy_n)$. For a finite time increment Δt, the change in the value of the parameters in the signal structure $y_i = y_i(t)$ can, from formula (2), be also expressed in the following way:

$$\Delta d_2(t) = \sqrt{\sum_{i=1}^{n} [y_i(t+\Delta t) - y_i(t)]^2}, \tag{9}$$

where

$$\Delta y_i = y_i(t+\Delta t) - y_i(t).$$

Similarly, the rate of changes in the signal structure in its transient state can be expressed by changes in the cosine of the angle between the respective vectors, becoming, from formula (4),

$$V_\varphi = \lim_{\Delta t \to 0} \frac{\Delta \cos\varphi}{\Delta t} = \frac{y_1(t)y_1(t+\Delta t)+y_2(t)y_2(t+\Delta t)+ \ \dots \ +y_n(t)y_n(t+\Delta t)}{\Delta t|s(t)|s(t+\Delta t)|}.$$

It is interesting to note in addition, that it follows from the research presented in study [1] that a change in the signal structure in a room depends essentially not only on the considered fragment of a time signal, but also on the position of the measurement point (see Figs. 4–6), which was not included in the theoretical part of the present study, making the considered problem even more complex.

To find certain qualitative relations between the space of acoustic states of the room and the space of the signal structure, it is essential to determine the dimensions of this space, corresponding to the establishing of the multi-dimensionality of the signal. On the assumption that it is periodic, the multi-dimensionality of the signal can be determined considering either its amplitude spectrum expressed by a set of Fourier series coefficients or a set of instantaneous values of time function. Having Fourier n-coefficients, each of which is a complex number containing two real numbers, it is possible to obtain altogether $n = 2k$ real numbers. From the theorem of the independence of the Fourier coefficients, and also the independence of their imaginary and real parts, it can be seen that from the amplitude spectrum of the periodic signal, one can obtain $2k$ independent parameters. These parameters can be considered as the coordinates of the multi-dimensional space of the signal structure. Just as from the signal with a duration T, with a spectrum limited by the highest frequency f_{max}, it is possible, as a result of sampling this signal at Δt intervals equal at least to $\Delta t \geqslant 1/(2f_{max})$, to obtain $N = T/dt \leqslant 2f_{max}$ independent time samples, which can also be treated as the coordinates of a multi-dimensional space of the signal structure. A different position of the vector in the space of the signal structure corresponds to each change in the signal structure caused by a change in the acoustic state of the room. The magnitude of this change can be determined from the distance between two points in the space of the signal structure, from formula (5), or on the basis of the value of the cosine of the angle between the two vectors s and s_0, determining a change in the signal structure with respect to a signal compared according to formula (4).

At this point, it is interesting to mention that both the space of acoustic states of a room and the space of the signal structure in the present study do not concern the whole room, but a specific measurement point.

4. The relation between the space of acoustic states of a room and the space of the signal structure

On the basis of the considerations presented above, it can be stated in general that the space of acoustic states of the room shapes the space of the signal structure,

or, in other words, the space of acoustic states of the room influences the space of the signal structure, causing as a result a change of its acoustic parameters. Hence, the room can be regarded as a "functional operator" of the vector of the state $\boldsymbol{p}$ with the coordinates $(x_1, x_2, \ldots, x_n)$ into a vector defining a change in the sound structure s with the coordinates $(y_1, \ldots, y_2, \ldots, y_n)$

$$s = F(\boldsymbol{p}) \tag{10}$$

From the above relation, each change in the parameters of the received signal is related to a change in the parameters of the acoustic state of the room. By writing formula (10) in the form of a set of equations in which n variables of the parameters of the vector of the acoustic state of the room $\boldsymbol{p}$ corresponds to each parameter of the vector of the signal structure s, it is obtained that

$$\begin{aligned} y_1 &= F_1(x_1^{(1)}, x_2^{(1)}, \ldots, x_n^{(1)}) \\ y_2 &= F_2(x_1^{(2)}, x_2^{(2)}, \ldots, x_n^{(2)}) \\ &\ldots\ldots\ldots\ldots\ldots\ldots \\ y_n &= F_n(x_1^{(n)}; x_2^{(2)}, \ldots, x_n^{(n)}). \end{aligned} \tag{11}$$

It is possible to determine these dependences more exactly by another change in the parameters of the acoustic state of the room and measuring the parameters describing a change in the signal structure, namely

$$dy_1 = \frac{\partial y_i}{\partial x_1^{(i)}} dx_1^{(i)} + \frac{\partial y_i}{\partial x_2^{(i)}} dx_2^{(i)} + \ldots + \frac{\partial y_i}{\partial x_n^{(i)}} dx_n^{(i)}; \quad i = 1, 2, \ldots, n. \tag{12}$$

The value of the partial derivatives $\partial y_i / \partial x_j^{(i)}$ determines the "sensitivity" of changes in the signal structure to a change in the parameter of the acoustic state of the room.

For the set of equations (11) to be solvable, the functions F_i – should be continuous differentiable in terms of $x_n^{(i)}$. A necessary condition for the solution of the set of equations is the value of determinant (13) which is different from zero,

$$\begin{vmatrix} \frac{\partial F_1}{\partial x_1^{(1)}} & \frac{\partial F_1}{\partial x_2^{(1)}} & \cdots & \frac{\partial F_1}{\partial x_n^{(1)}} \\ \frac{\partial F_2}{\partial x_1^{(2)}} & \frac{\partial F_2}{\partial x_2^{(2)}} & \cdots & \frac{\partial F_2}{\partial x_n^{(2)}} \\ \ldots\ldots\ldots\ldots\ldots\ldots\ldots\ldots \\ \frac{\partial F_n}{\partial x_1^{(n)}} & \frac{\partial F_n}{\partial x_2^{(n)}} & \cdots & \frac{\partial F_n}{\partial x_n^{(n)}} \end{vmatrix} \neq 0. \tag{13}$$

The basic task in looking for the relation between the space of acoustic states of the room and the space of the signal structure is to determine the form of the

function F in formula (11) describing the relation in general. Assuming in the first approximation the function F to be linear, the set of equations (11) can be written in the form

$$\begin{aligned} y_1 &= a_1^{(1)}x_1^{(1)} + a_2^{(1)}x_2^{(1)} + \ldots + a_n^{(1)}x_n^{(1)} \\ y_2 &= a_1^{(2)}x_1^{(2)} + a_2^{(2)}x_2^{(2)} + \ldots + a_n^{(2)}x_n^{(2)} \\ &\ldots\ldots\ldots\ldots\ldots\ldots\ldots \\ y_n &= a_1^{(n)}x_1^{(n)} + a_2^{(n)}x_2^{(n)} + \ldots + a_n^{(n)}x_n^{(n)} \end{aligned} \tag{14}$$

It is necessary to note that the set of equations (14), when written in form (15), can serve to determine the parameters of the acoustic state of the room on the basis of the measured parameters of changes in the signal structure

$$\begin{aligned} x_1 &= b_1^{(1)}y_1^{(1)} + b_2^{(1)}y_2^{(1)} + \ldots + b_n^{(1)}y_n^{(1)} \\ x_2 &= b_1^{(2)}y_1^{(2)} + b_2^{(2)}y_2^{(2)} + \ldots + b_n^{(2)}y_n^{(2)} \\ &\ldots\ldots\ldots\ldots\ldots\ldots\ldots \\ x_n &= b_1^{(n)}y_1^{(n)} + b_2^{(n)}y_2^{(n)} + \ldots + b_n^{(n)}y_n^{(n)} \end{aligned} \tag{15}$$

Analyzing the set of equations (14), it can be seen that a change in successive parameters of the acoustic state of the room should involve a specific change in the parameters of the signal. The coefficients a_i^j which occur in these equations can be determined by a change in the parameters x_i – by the value Δx_i for the other parameters of the acoustic state of the rom being stationary.

The set of equations (14) can be solved if determinant (16) is different from zero

$$\begin{vmatrix} a_1^{(1)}a_2^{(1)}\ldots a_n^{(1)} \\ a_1^{(2)}a_2^{(2)}\ldots a_n^{(2)} \\ \ldots\ldots\ldots \\ a_1^{(n)}a_2^{(n)}\ldots a_n^{(n)} \end{vmatrix} \neq 0. \tag{16}$$

In the case the i-th row of the matrix of coefficients consists of zero terms, this means that the parameter of the signal y_i does not depend on any of the parameters of the acoustic state of the room. With the zero value of the i-th column the parameter of the state of the room x_i does not influence any of the parameters of the signal. On the other hand, if the terms of two rows or two columns differ with a constant coefficient, this means that there is a linear dependence between two parameters of the signal or two parameters of the acoustic state of the room.

5. The determination of the acoustic states of the room on the basis of a classification of changes in the signal structure

In a general case, all the possible acoustic states of the room can be divided into a number of classes. This classification can be carried out in various ways, nevertheless, considering its practical aspect, it would be convenient to perform it, e.g., from the point of view of chosen criteria of subjective evaluation of the acoustic quality of the room. The set of the possible acoustic states of the room could then be divided into two basic classes: the class of the states of the room which is satisfactory and their class which is unsatisfactory from the point of view of these criteria. Such a division could be made by marking a threshold value x_{0i} (or a few threshold values) on each coordinate axis of a multi-dimensional space of acoustic states of the room. A plane perpendicular to each axis, crossing the point x_{0i}, would then separate the space into two regions or a correspondingly greater number of them, determining the satisfactory or unsatisfactory acoustic states of the room. It is possible to subordinate an appropriate classification of changes in the signal structure to a classification of acoustic states of the room performed in this way, which is essential from the practical point of view. The threshold values of these changes plotted on the coordinate axes of the multi-dimensional space of the signal structure could be determined from psychoacoustic investigations.

In real conditions the precise description of the acoustic state of the room requires considering a very large number of the parameters of the state, which would be very troublesome and tedious in practice. On the other hand, this problem can be approached in a slightly different way. Namely, instead of describing the acoustic state of the room by the set of parameters $x_1, x_2, \ldots, x_n$, all the acoustic states of the room could be divided into t class $c_l (l = 1, 2, \ldots, t)$ and a certain representative state $p_l = (x_1^{(l)} x_2^{(l)}, \ldots, x_n^{(l)})$ could be chosen for them. Thus, the determination of the measured acoustic state of the room would consist in finding to which class c_l the studied state $\boldsymbol{p}$ belongs, requiring comparison of this state and the representative $\boldsymbol{p}_l$ of each class. On the basis of the relation between the space of acoustic states of the room and the space of the signal structure, one can note that the classification of acoustic states of the room is equivalent to the classification of changes in the signal structure. This means that, instead of the states $\boldsymbol{p}_l = (x_1^l, x_2^l, \ldots, x_n^l)$ representative of each class, it is possible to assume the vectors of changes in the signal structure $\boldsymbol{s}_l = (y_1^{(l)}, y_2^{(l)}, \ldots, y_n^{(l)})$ corresponding to these states, involving the transformation of the problems of the classification of acoustic states of the room into the field of psychoacoustic investigations.

Let us assume that, on the basis of certain psychoacoustic criteria, certain classes of changes in the signal structure were established to which the corresponding vectors $s_l = (y_1^{(l)}, y_2^{(l)}, \ldots, y_n^{(l)})$, where $l = 1, 2, \ldots, t$, are subordinated. A certain change in the signal structure $\boldsymbol{s}_1 = (y_1^{(l)}, y_2^{(l)}, \ldots, y_n^{(l)})$ measured for a given acoustic state of the room, can be classified into one of the established classes represented by

the vectors s_l from the determined distance between points in the space of the signal structure, or the value of the cosine of the angle contained between the vectors of changes in the signal structure.

According to the formulae given in chapter 1, the distance between points in a n-dimensional space can be calculated by applying the formulae

$$d(s_1, s_l) = \sqrt{\sum_{i=1}^{n} (y_i^{(1)} - y_i^{(l)})^2}, \tag{17}$$

or

$$d_\infty(s_1, s_l) = \max |y_i^{(1)} - y_i^{(l)}|, \tag{18}$$

for

$$1 \leqslant i \leqslant n; \quad 1 \leqslant l \leqslant t.$$

It can be seen from (17) that the difference between the signals: the reference signal, representative of a given class, and the signal in question, is equal to the standard deviation of all the parameters of the two signals. In turn, according to (18), the difference between the reference signal and one in question is determined by the maximum value of the absolute difference between the parameters of these signals.

The vector of changes in the signal structure $s_1 = (y_1^{(1)}, y_2^{(1)}, \ldots, y_n^{(1)})$ can be classified into one of the classes represented by the vectors s_l, as was already mentioned, also by calculating the value of the cosine of the angle contained between the respective vectors (see(4)). The greatest value of the cosine of this angle makes it possible to include the vector s_1 representing a given class of changes in the signal structure.

In determining the acoustic state of the room on the basis of the classification of changes in the signal structure, it is necessary to note the presence of external interferences generating into the room. These interferences could be the cause of error in classification, as the vector of changes in the signal structure s, corresponding to a given acoustic state of the room p, would contain the additional component s_e related to the occurrence of the interferences e, which could be written in the following way:

$$s + s_e = F(p, e). \tag{19}$$

Moreover, in the above considerations it was assumed that the acoustic state of the room is fully described by n parameters $x_1, x_2, \ldots, x_n$, apart from which there are no other parameters characterizing the acoustic properties of the room. This assumption is not entirely valid, since theoretically many parameters can be attributed to each room. However, in practice only a few parameters, are assumed, being regarded as the most characteristic parameters describing the acoustic state of the room. Therefore, hence, two acoustic states of the room which are considered equal in terms of the set of the assumed parameters $x_1, x_2, \ldots, x_n$ need not to be the same, since they can differ in the values of the parameters $x_{n+1}, x_{n+2}, \ldots, x_{n+\alpha}$

which are not included in this set. As a result of this changes the in the signal structure, measured parameters for these two "identical" acoustic states of the room, are not exactly the same, namely

$$y_i + \Delta y_i = F_i(x_1^{(i)}, x_2^{(i)}, \ldots, x_n^{(i)}, x_{n+1}^{(i)}, x_{n+2}^{(i)}, \ldots, x_{n+\alpha}^{(i)})$$

moreover y_1 is the parameter of a signal corresponding to the state of the room p_i if $x_{n+1}^{(i)}, x_{n+2}^{(i)}, \ldots, x_{n+\alpha}^{(i)} = 0$, or more generally

$$s + s_e = F'(p, p', e).$$

where e is the vector accounting for the value of the external interferences.

6. The results of preliminary experimental research

Apart from the theoretical considerations presented above, which constitute the essential part of the research, within the framework of the present study, preliminary experimental investigations were also undertaken. It is necessary to note that the results of these investigations are rather reconaissance in character, being an attempt to represent a change in the spectral envelope of a sound in the room in the so-called physical and subjective space of changes in the signal structure. The experimental research on changes in the amplitude-frequency structure of the acoustic signal propagating in rooms with different acoustic properties was discussed in detail in study [1].

The range of these studies included the following elements:
– the determination of changes in the spectral structure of a sound, successively in its growth process, the steady state and the decay process, for different acoustic parameters of the room; and
– the determination of changes in this structure depending on the spatial configuration of rooms shaped as acoustically coupled ones.

The studies were carried out in a special room permitting the shaping of four types of rooms with different acoustic properties. The applied measurement equipment made it possible to register and process in the analogue-digital way any time fragment, chosen from the analyzed course, having an essential significance for the study of its transient states (the growth, the decay).

The object of the study were the sounds of two natural vowels „a" and „e", a combination of these vowels in the word „rzeka" and a white noise signal, reproduced in a room with diversified acoustic properties. For each of these sounds, three characteristic time fragments were distinguished, representing successively the process of their growth the steady state and the decay process which were then subject to detailed spectral analysis by means of the Fast Fourier Transform (the FFT method), implemented on an Eliot 4130 computer. The ample experimental material presented in study [1] was carefully analyzed quantitatively and qualitatively over the range of which a number of quantitatives were determined, charac-

terizing the amplitude-frequency changes in the harmonic and formant structures of the studied sounds in the range of their particular time fragments.

Figs. 1–3 present, as an example, for one of the analyzed sounds (the vowel „a"), computer records of chosen time fragments: of the growth process, the steady state and the decay process of this sound, and the corresponding spectra gained by the FFT method. These courses were obtained in three rooms different acoustically, namely in a room with properties close to those of anechoic chamber, denoted further as A, with the reverberation time $T_A = 50$ ms; in the so-called damped room, denoted as B, with the reverberation time $T_B = 250$ ms; and in an undamped room, denoted as C, with the reverberation time $T_C = 1s$. A preliminary qualitative analysis of these spectra indicates that as a result of the influence of the acoustic parameters of the room different in terms of their value, on the form of the signal it is possible to note different changes in its spectral structure, expressed in a change in the amplitude relations between successive harmonics, a change in the half-width of the formants etc.

As can be seen, the quantity of these changes depends on the time section of the analyzed signal namely, the growth, steady state and the decay and on the acoustic properties of the room. A detailed quantitative analysis of changes in the spectral structure of this sound, and other signals too, which were mentioned above, depending on the acoustic properties of the considered rooms, the choice of the measurement point, were presented in study [1].

On the basis of the conception, given in the chapter 2, of representing changes in the sound structure in the aspect of the multi-dimensional space, in keeping with expression (5), the so-called vectors of changes in the signal structure were determined for the considered speech sounds, respectively in their growth process, the steady state and the decay process. The lengths of these vectors map the resultant difference between the sound spectra recorded in a room with properties close to those of an anechoic chamber, treated as reference spectra and the spectra of this sound recorded at a given measurement point P_x of a given room respectively for the growth process the steady state and the sound decay process

$$d(P_0, P_x)|\boldsymbol{p}_x| = \sqrt{\sum_{i=1}^{n} (L_i^{(P_0)} - L_i^{(P_x)})^2}, \tag{20}$$

where $L_i^{(P_0)}$ and $L_i^{(P_x)}$ are the acoustic pressure levels determined in the i-th frequency band, respectively for the reference spectrum and the spectrum measured at a chosen measurement point in a given room and n is the total number of frequency bands.

A similar conception of the quantitative evaluation of the spectral differences in the aspect of a multi-dimensional space was presented in study [3], concerned with the problems of changes in the sound timbre in depending on the position of the measurement point.

Assuming further that the essential information on the analyzed sound is contained in the bands of the first three formants, the n-dimensional space of the signal structure was limited to a three-dimensional space, subordinating, in keeping

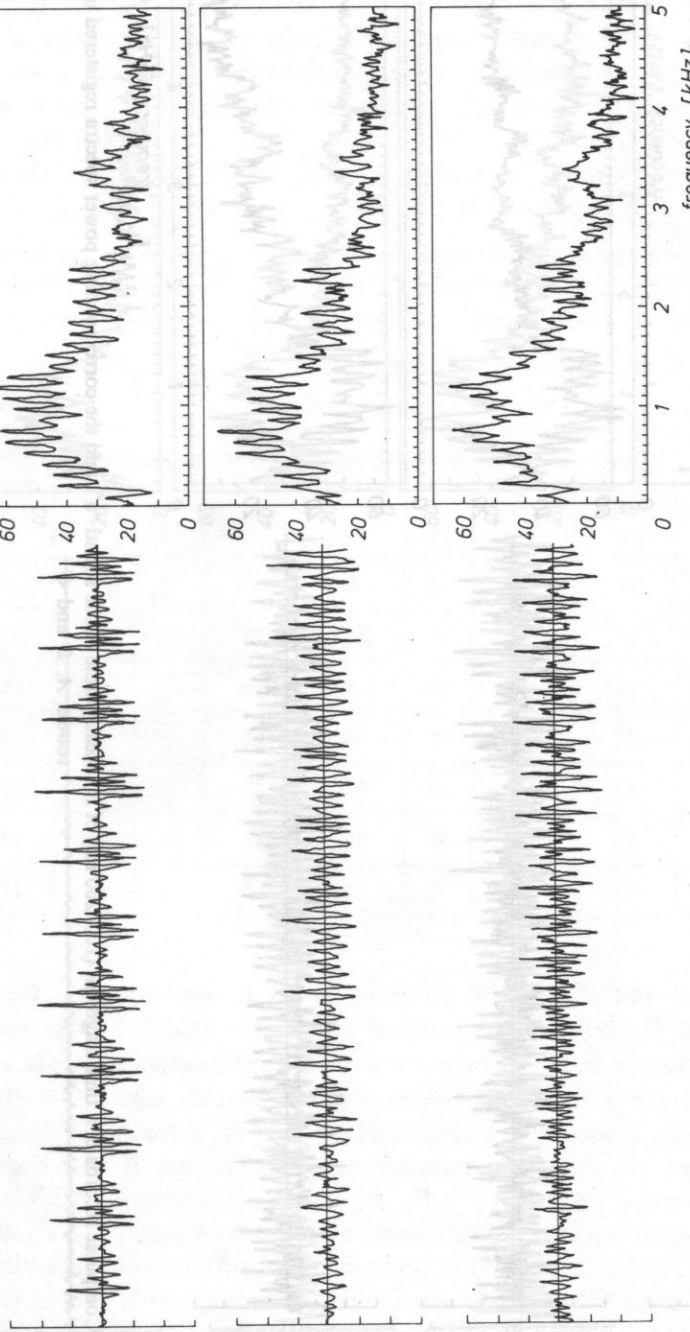

Fig. 1. Computer records of a time fragment of the growth (0–100 ms) of the sound "a", and the corresponding power spectra registered in three rooms *A*, *B* and *C*

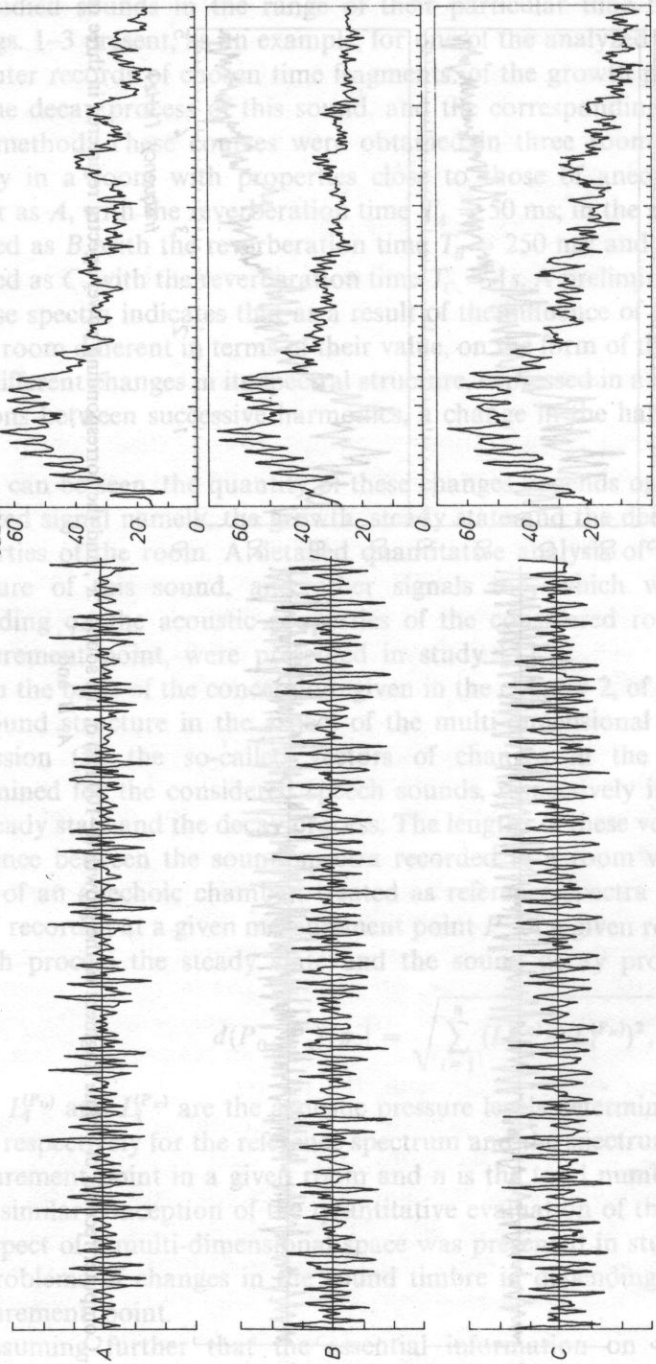

Fig. 2. Computer records of a time fragment (160–260 ms) of the steady state of the sound "a", and the corresponding power spectra registered in three rooms *A*, *B* and *C*

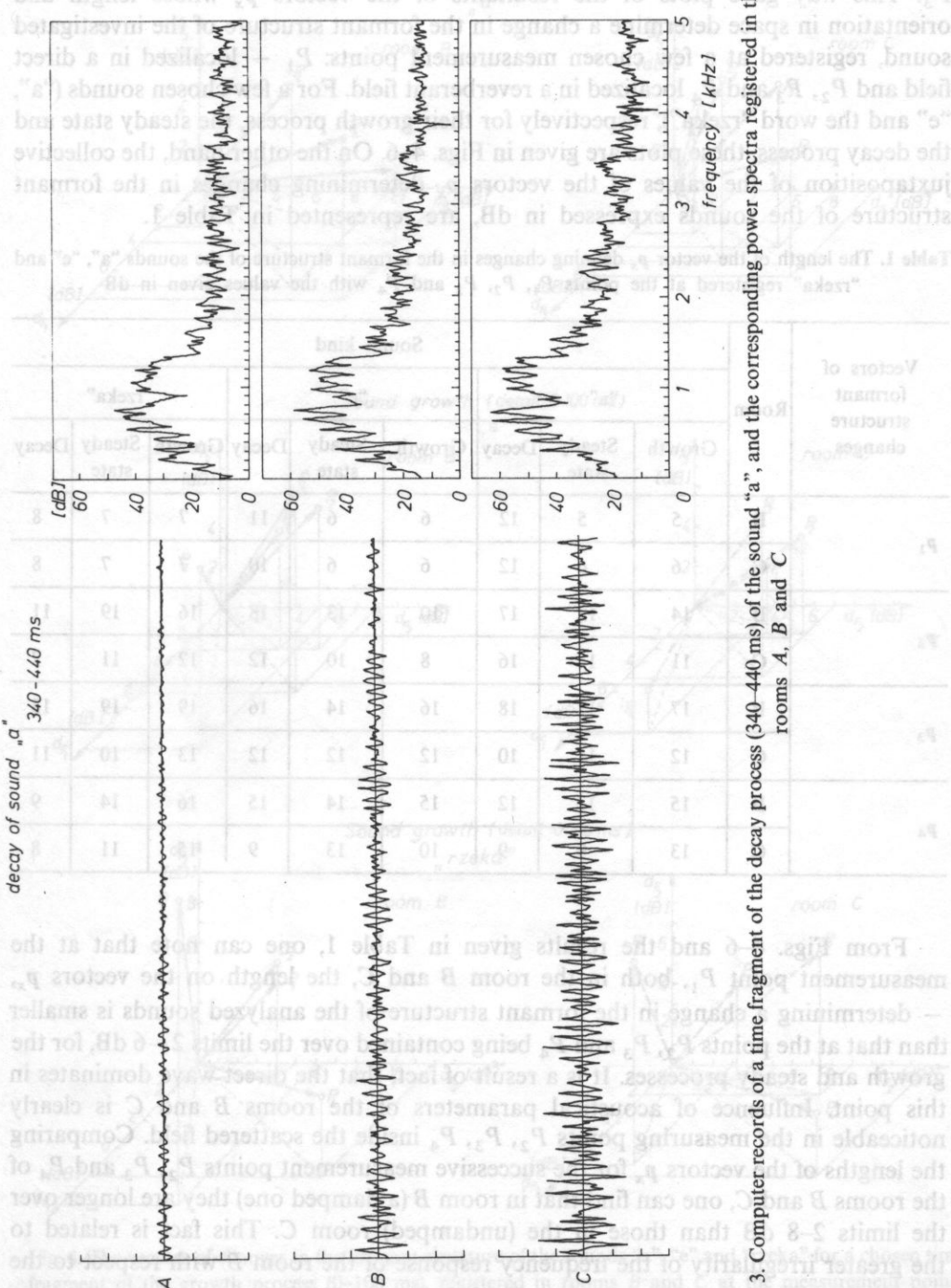

Fig. 3. Computer records of a time fragment of the decay process (340–440 ms) of the sound "a", and the corresponding power spectra registered in three rooms *A*, *B* and *C*

with formula (20), the vectors $\boldsymbol{p}_x$ to the energy maxima of the formants F_1, F_2 and F_3. This way gave plots of the resultants of the vectors $\boldsymbol{p}_x$ whose length and orientation in space determine a change in the formant structure of the investigated sound, registered at a few chosen measurement points: P_1 – localized in a direct field and P_2, P_3 and P_4 localized in a reverberant field. For a few chosen sounds ("a", "e" and the word "rzeka"), respectively for their growth process, the steady state and the decay process, these plots are given in Figs. 4–6. On the other hand, the collective juxtaposition of the values of the vectors $\boldsymbol{p}_x$ determining changes in the formant structure of the sounds expressed in dB, are represented in Table 1.

Table 1. The length of the vector $\boldsymbol{p}_x$ defining changes in the formant structure of the sounds "a", "e" and "rzeka" registered at the points P_1, P_2, P_3 and P_4 with the values given in dB

Vectors of formant structure changes	Room	Sound kind								
		"a"			"e"			"rzeka"		
		Growth	Steady state	Decay	Growth	Steady state	Decay	Growth	Steady state	Decay
$\boldsymbol{p}_1$	B	5	5	12	6	6	11	7	7	8
	C	6	6	12	6	6	10	7	7	8
$\boldsymbol{p}_2$	B	14	12	17	10	13	18	16	19	11
	C	11	12	16	8	10	12	12	11	7
$\boldsymbol{p}_3$	B	17	12	18	16	14	16	19	19	13
	C	12	11	10	12	12	12	13	10	11
$\boldsymbol{p}_4$	B	15	12	12	15	14	15	16	14	9
	C	13	9	9	10	13	9	15	11	8

From Figs. 4–6 and the results given in Table 1, one can note that at the measurement point P_1, both in the room B and C, the length on the vectors $\boldsymbol{p}_x$, – determining a change in the formant structure of the analyzed sounds is smaller than that at the points P_2, P_3 and P_4 being contained over the limits 2–6 dB, for the growth and steady processes. It is a result of fact, that the direct wave dominates in this point. Influence of acoustical parameters of the rooms B and C is clearly noticeable in the measuring points P_2, P_3, P_4 inside the scattered field. Comparing the lengths of the vectors $\boldsymbol{p}_x$ for the successive measurement points P_2, P_3 and P_4 of the rooms B and C, one can find that in room B (a damped one) they are longer over the limits 2–8 dB than those in the (undamped) room C. This fact is related to the greater irregularity of the frequency response of the room B with respect to the

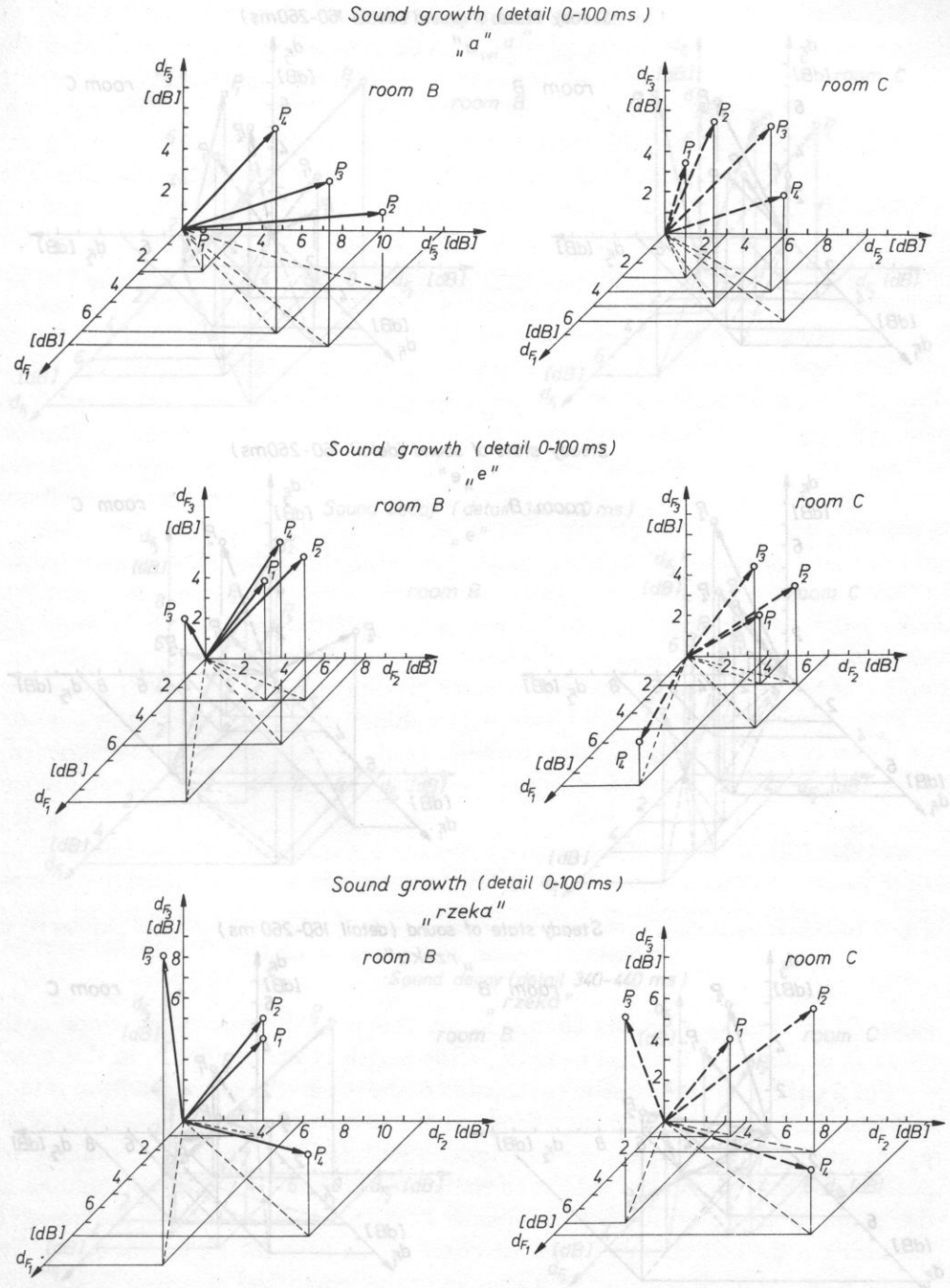

Fig. 4. The vectors of changes in the formant structure of the sounds "a", "e" and "rzeka" for a chosen time fragment of the growth process (0–100 ms), registered in rooms *B* and *C* at the measurement points P_1, P_2, P_3 and P_4

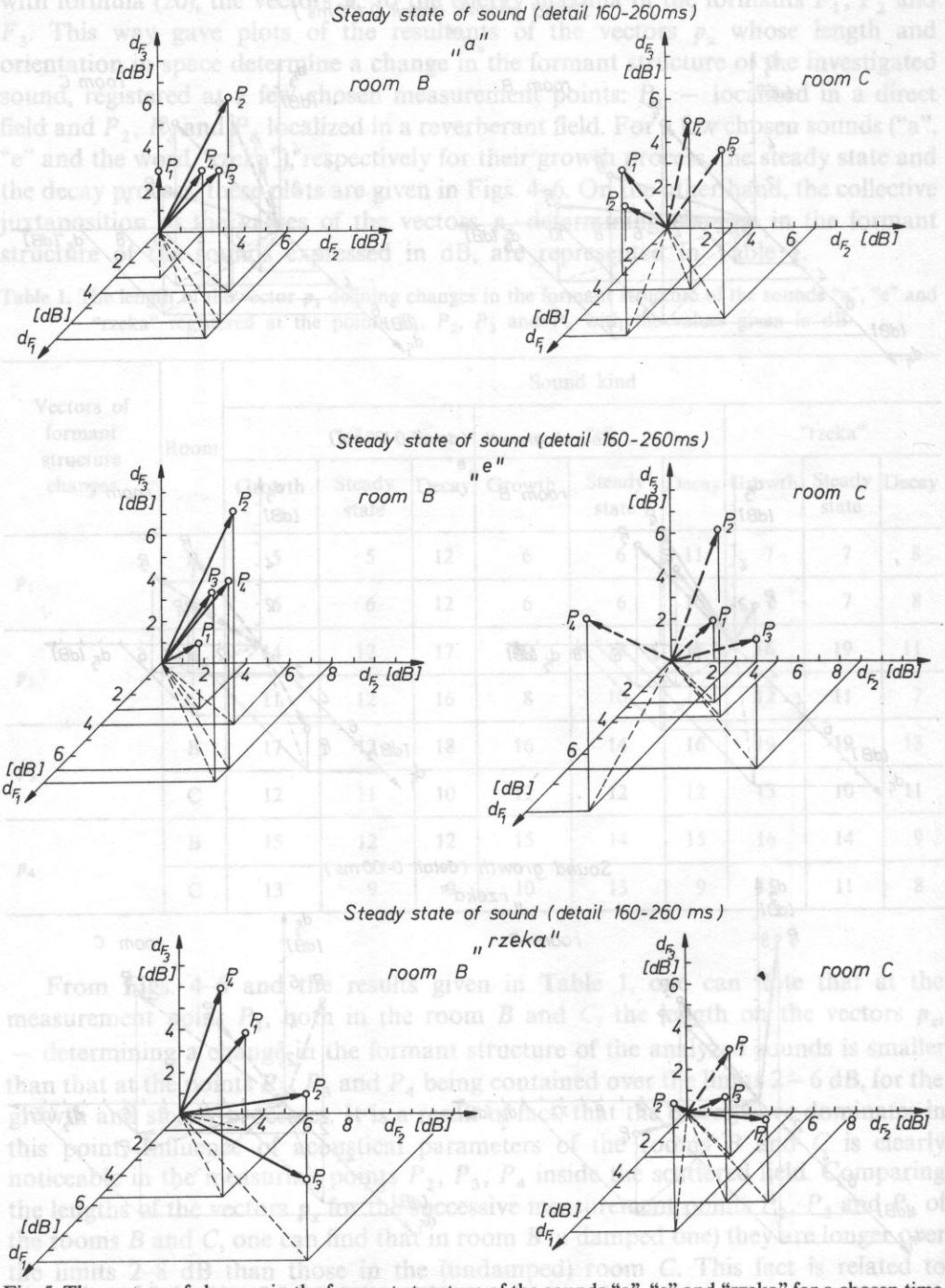

Fig. 5. The vectors of changes in the formant structure of the sounds "a", "e" and "rzeka" for a chosen time fragment of the steady state (160–260 ms), registered in rooms B and C at the measurement points P_1, P_2, P_3 and P_4

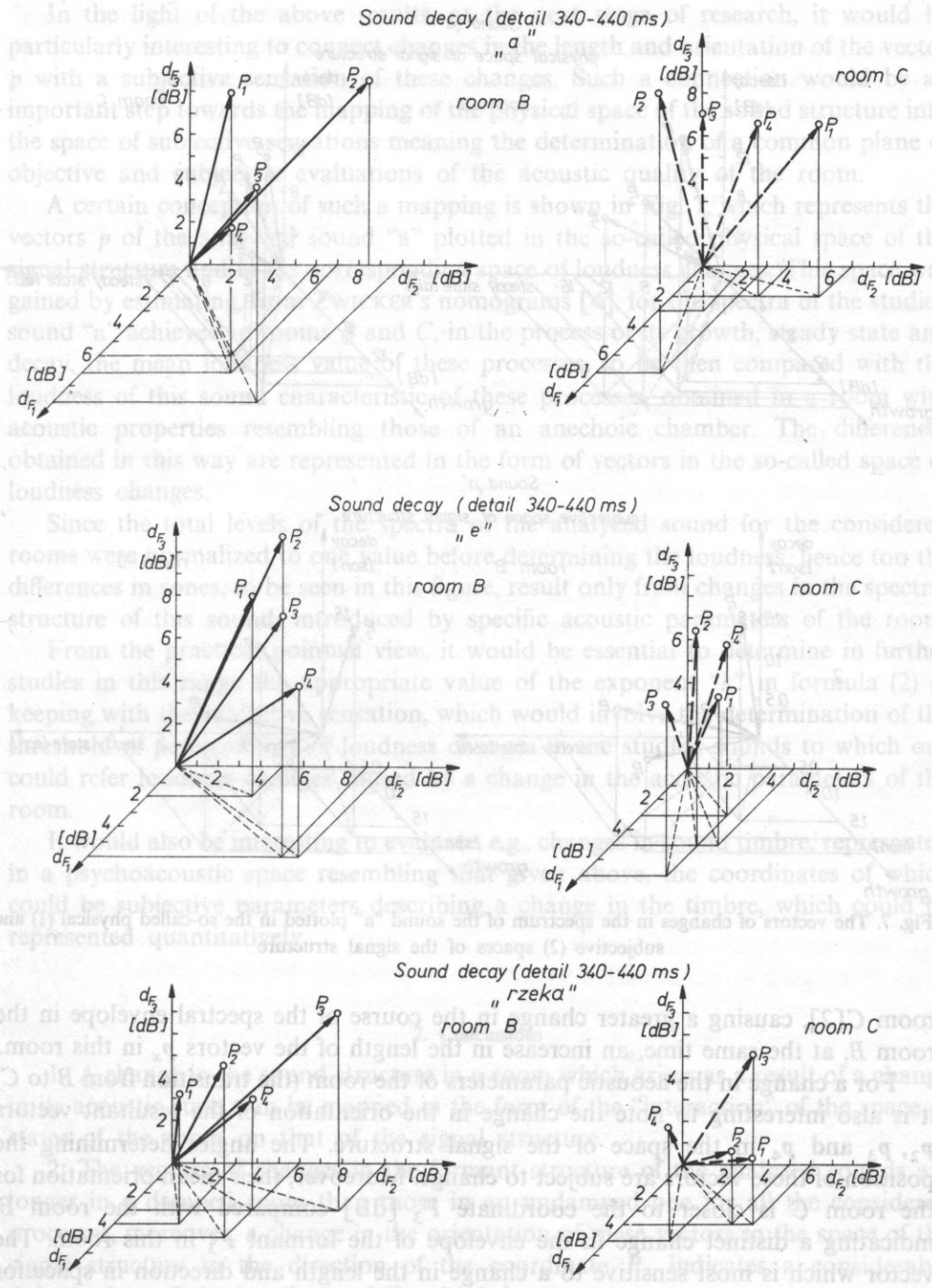

Fig. 6. The vectors of changes in the formant structure of the sounds "a", "e" and „rzeka" for a chosen time fragment of the decay process (340–440 ms), registered in rooms *B* and *C* at the measurement points P_1, P_2, P_3 and P_4

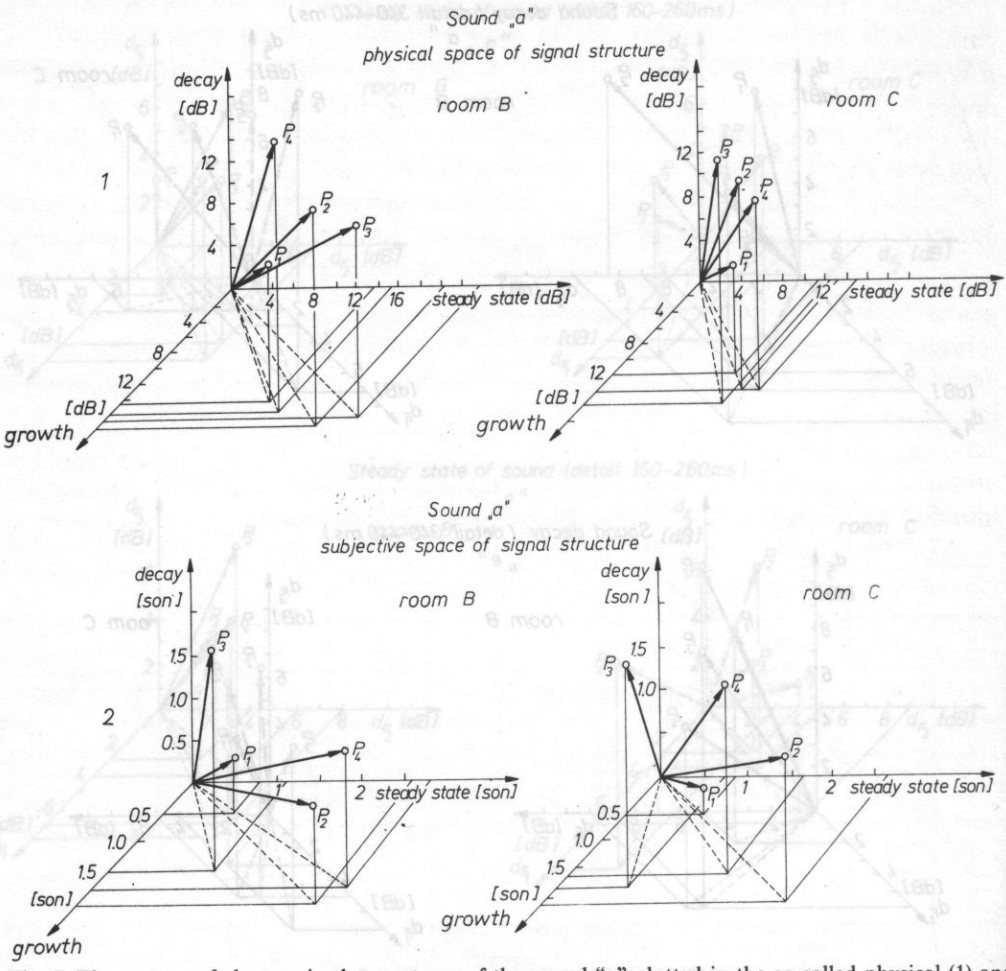

Fig. 7. The vectors of changes in the spectrum of the sound "a" plotted in the so-called physical (1) and subjective (2) spaces of the signal structure

room C[2], causing a greater change in the course of the spectral envelope in the room B, at the same time, an increase in the length of the vectors $\boldsymbol{p}_x$ in this room.

For a change in the acoustic parameters of the room (the transition from B to C) it is also interesting to note the change in the orientation of the resultant vectors $\boldsymbol{p}_2$, $\boldsymbol{p}_3$ and $\boldsymbol{p}_4$ in the space of the signal structure. The angles determining the position of these vectors are subject to change. Moreover, their mean orientation for the room C is closer to the coordinate F_3 [dB] compared with the room B, indicating a distinct change in the envelope of the formant F_3 in this room. The vector which is most sensitive to a change in the length and direction in space for a change in the acoustic parameters of the room, is the vector $\boldsymbol{p}_3$ characterizing the magnitude of changes in the formant structure of a sound registered at the measurement point P_3.

In the light of the above results, at the next stage of research, it would be particularly interesting to connect changes in the length and orientation of the vector $\boldsymbol{p}$ with a subjective sensation of these changes. Such a connection would be an important step towards the mapping of the physical space of the sound structure into the space of subjective sensations meaning the determination of a common plane of objective and subjective evaluations of the acoustic quality of the room.

A certain conception of such a mapping is shown in Fig. 7, which represents the vectors $\boldsymbol{p}$ of the analyzed sound "a" plotted in the so-called physical space of the signal structure and in the corresponding space of loudness changes. This space was gained by estimating, from ZWICKER'S nomograms [4], for the spectra of the studied sound "a" achieved in rooms *B* and *C*, in the process of its growth, steady state and decay, the mean loudness value of these processes, to be then compared with the loudness of this sound characteristic of these processes, obtained in a room with acoustic properties resembling those of an anechoic chamber. The differences obtained in this way are represented in the form of vectors in the so-called space of loudness changes.

Since the total levels of the spectra of the analyzed sound for the considered rooms were normalized to one value before determining the loudness, hence too the differences in sones, to be seen in this figure, result only from changes in the spectral structure of this sound, introduced by specific acoustic parameters of the room.

From the practical point of view, it would be essential to determine in further studies in this range the appropriate value of the exponent "*k*" in formula (2) in keeping with the subjective sensation, which would involve the determination of the threshold of perceptibility of loudness changes in the studied sounds to which one could refer loudness changes caused by a change in the acoustic parameters of the room.

It would also be interesting to evaluate, e.g., changes in sound timbre, represented in a psychoacoustic space resembling that given above, the coordinates of which could be subjective parameters describing a change in the timbre, which could be represented quantitatively.

7. Conclusions

1. A change in the sound structure in a room which arises as a result of a change in its acoustic state, can be mapped in the form of the "interaction" of the space of states of the room on that of the signal structure.

2. The vectors of changes in the formant structure of the analyzed sounds are longer in a damped room than those in an undamped one for all the considered processes, moreover, a change in the orientation of these vectors in the space of the signal structure in the direction of the coordinate P_3 indicates a considerable deformation of the envelope of the third formant.

3. The physical space of the signal structure can be mapped into the space of subjective sensations with coordinates which are the respective psychoacoustic

quantities. Such a mapping can be an important step towards the determination of a common plane of objective and subjective evaluations of the acoustic quality of a room which is still sought for in the problems of room acoustics.

References

[1] E. OZIMEK, *Research on a change in the spectral structure of a sound propagating in a room* (in Polish) Scientific Publications of Adam Mickiewicz University, Poznań 1977 (Habilitation thesis).

[2] E. OZIMEK, *The functions of the intensity level distribution of the frequency response of a room* (in Polish), Archiwum Akustyki, 3, 342–355 (1984).

[3] R. PLOMP, H. STEENKEN, *Place dependence of timbre in reverberant sound fields*, Acustica **28**, 50–59 (1973).

[4] E. PAULUS, E. ZWICKER, *Programme zur automatischen Bestimmung der Lautheit aus Terzpegeln oder Frequenzgruppenpegeln*, Acustica, **27**, 253 (1972).

Received August 8, 1987.

ARCHIVES OF ACOUSTICS
12, 3–4, 273–289 (1987)

DIFFERENCE LIMENS OF AMPLITUDE MODULATED SIGNALS[1]

EDWARD OZIMEK, ALEKSANDER SĘK

Institute of Acoustics, A. Mickiewicz University (60–769) Poznań, ul. Matejki 48/49)

Presented in the literature studies on the perception of amplitude modulated signals concentrate mainly on the determination of modulation thresholds, and of the so-called roughness and amplitude of a signal. Whereas papers concerned with difference limens of amplitude modulation of carriers more complex than a tonal signal are lacking. With this in mind, research aimed in principle at the determination of difference limens of noise octave bands amplitude modulated with sinusoidal signals was undertaken. A comparison of these limens with values of STI which is an objective measure of speech intelligibility in a room was another important aim of performed studies. Such a comparison was a certain psychoacoustic verification of the perception ability of definite changes of the STI by a listener.

Research results proved that difference limens depend significantly on the modulation factor of the reference signal. It was also found that difference in the STI values, determined with the objective method (the so-called RASTI method), which determine room quality from the point of view of speech intelligibility are found in the range of difference limens of amplitude modulated signals or below these limens.

1. Introduction

Research performed up to the present on the perception of amplitude modulated signals concern mainly the determination of modulation thresholds and the evaluation of the so-called roughness and amplitude fluctuation of a signal. Several papers can be found which indirectly are concerned with difference limens of amplitude modulation however with respect only to a simplest case of a modulation of a sinusoidal signal with another sinusoidal signal. Hence, it seems interesting to carry out research on the determination of difference limens of amplitude modulation for a more complex carrier than a tonal signal. Performed studies are directly related to results of papers [3, 4] which prove that changes of the amplitude modulation index of definite white noise bands propagating in a room allow a direct evaluation of speech intelligibility in this room. The so-called speech transmission index – STI is the measure of such intelligibility. With respect to these papers, the problem of difference perception between modulated signals with various values of modulation indices requires further analysis. In principle this problem resolves itself into the deter-

[1] Research was performed within the framework of problem CPSP 02.03.7.4

mination of difference limens for these signals. In terms of experimentally determined values of the STI, these limens can be their interesting psychoacoustic verification. It is obvious that in order to have changes of the modulaton index observed in a room for example percepted by a listener, they have to exceed determined difference limens. The results of our research show that differences of the STI which are important to the diversification of speech intelligibility evaluation in rooms are found at the same level or below difference limens.

2. Review of studies concerned with perception of amplitude modulated signals

Many scientists have dealt with the perception of amplitude modulated sounds [1, 2, 6, 7, 8, 9, 10, 12, 13]. Two fundamental groups of papers can be isolated. The first one is concerned with the determination of amplitude modulation thresholds with the applicaton of a wide class of carrier and modulating signals. The second group of papers is concerned with investigations of the fluctuation intensity of amplitude modulated sounds and of roughness.

2.1. Thresholds of amplitude modulation of signals

ZWICKER's and FELDTKELLER's paper [13] widely presents the problem of amplitude modulation thresholds. Apart from classical modulation thresholds, i.e. modulation of a sinusoidal signal by another sinusoidal signal, this paper presents a series of relationships for the preception of amplitude modulated complex signals – especially amplitude modulation of various bands of white noise.

ZWICKER [12] univocally determined relationships between the thresholds amplitude modulation factor, amplitude and frequency of the carrier tone, frequency of modulating signal for a case of investigations of amplitude modulation performed with the utilization of tonal signals only. This led to the identification of certain significant perception ranges of modulated signals, i.e. the so-called "follow-up" range, roughness range and range of separation of side components also characteristic for frequency modulation. Results of this research have contributed to the formulation of a certain perception theory of the monaural phase effect and to the perception of modulated signals [13].

ZWICKER and FELDTKELLER [13] have also stated certain fundamental relationships which govern the perception of various noise bands amplitude modulated with the utilization of various modulating signals. The assignation of relationships between the threshold amplitude modulation factor and band width of carrier signal for a regular (sinusoidal or rectangular) modulating signal with constant frequency equal to 4Hz was the most important problem. It was stated that every increase of the width of the carrier signal band causes a proportional decrease of amplitude modulation thresholds. This dependence is valid for all noise bands with width not exceeding the width of one critical band. In this case, the width of the critical band is

of great importance because in accordance with paper [13], when this width is exceeded by a modulated sound then a different in quality perception mechanism is acutated. We have to do with the so-called separation sidebands, or with so-called spectral mechanism of perception in such a case [6].

In the course of detailed analysis of relationships between amplitude modulation thresholds and modulating frequency for various widths of the band of carrier noise it was stated that for a noise with spectrum range not exceeding the width of one critical band, these thresholds in quality are close to thresholds of modulation of a sinusoidal signal with another sinusoidal signal. When the spectrum of carrier signal exceeds the width of the critical band then the effect of separation of side bands is of constant character and does not depend on the value of modulating frequencies. In such a case thresholds of amplitude modulation of such a noise become identical to thresholds of broad-band noise which are approximately proportional in a wide range of modulating frequencies to values of these frequencies.

Presented above conclusions find practical application, because natural sounds of music or speech are broad-band signals and so their perception is governed by principles valid in this range for a broad-band noise.

Also VIEMEISTER's research [10] was concerned with amplitude modulation perception. He studied the so-called temporal modulation transfer function (TMTF) which is determined on the basis of thresholds of amplitude modulation. Viemeister's research is partly a repetition, but also an extension of results presented in paper [13] for various bands of white noise as the carrier signal.

The temporal modulation transfer function (TMTF) was defined by Viemeister as

$$\text{TMTF} = 20\lg m \quad [\text{dB}],$$

where m is the threshold amplitude modulation factor.

Viemeister's experimental results are consistent with results given in paper [13] for broad-band noise and they supplement them in many matters. They have proved that thresholds of amplitude modulation of a wide noise band depend on the modulation frequency up to the value of 2 KHz. Whereas a further increase of the value of this frequency does not influence the value of the threshold. This is most apparent in the diagram: TMTF versus modulating frequency.

Like Zwicker, Viemeister noticed that an extension of the carrier signal band distinctly decreases thresholds of amplitude modulation. The value of the determined threshold is strongly influenced by the mid-band frequency in this relationship. According to Viemeister's investigations, decisively higher thresholds are observed for lower mid-band frequencies of carrier signal bands.

Besides presented above conclusions, VIEMEISTER's paper [10] gives also a development of TERHARDT's model [8]. According to this model thresholds of amplitude modulation can be interpreted on the basis of a low-pass filter with an adequate limit frequency. TERHARDT [8] grounded his hypothesis on amplitude modulation thresholds derived by Zwicker for tones. This gave a great discrepancy between his

theory and experimental data – mainly in frequency range in which the so-called separation of sidebands of the modulated sound is observed. Such an effect took place, because the spectrum of the modulated signal exceeded the width of one critical band. Viemeister applied a wide noise band as the carrier signal and thus completely eliminated the effect of separation of sidebands and obtained absolute (accurate to standard deviation value) compatibility of experimental data with theoretical assumptions.

2.2. Roughness and intensity of amplitude fluctuation of amplitude modulated signals

The problem of perception of the so-called roughness and intensity of amplitude fluctuation intensity of amplitude modulated signals is fairly widely discussed in papers [1, 2, 7, 8, 9]. Roughness as well as amplitude fluctuations are treated in these papers as two independent phenomena. Amplitude fluctuations are such changes of the amplitude which occur not more often than 20 times per second ($f_{mod} \leqslant 20$ Hz). These changes are perceived as succesive minima and maxima of the amplitude of the signal. This means that the organ of hearing "follows-up" with these changes. The sensation of sound roughness is achieved at changes of the signal amplitude greater than 20 times per second ($f_{mod} \geqslant 20$ Hz). In such a case the organ of hearing does not "follow-up" with the observation of succesive amplitude maxima and minima, and receives a global impression of such a type of signal – called roughness in short.

TERHARDT'S paper [9] is one of the first which concerns the perception of signal amplitude fluctuations in the conditions of amplitude modulation. The author is interested in the determination of amplitude fluctuation intensity and roughness in terms of physical parameters of signals, i.e. carrier frequency, modulating frequency and amplitude of the signal.

Terhardt stated that amplitude fluctuation intensity and roughness is proportional to the intensity level of a signal in the range from 40 to 80 dB.

The relationship between roughness and carrier frequency f_c can be characterized in two intervals. And so, for $f_c \in (125\text{–}500\,\text{Hz})$ an increase of roughness accompanying an increase of carrier frequency is observed. When f_c reaches the value of 500 Hz roughness assumes a constant value independent from further increase of carrier frequency. Whereas, amplitude fluctuation intensity is independent from carrier frequency.

Yet the relationship between fluctuation intensity and roughness, and modulation factor is the most important relation determined in paper [9]. It was stated that fluctuation intensity as well as roughness is proportional to the square of the amplitude modulation factor.

Another paper written by TERHARDT [8] is concerned with similar problems. Besides information on roughness due to amplitude modulation, also information on roughness in the conditions of frequency modulation and on effects related to the summation of roughness in the conditions of amplitude modulation can be found in this paper.

It should be noted that both mentioned papers by Terhardt are concerned with the classical problem of amplitude modulation, namely modulation of a sinusoidal signal with another sinusoidal signal.

GUIRAO's paper [2] is another paper which deals with roughness in the conditions of amplitude modulation of a sinusoidal signal with another sinusoidal signal and of a narrow noise band with a simple tone. A correlation between the parameters of a modulated signal (especially between modulating frequency and modulation factor) and roughness intensity was sought in this paper. It was stated that roughness is linearly correlated with modulating frequency (in the range 12–55 Hz), and non-linearly correlated with the modulation factor. This refers to tonal as well as noise signals.

Also SCHÖNE's paper [7] is concerned with similar problems. Among others it presents difference limens of amplitude modulation. However, here these limens are investigated with respect to investigations of amplitude fluctuation intensity of an amplitude modulated signal.

However, unlike in paper [2] SCHÖNE did not deal with roughness, but with amplitude fluctuation intensity only. He applied modulating frequencies from the range 1–10 Hz. Among others Schöne stated that amplitude fluctuation intensity is independent from the intensity level of a signal and from modulating frequency. In this range of modulating frequencies the amplitude fluctuation intensity is linearly correlated with the modulation factor, i.e. every increment of the modulation factor (defined here as $d = L_{max} - L_{min}$, where L_{max} and L_{min} denote the maximum and minimum pressure level of the signal, respectively) causes a proportional increment of fluctuation intensity.

It should be stressed that Schöne performed his studies for several discrete values of the reference amplitude modulation factor which do not exhaust the full range of modulation variability, especially for $m > 0.75$. The greatest value was equal to 75%.

Also FASTL's paper [1] is concerned with the evaluation of fluctuation intensity of signal amplitude. His research was aimed at the evaluation amplitude fluctuation intensity of a wide noise band amplitude modulated by a tone in terms level of the intensity level, amplitude modulation factor and modulating frequency. Fastl stated that an increase of amplitude fluctuation intensity accompanies an increase of the modulating frequency and reaches a maximum for $f_m = 4$ Hz. An increase of the intensity level in the range 40 – 80 dB induces an increase of fluctuation intensity.

Paper [1] states that fluctuation intensity is proportional to the logarithm of the amplitude modulation factor for a noise signal.

It should be particularly noticed that mentioned above papers concerned with roughness and amplitude fluctuations present divergent results, but their general conclusions are rather consistent. Already TERHARDT [8, 9] has noticed this fact and stated that results of such experiments can significantly depend on the choice of reference signal.

The presented above review of literature shows that a majority of papers is concerned with problems of determining perception thresholds of relatively simple

modulation, i.e. a modulation of a sinusoidal signal with another sinusoidal signal, and with problems of evaluation of so-called roughness or signal amplitude fluctuations. Therefore it seems useful to carry out research on the determination of difference limens of amplitude modulation for spectrally more complex carrier signals. Thus, achieved results could be referred to evaluation criteria of room quality from the point of view of speech intelligibility given in paper [4].

3. Temporal and spectral structure of a noise band amplitude modulated by a tone

The calculation of the spectrum of a modulated signal is simple in the case of amplitude modulation of a sinusoidal signal, because it is based on simple trigonometric transformations. This simple mathematical procedure can not be applied to determine the spectrum of modulated random signals (irregular), because there is no analytic form of the temporal function of such signals. The spectral structure of this type of signals is derived on the basis of the theory of the autocorrelation function and the Wiener-Chińczyn theorem.

Let us consider a white noise band described with function $S(t)$ with power spectral density $G_s(\omega)$,

$$G_s(\omega) = \begin{cases} G_s \text{for } \omega_{\min} < \omega < \omega_{\max} \\ 0 \text{ for other } \omega \end{cases}. \tag{1}$$

Let us assume that signal $S(t)$ is amplitude modulated by a sinusoidal function $b(t)$

$$b(t) = B\cos\omega_m t \tag{2}$$

where

$$\omega_m < \omega_{\min}.$$

Furthermore, let us assume that this signal is a stationary ergodic process with mean value equal to zero and root-mean-square value σ. In order to determine the power spectral density of a signal under consideration, first of all we have to determine its autocorrelation function and then use the Wiener-Chińczyn theorem. In consequence, the power spectral density for a band noise modulated with a tonal signal can be noted as follows:

$$G_a(\omega) = G_s(\omega) + \frac{1}{2}k^2B^2[G_s(\omega-\omega_m) + G_s(\omega+\omega_m)], \tag{3}$$

where G_s power spectral density of carrier signal, B and ω_m is the amplitude and pulsation of modulating signal, respectively.

It results from expression (3) that power spectral density of a noise signal amplitude modulated with a tone consists of three bands. The central band is the carrier band, while two sidebands which lie symmetrically with respect to the central band at a distance equal to the value of modulating frequency from it are

modulation products. Mentioned three bands overlap at small values of modulating frequencies.

The problem of defining the measure of modulation is an important problem in the discussion of the temporal and spectral structure of modulated noise signals. The modulation factor is such a measure in classical considerations, i.e. in the case of modulation of a sinusoidal signal with another sinusoidal signal. It has the following form

$$m = \frac{kB}{A_0}, \tag{4}$$

where B and A_0 are amplitudes of modulating and carrier signal, respectively, and k is the apparatus constant. In the case under consideration, when value m is determined for an amplitude modulated noise, expression (4) can not be applied directly. The m_{sk} quantity which expresses the ratio of root-mean-square values of the modulating and carrier signal was accepted as the measure of modulations

$$m_{sk} = k \cdot \sqrt{\frac{B^2}{\sigma^2}}, \tag{5}$$

where B – amplitude of modulating signal, σ – root-mean-square value of carrier signal, k – apparatus constant.

Achieved threshold values or their differences will be expressed with this quantity, m_{sk}, in the further part of this paper.

It should be added that apart from presented here analytical expressions which enable the determination of spectral density of a modulated noise, also an experimental spectral analysis of modulated noise was performed. This analysis fully confirmed obtained theoretical data.

4. Aim of research, apparatus and measurement methods

Undertaken research was aimed at the determination of difference limens of amplitude modulation of white noise octave bands, performed with sinusoidal signals with chosen frequencies, the reference of these limens to values of the STI which determine the quality of a room from the point of view of speech intelligibility.

The block diagram of the applied apparatus is presented in Fig. 1. White noise generated by noise generator – 1, subjected to filtration in an octave filter – 2 with adequate mid-band frequency f_c and fed to modulator – 6, was the carrier signal. A sinusoidal function generated by generator – 3 was the modulating signal. It was supplied to the switching device – 5 which by turns attached it directly to the modulator and a so-called reference signal was obtained, or indirectly to the modulator through a system of potentiometers – 7,8 and then a test signal was obtained. The listener could set a definite value of the modulation index for a signal

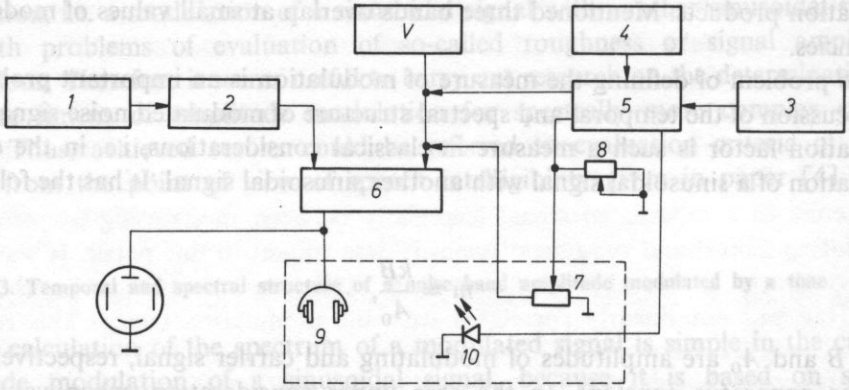

Fig. 1. Block diagram of measuring apparatus. 1 – noise generator, 2 – octave filter, 3 – tone generator, 4 – pulse generator, 5 – switching device, 6 – modulator, 7, 8 – potentiometers, 9 – earphones 10 – diodek

with a potentiometer – 7. This value was signalled with a diode – 10. The switching device – 5 was controlled with a signal from the pulse generator – 4 which generated a symmetric rectangular signal.

The described above set-up could be used to obtain pairs of signals containing a reference signal with a constant value of the modulation index m and test signal with modulation index regulated by the listener.

Duration times of test signals and reference signals were identical and were equal to 2, 3 seconds.

The following four white noise octave bands with mid-band frequencies $f_c = 250$, 500, 1000, 2000 Hz and seven various frequencies of the modulating tone: $f_m = 1, 2, 4$, 8, 16, 32, 64 Hz were applied in performed research. The level of acoustic pressure of the modulated signal was constant and equal to 75 dB (SPL). Difference limens were determined for the following amplitude modulation indexes of the reference signals: $m_w = 25\%$, 50%, 75% 100%. For comparative reasons also measurements of classical threshold of amplitude modulation were carried out in the same cycle of experiments with the same methods and in the same apparatus.

Applied research methods are a certain modification of the adjustment method and method of limits [11]. In the course of experiments listeners compared the following pairs of signals consisting of a reference signal with a constant value of modulation factor and test signal with a modulation factor regulated within the range from zero to the value set in the reference signal.

Two separate series of measurements were performed: ascending series (↑) in which the listener was to increase gradually the amplitude modulation factor in the test signal from zero to a moment in which the test signal and reference signal were identical in his assessement; descending series (↓) in which the listener was to decrease gradually the amplitude modulation factor in the test signal from the value set in the reference signal to the moment when the test signal and reference signal differed insignificantly (on threshold level).

Every threshold value was determined on the basis of five ascending series and five descending series. Then threshold values averaged for these series were statistically tested with the F-Snedecor test, the compatibility test and the test of ranks sum at the significance level $\alpha = 0.05$. Tests gave a positive result for a majority of data, whereas in a case of negative test results measurements were supplemented with additional two series.

Thanks to statistic testing results of both series could be considered jointly, and mean values and standard deviations could be determined for them.

Two listeners with audiologically normal hearing participated in experiments.

5. Research results and their analysis

5.1. Thresholds of amplitude modulation

In the first place classical amplitude modulation thresholds were determined. They are presented in Figs. 2 and 3 for listeners EO and AS, respectively. The threshold value of the amplitude modulation factor m, in percentage, is expressed in terms of modulating frequency f_m. The midband frequency of a noise octave band (carrier signal) is the parameter of these curves.

It can be seen from these figures that two independent ranges in determined thresholds can be separated in terms of the value of modulating frequency. Modulation thresholds are constant, independent from modulating frequency with an accuracy of confidence interval (marked by a vertical line) for a modulating frequency range up to approximately 16 Hz. This is the so-called "follow-up" range in which the organ of hearing follows-up with temporal changes of signal intensity, i.e. its successive minima and maxima. These changes take place relatively slowly, so the

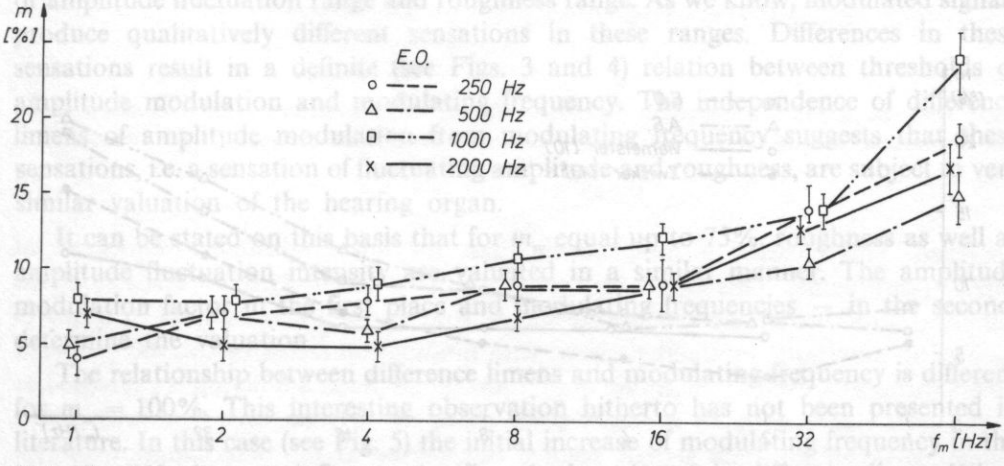

Fig. 2. Thresholds of amplitude modulation of a noise octave band versus modulating frequency for listener EO. The mid-band frequency of the noise octave band is the parameter of these curves

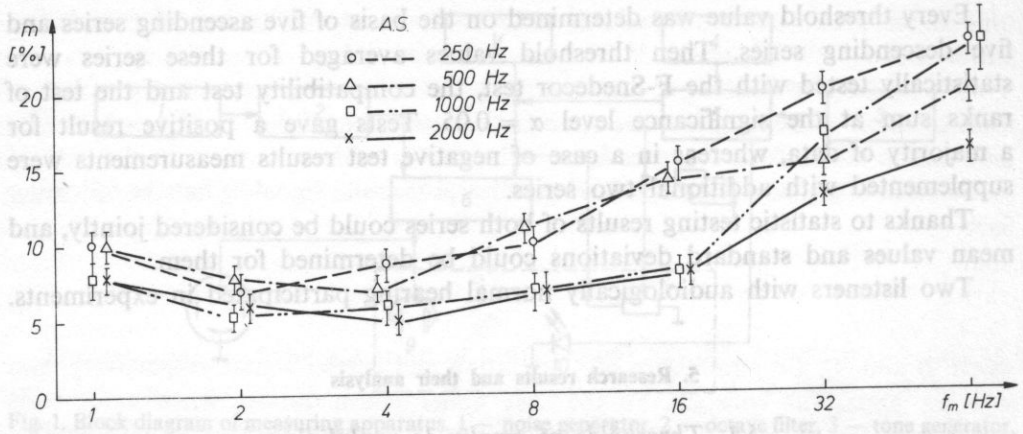

Fig. 3. Thresholds of amplitude modulation of a noise octave band versus modulating frequency for listener *AS*. The mid-band frequency of the noise octave band is the parameter of these curves

so-called temporal mechanism of the organ of hearing can be accepted responsible for their perception in this range.

In the range from 16 to 64 Hz an increase of the value of the modulation factor *m* greater than it was stated in the range up to 16 Hz is observed to accompany an increase of modulating frequencies. This is the so-called roughness range in which the ear no longer follows-up with temporal changes of signal intensity, because of a too great modulating frequency. The spectral structure of the modulated signal is the decisive factor in this case.

Achieved relationships between thresholds and modulating frequency were compared with analogical relationships presented by VIEMEISTER [10], and ZWICKER and FELDTKELLER [13] and shown in Fig. 4. Results obtained by the authors of

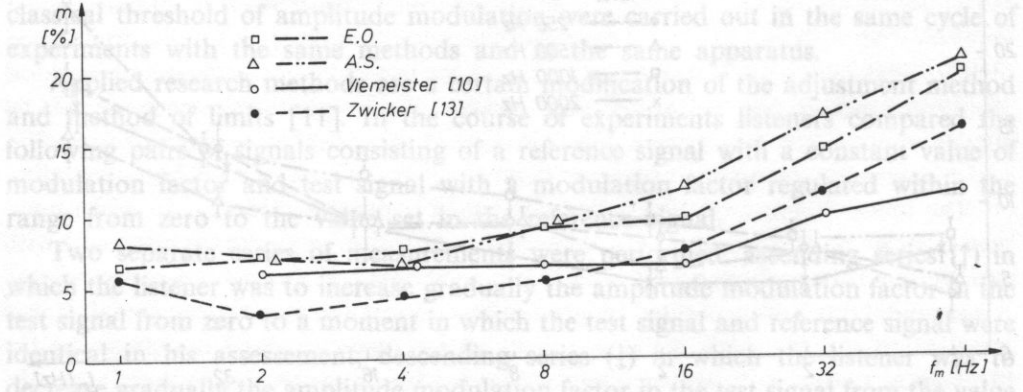

Fig. 4. A comparison of threshold of amplitude modulation in terms of modulating frequency achieved by various authors

this paper, shown in this figure, present average values of the amplitude modulation factor for a noise octave band, whereas VIEMEISTER'S results [10] and ZWICKER'S-FELDTKELLER'S results [13] refer to broad-band noise. A good consistency of results can be observed in the range of low modulating frequencies, which do not exceed 16 Hz.

Whereas, for frequencies $f_m > 16$ Hz, obtained threshold increments are much larger than values given in papers [10, 13]. This discrepancy results from the fact that results in papers [10, 13] refer to a broad-band noise, while results of research carried out by the authors of this paper refer to octave bands.

However, generally it can be stated that obtained values of amplitude modulation thresholds are consistent with data published in literature and they confirm the so-called "narrow-band" hypothesis of amplitude modulation perception given by VIEMEISTER [10].

5.2. *Difference limens of amplitude modulation*

The fundamental part of research was concerned with the determination of difference limens of amplitude modulation. It was aimed at the determination of the smallest, just noticeable difference between a reference signal with a set value of the modulation factor, $m_w = 25, 50, 75, 100\%$ and test signal in which the value of this factor could be changed in a range from 0 to m_w.

Research results for noise octave bands with mid-band frequencies $f_c = 250, 500, 1000, 2000$ Hz are presented in Fig. 5 a for listener EO and in Fig. 5b for listener AS. It results from Fig. 5 that difference limens for $m_w = 25, 50, 75\%$ are approximately independent of the modulating frequency from the band 1–64 Hz for both listeners. This is a rather surprising fact, because the mentioned modulating frequency range includes two characteristic perception ranges of modulated signals, i.e. the follow-up or amplitude fluctuation range and roughness range. As we know, modulated signals produce qualitatively different sensations in these ranges. Differences in these sensations result in a definite (see Figs. 3 and 4) relation between thresholds of amplitude modulation and modulating frequency. The independence of difference limens of amplitude modulation from modulating frequency suggests that these sensations, i.e. a sensation of fluctuating amplitude and roughness, are subject to very similar valuation of the hearing organ.

It can be stated on this basis that for m_w equal up to 75%, roughness as well as amplitude fluctuation intensity are valuated in a similar manner. The amplitude modulation factor in the first place and modulating frequencies – in the second, determine the valuation.

The relationship between difference limens and modulating frequency is different for $m_w = 100\%$. This interesting observation hitherto has not been presented in literature. In this case (see Fig. 5) the initial increase of modulating frequency in the range 1–16 Hz does not influence significantly the value of the difference limen. When f_m exceeds the value of approximately 16 Hz a distinct increase of the threshold is

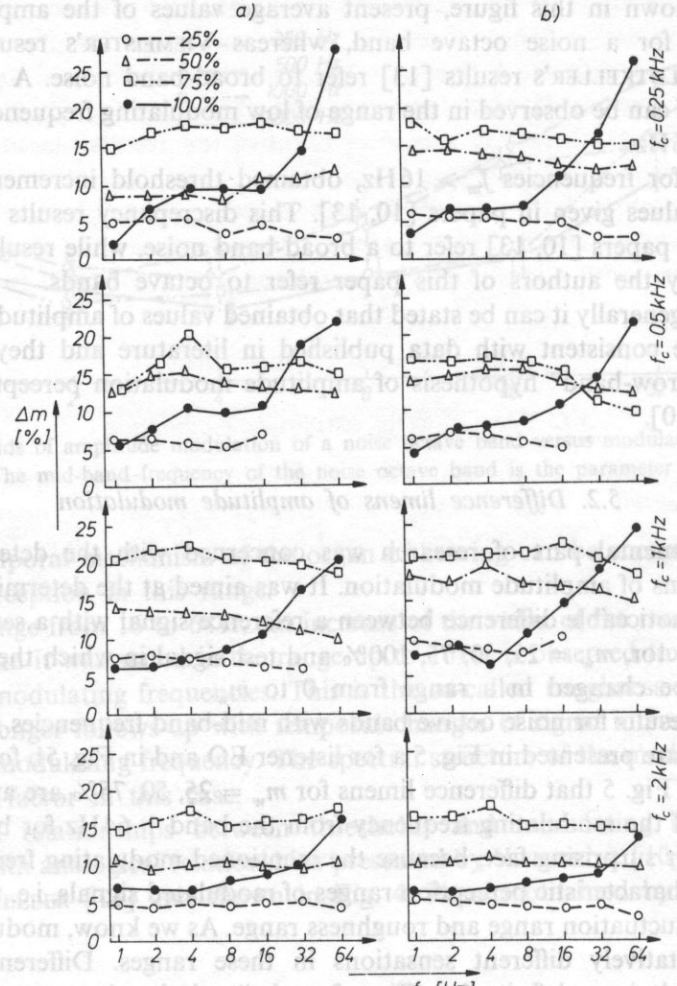

Fig. 5. Difference limens of amplitude modulation for various mid-band frequencies of noise octave bands. The modulation factor of the reference signal is the parameter of these curves: a) — for listener EO, b) — for listener AS

observed. This increase is quite considerable for lower mid-band frequencies of carrier noise bands. This effect can be explained on the basis of an analysis of the temporal structure of the modulated signal. And so the intensity level in terms of time of an amplitude modulated signal with modulation factor below 100% always differs from zero, even at minimum amplitude values. Such a function is percepted as a constant signal with an intensity level changing in time. Investigations of the difference limen for such signals resolve themselves to the determination of just noticeable difference between the reference signal and test signal. This difference can be determined on the basis of the difference of intensity levels in the range of maxima

and minima of this signal, or on the basis of the evaluation of the changes of its dynamics, i.e. simultaneously on the basis of the level difference in maxima and minima.

However, for a case of the amplitude modulation factor of a reference signal equal to 100%, the perception of such a signal is completely different. This results from the fact that at a maximum of the amplitude of a signal with 100% modulation its intensity level considerably differs from zero, while at a minimum of the amplitude the intensity level of this signal is close to zero. Therefore, research of modulated signals is qualitatively different in the perception process for signals with $m_w = 100\%$ and signals with $m_w < 100\%$, in spite of the fact that these signals belong to the same class of modulated signals.

It is also worth noticing that in accordance with Fig. 5, a distinct increase of the difference limen level accompanies the increase of value m_w up to $m_w \leqslant 75\%$.

On the basis of data presented in Fig. 5 it can be assumed that difference limens of amplitude modulation are approximately constant and independent from modulating frequency for $f_m < 16\,\text{Hz}$, i.e. for the so-called "follow-up" range (i.e. amplitude fluctuations).

On this basis these limens were averaged with respect to modulating frequency in the range 1–16 Hz. So obtained functions are presented in Figs. 6 and 7 for listeners EO and AS, respectively. The mid-band frequency of noise octave bands was the parameters of these curves. These figures present also results of certain additional research on difference limens of amplitude modulation carried out in the range of m_w from 75–100% for a noise octave band with mid-band frequency equal to 1000 Hz. These additional studies were to give a more accurate determination of the position of the limen value maximum in terms of function f_m.

It results from Figs. 6 and 7 that an increase of the amplitude modulation factor of a reference signal in the range from zero to 75% causes an approximately linear

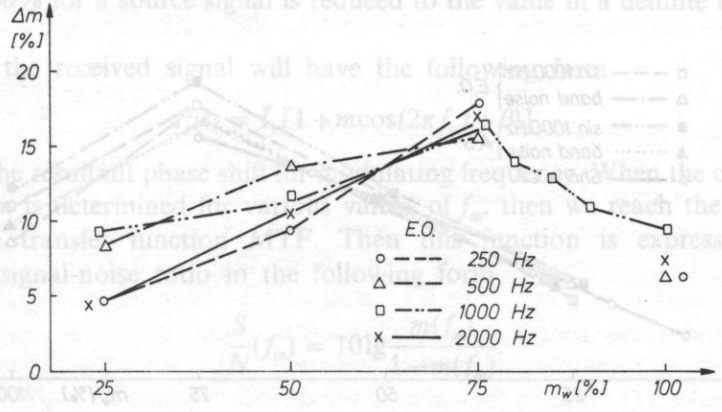

Fig. 6. Values of difference limens averaged with respect to modulating frequencies versus amplitude modulation factor m_w, for listener EO.

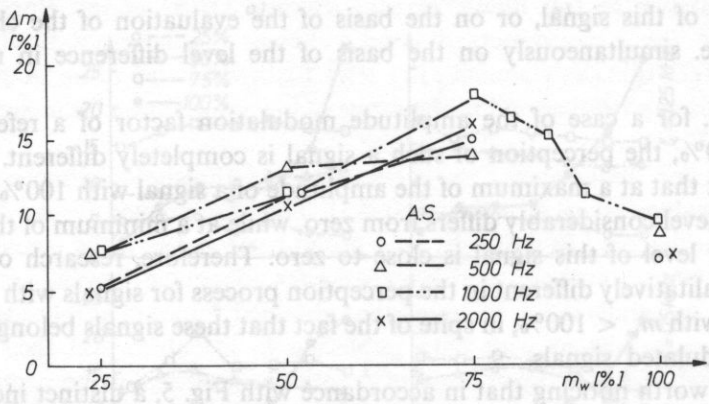

Fig. 7. Values of difference limens averaged with respect to modulating frequencies versus amplitude modulation factor m_w, for listener AS

increase of difference limens up to a maximum in the range $m_w = 75\%$. A further increase of m_w values above the value of 75% induces a considerable decrease of difference limens.

An analysis of data presented in Figs 6 and 7 proves also that in principle difference limens of amplitude modulation are independent from the mid-band frequency of the carrier noise band. On this basis these limens were averaged with respect to mid-frequency of noise bands. Fig. 8 presents the result of averaging for individual listeners. It also shows difference limens of amplitude modulation of a tonal signal with frequency $f_c = 1000\,\text{Hz}$, and results of SCHÖNE's research [7].

It results from Fig. 8 that difference limens of amplitude modulation do not depend on the type of carrier signal. This statement corresponds with FASTL's conclusion [1], according to which the fluctuation intensity of a tone and noise band are governed by similar principles. It also results from the figure that difference

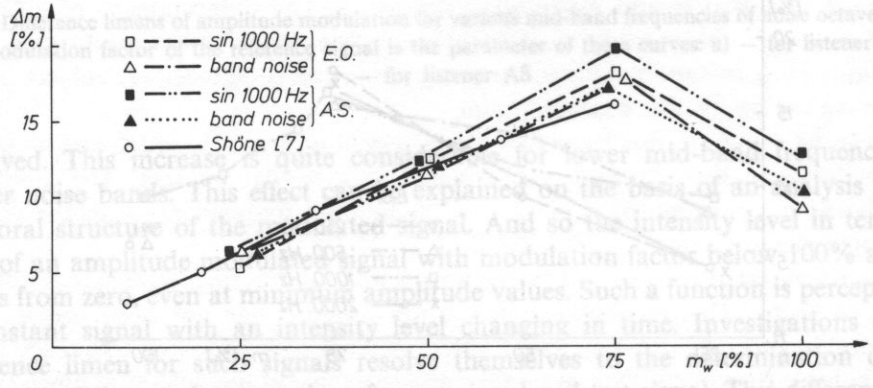

Fig. 8. A comparison of averaged difference limens of a noise and tonal signal, achieved by the authors with results of SCHÖNE research [7]

limens of amplitude modulation are linearly correlated with amplitude modulation factor m_w in the range of m_w up to 75%. A regression analysis performed in this range proves that this dependence can be noted analytically as follows

$$\Delta m = 0.24 \cdot m_w. \tag{6}$$

SCHÖNE [7] in such case reached a dependence: $d_{DL} = 0.3 \cdot d$ where $d = L_{max} - L_{min}$, L_{max} and L_{min} denote respectively the maximum and minimum level of acoustic pressure. A difference in the numerical coefficient results from the fact that expression (6) presents linear quantities, while Schöne's relation presents logarithmic quantities.

5.3. *Difference limens of amplitude modulation related to the index of speech intelligibility in a room (The* RASTI *method)*

In the course of further studies achieved difference limen values were related to the index of speech intelligibility in a room. As we know, such intelligibility is an important criterion of room acoustic quality. During the last several years an interesting method of speech intelligibility measurement in a room was developed. It is called the RASTI method [5]. This method is based on the determination of the so-called modulation transfer function MTF for a given room. It is characteristic for the MTF that the value of the modulation factor of a noise signal is decreased on its path from the sound source to the microphone [4]. A white noise band with a definite mid-band frequency and a 100% modulation factor was the test signal in this method

$$I(t) = \bar{I}(1 + \cos 2\pi f_m t), \tag{7}$$

where f_m is the modulating frequency.

Due to the room's reverberation and the interfering noise, the modulation factor equal to 100% for a source signal is reduced to the value in a definite measurement point.

Hence, the received signal will have the following form

$$I_r(t) = \bar{I}_r[1 + m\cos(2\pi f_m t + \theta)], \tag{8}$$

where θ is the resultant phase shift for modulating frequency. When the change of the coefficient m is determined for various values of f_m, then we reach the form of the modulation transfer function MTF. Then this function is expressed with an equivalent signal-noise ratio in the following form

$$\frac{S}{N}(f_m) = 10\lg\frac{m(f_m)}{1 - m(f_m)}. \tag{9}$$

As a result of a certain limitation of the variability of quantity S/N (f_m), its averaging in the whole interval of frequency f_m and certain standarization, we achieve

the so-called sound transmission index STI

$$\mathrm{STI} = \frac{\frac{S}{N} + 15}{30}. \tag{10}$$

A special measurement method, called RASTI (Rapid STI), is used to calculate the value of this index.

According to the authors of this method the STI is an objective measure of speech intelligibility in a room. This is illustrated in Fig. 9[4]. Values of speech

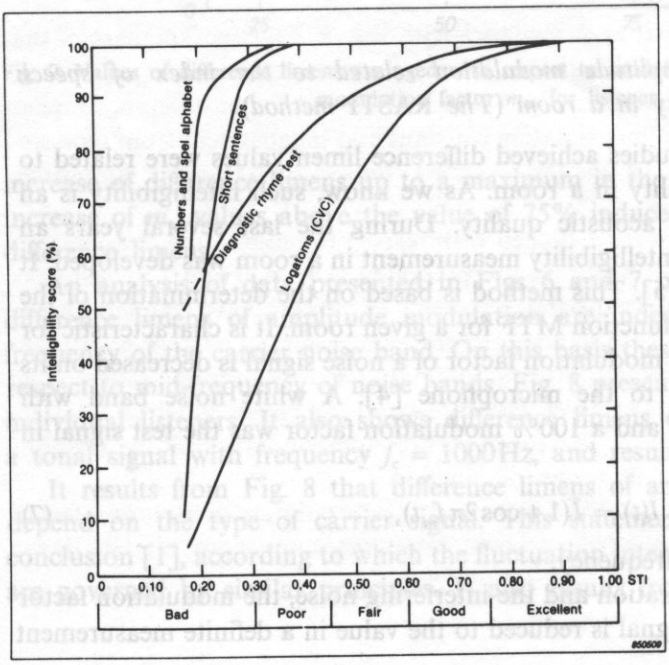

Fig. 9. Relationships between speech intelligibility expressed in percentages and the STI for various test signals [4]

intelligibility in percentage, determined subjectively by listeners which participated in the experiment, are marked on the Y-axis and standarized values of the STI which change from 0 to 1 are marked on the X-axis. A classification scale of room quality from the point of view of speech intelligibility is given below the axis of abscissae. It varies from bad to excellent. This classification corresponds to intervals equal to 0.15 STI in the middle STI variability range. This means that a change of the STI value of a signal measured in a room with 0.15 is clearly perceptible by the listener and significantly influences speech intelligibility evaluation.

With regard to research presented in papers [4, 5] it is interesting to relate the mentioned above STI value to the value of the difference limen for $m_w = 100\%$. This limen expresses the smallest change of the value of m (amplitude modulation factor), just noticeable by the listener.

In order to relate these values, the value of the difference limen for $m_w = 100\%$ had to be expressed in STI units. To this end, values of $\frac{S}{N}(f_m)$ were calculated according to expression (9) for the white noise octave bands with mid-band frequencies equal to 500 and 2000 Hz, and for successive modulating frequencies f_m from the range 1–16 Hz. Then the variability range of the $\frac{S}{N}(f_m)$ value was reduced to an interval $\pm$ 15dB in accordance with expression (10) and the mean value of this quantity was calculated for all f_c and f_m. A difference value equal to 0.16 STI was achieved from formula (10) for $m_w = 100\%$. This means that the listener can univocally state amplitude changes in the modulated test signal at STI values $\geqslant 0.16$. This considerable value of the difference limen does not confirm the conclusion resulting from paper [5], according to which STI changes of about 0.15 radically influence speech intelligibility in a room, i.e. speech sounds have to be univocally percepted by the listener.

It is also worth noticing that in accordance with Fig. 8 the perception of threshold amplitude changes of an amplitude modulated signal depends significantly on the value of the modulation factor of the reference signal (i.e. the m_w value). Therefore, it would be interesting to relate achieved values of difference limens (for $m_w < 100\%$) to changes of the amplitude ("modulation") occurring in real speech signals in further research.

References

[1] H. FASTL, *Fluctuation strength and temporal masking patterns of sinusoidally amplitude-modulated broad-band noise*. Hear. Res. **8**, 59–69 (1982).

[2] M. GUIRAO, J. M. GARAVILLA, *Perceived roughness of amplitude modulated tones and noise*, JASA, **60**, 1335-1338 (1976).

[3] T. HOUTGAST, H. J. M. STEENEKEN, *A review of the MTF concept in room acoustic and its use for estimating speech intelligibility in auditoria*, JASA, **77**, 1060-1077 1985.

[4] T. HOUTGAST, H. J. M. STEENEKEN, *The modulation transfer function in room acoustics*, Tech. Rev. No. 3, 1985.

[5] H. J. M. STEENEKEN, T. HOUTGAST, RASTI – *A tool for evaluating auditoria*, Tech. Rev. No. 3, (1985).

[6] E. OZIMEK, A. SĘK, *Perception of amplitude and frequency modulated signals (Mixed modulation)*, JASA, **82**, 5, 1598-1603 (1987).

[7] R. SCHÖNE, *Messungen zur Schwankungsstärke von amplituden-modulierten Sinustönen*, Acustica **41**, 4, 252–257 (1979).

[8] E. TERHARDT, *On the perception of periodic sound fluctuations (Roughness)*, Acustica **30**, 201–213 (1974).

[9] E. TERHARDT, *Über akustische Rauhigkeit und Schwankungsstärke*, Acustica **20**, 213–224 (1968).

[10] N. F. VIEMEISTER, *Temporal modulation transfer function based upon modulation thresholds*, JASA, **66**, 5, 1364–1380 (1979).

[11] R. S. WOODWORTH, H. SCHLOSBERG, *Experimental psychology* (in Polish), PWN, Warszawa 1963.

[12] E. ZWICKER, *Die Grenzen der Horbarkeit der Amplitudemodulation und Frequensmodulation eines Tones*, Acustica, **2**, 3, 125–133 (1952).

[13] E. ZWICKER, R. FELDTKELLER, Das Ohr als Nachrichten-empfänger, S. Heinel Verlag, Stuttgart 1967.

Received August 26, 1986.

ARCHIVES OF ACOUSTICS
12, 3-4, 291-299 (1987)

A PHYSIOLOGICAL EVALUATION OF THE EFFICIENCY OF PLAYING THE WIND INSTRUMENTS – AN AERODYNAMIC STUDY

ZYGMUNT PAWŁOWSKI, MAREK ŻÓŁTOWSKI

Phoniatry Department, Frederic Chopin Music Academy
(00–368 Warsaw, Okólnik Street 2)

The purpose of this study was to present mean values of particular aerodynamic parameters to determine the physiological standard of playing. The authors applied the aerodynamic method in examinations of musicians playing the orchestral wind instruments. Direct results of the measurements for each person were the following quantities: the pressure before the instrument inlet (SP), the mean air flow rate (MFR) through the mouthpiece or the reed, and the play time (MPT). On the basis of these quantities, the lips or reed resistance (GR), the expiration power (EP) and the work performed during playing (S) were calculated. The measured results were so elaborated that the measured results were calculated separately for those persons for whom the play time was no less than the mean time of persons playing the same instrument. For such a division of the examined persons, the mean values of the aerodynamic parameters were calculated. The efficiency of playing is essentially affected by the value of the lips or reed resistance (GR).

1. Introduction

This paper is concerned with the set of the values of aerodynamic parameters occurring for musicians as they play the wind instruments. In 1981–1985, the present authors carried out clinical studies, using a purpose-modified aerodynamic method [3, 4]. This method made it possible to register and then calculate the occurring parameter values, namely the maximum play time (MPT), the air pressure before the instrument inlet (SP), the mean air flow rate (MFR) through lips or the reed, the lip or reed resistance (GR), the expiration power (EP) and the work performed in the course of the play (S).

In previous publications, the present authors described the aerodynamic method [3, 4], chosen problems related to the aerodynamics of playing [5] and the phenomenon of initiation, i.e. the sound formation [6]. These papers also considered the hyperbaric phenomenon significant for the activity and efficiency of the

The work was supported by the Polish Academy of Science Project MR.I.24.IX.10

musicians' respiratory organ. It has been shown that there is a defensive automatism of the respiratory organ during playing, consisting in the compensation of the large value (100 cm H_2O) of the air pressure during playing in forte and at a high frequency (trumpet). Therefore, we should believe that, apart from other factors, such as age, allergy, nicotinism [2], the compensation phenomenon makes it possible to continue the long-term work of musicians without the occurrence of symptoms of emphysema.

The present authors believe that the presented mean values of the aerodynamic parameters should serve in elaborating physiological standards for playing the wind instruments, within the limits assumed for the population in Poland. Because of lack of literature on the subject, the present study may contribute to the undertaking of further research.

2. Selected literature review

Results of spirometric examinations carried out on instrumentalists [2], collected from various points of view, are uniform for the group of those who play the same instrument. No characteristic changes were found in terms of age groups or the number of years of playing.

It is interesting to note ventilation changes. A large percentage of the examined persons exhibit obstructive ventilation changes characteristic of increased resistance of the respiratory tract. On the other hand, no changes of restrictive type were found, which would result from increased resistance of lung tissue.

Obstructive changes occur in 80% of the examined young and middle-aged persons aged between 20 and 40. On the other hand, in elder persons, aged between 40 and 60, ventilation changes occurred in 58% of cases. This is probably caused by the fact that professional instrumentalists in whom, when they were still young, large ventilation changes occurred, had to abandon their profession. Apart from other factors, such as nicotinism or chronic catarrh of bronchi, the symptoms of ventilation insufficiency are to a deciding degree caused by the way of playing a given wind instrument. It seems that the age of the examined persons is of greater significance than the duration of professional work.

Problems related to the technique of hyperbaric breathing [7, 8] have been the object of numerous studies. In hyperbaric condition the lung pressure is greater than that in normal conditions and depends on the diver's submersion depth under water, the gas flow intensity and the kind of used respiration mixture. Respiratory hyperpressure consists in supplying a mixture of respiratory gases to the respiratory tract under increased pressure, i.e., one greater than that of the ambient atmosphere, to increase the molecular pressure of oxygen.

It follows from studies carried out by A. MURAS [1] that an increase in pressure in musicians' lungs during playing the wind instruments occurs only in the expiratory phase as it is considerable but short compared with hyperpressure occurring in divers. Hyperpressure in divers' lungs in hyperbaric conditions occurs in

two respiration phases, and has a long-term effect, because of changes of respiratory gas distribution which it causes.

It follows from the results obtained by the authors [5] for the values of aerodynamic parameters concerned with the technique of hyperbaric respiration that there is a compensation for a rapid increase in the lung pressure. This pressure is necessary for the intonation of a sound with given pitch and intensity.

3. Assumptions and purpose of the study

Because of some operational mechanisms have not been determined in detail, it is necessary to analyze the cooperation between the respiratory and articulatory organs, namely the actions of the tongue and lips in playing the wind instruments. The results obtained from both experimental and clinical researches would provide the basis for elaborating the optimum standards (physiological standards of playing). These standards would make it easier to ensure diagnosis in considering cases of insufficiency of the respiratory and articulatory organs in the teaching process. The characteristics of playing the wind instruments have been presented in the literature above all from the points of view of aesthetics, playing technique, educational problems, choice of repertoire in the course of education etc.

Phoniatric problems are related above all to the explanation of the physiological mechanism of sound formation, i.e., the cooperation of the functions of the respiratory and articulatory organs. Quite purposefully, the authors do not consider the problem of cooperation between playing and the functions of the central nervous system and the hearing organ – as it will be the object of further studies.

The purpose of this study is to analyze the mutual dependence of aerodynamic parameters. An ideal vibrating system, i.e., one exciting vibrations, which would be characterized by constant resistance independent of the pitch and intensity of sound, would require constant pressure to excite vibrations. Pressure changes would determine those in the vibration amplitude, i.e., in the sound intensity. To change the sound pitch, it would not be necessary to change the pressure before the instrument inlet. A real vibrating system, such as the reed or the mouthpiece of the instrument, varies its resistance, depending on the sound pitch and intensity.

The authors' intention was to determine the values of aerodynamic parameters and the correlations between them in the course of playing.

The purpose of this paper is to present mean values of particular aerodynamic parameters and gain data for determining the physiological standard of playing.

4. Selection of the examined persons and the research method

The study was carried out on a group of students and teachers of the Academy of Music in Warsaw. Moreover, they were performed on professional musicians who applied for medical treatment. In all, 87 persons were examined. The study used the

results for 66. Because of the poor technical quality, resulting from insufficient cooperation with the examined persons, 21 cases were not interpreted.

Prior to the study, general otolaryngological examinations were performed, whose results showed no deviations from normal in the range of interest.

The study was carried out according to the method elaborated and published by the authors [5]. The direct measured results for each person were the quantities: – the pressure before the instrument inlet (SP), the flow rate (MFR) through the mouthpiece or reed, and the play time (MPT). On the basis of these quantities, the lip or reed resistance (GR), the expiration power (EP) and work (S) were calculated.

Apart from theses aerodynamic parameters, sound signals were recorded for further studies. The results of aerodynamic measurements and mean values were computed on a RIAD computer.

5. Results of the study and their interpretation

The results of aerodynamic measurements were elaborated in such a way that the results of measurements for those persons for whom the duration of playing sounds from the lower and upper frequency scale was equal to or longer than the mean play time for persons playing the same instrument were included in the group of persons with normal play time. For such a division of the examined persons, into groups with normal or shorter play times, mean values of aerodynamic parameters were calculated. Quite purposefully, the authors did not include in this publication the standard deviations (SD), on the assumption that the number of persons playing the

Table 1. Mean values of aerodynamic parameters obtained for instrumentalists with normal play time

	flute		clarinet		oboe		bassoon		trumpet		trombone		French horn		tuba	
frequency of play. soun.	c_1	c_4	e	b_3	c_1	c_3	c	c_2	c_1	c_3	F	c_2	c	c_3	F	b_1
MPT [s] P	31,0	12,2	37,4	27,6	32,0	28,0	19,1	28,6	40,0	21,3	17,4	17,0	32,0	23,0	21,0	21,0
MPT [s] F	20,3	8,2	32,5	24,0	31,0	30,0	16,5	18,6	11,2	11,3	15,0	8,5	14,2	0,5	10,5	7,0
SP [cmH_2O] P	4,8	15,7	37,5	24,0	53,4	55,0	39,5	69,8	60,0	82,1	21,2	38,1	22,2	70,8	14,8	74,0
SP [cmH_2O] F	9,0	26,9	51,5	37,0	57,3	68,5	50,2	87,1	48,0	153,8	24,7	53,5	37,5	118,5	40,0	103,0
MFR [1/s] P	0,18	0,53	0,18	0,23	0,19	0,27	0,30	0,20	0,13	0,25	0,44	0,58	0,17	0,25	0,29	0,29
MFR [1/s] F	0,26	0,85	0,21	0,26	0,18	0,20	0,36	0,30	0,47	0,63	0,77	0,91	0,40	0,55	0,59	0,29
GR $\left[\frac{cmH_2O}{1/s}\right]$ P	25,4	40,5	228,0	112,5	326,0	272,0	140,0	388,0	536,0	488,0	48,0	99,6	136,0	299,0	50,0	250,8
GR $\left[\frac{cmH_2O}{1/s}\right]$ F	34,6	36,0	278,0	154,0	336,0	390,5	160,6	305,0	93,0	282,0	59,8	58,8	101,0	235,0	67,4	116,4
EP [W] P	0,10	0,65	0,67	0,54	0,99	1,54	1,13	1,29	0,69	1,51	0,93	2,04	0,37	1,73	0,42	2,14
EP [W] F	0,23	2,80	1,11	0,93	1,02	1,32	1,67	2,5	2,49	9,35	1,69	4,77	1,43	6,15	2,30	8,95
S [kGm] P	0,30	1,00	2,13	1,74	3,53	3,63	2,75	4,92	3,77	4,36	1,97	3,46	1,57	4,91	1,18	5,92
S [kGm] F	0,56	1,87	3,16	2,66	3,81	4,48	3,55	6,12	2,43	8,03	2,24	4,76	2,61	8,24	3,18	8,24

parameters P = piano , F = forte

Table 2. Mean values of aerodynamic parameters obtained for instrumentalists with reduced play time

		flute		clarinet		oboe		bassoon		trumpet		trombone		French horn		tuba	
frequency of play. soun.		c_1	c_4	e	b_3	c_1	c_3	c	c_2	c_1	c_3	F	c_2	c	c_3	F	b_1
MPT[s]	P	14,9	8,6	27,8	16,3	11,7	16,7	13,5	13,8	15,9	19,5	15,2	9,5	19,2	3,1	5,0	5,0
	F	12,2	6,2	17,6	10,6	13,1	14,2	11,3	14,5	8,0	8,15	4,6	5,9	8,0	6,2	2,5	12,0
SP[cmH_2O]	P	4,0	7,0	27,7	25,2	54,0	41,8	21,0	34,2	37,5	64,7	30,3	53,3	49,0	70,0	17,4	42,2
	F	6,7	14,0	29,5	37,3	45,7	60,8	26,3	55,0	60,8	109,7	42,4	87,9	18,8	69,3	26,5	69,3
MFR[l/s]	P	0,39	0,68	0,31	0,41	0,48	0,35	0,50	0,49	0,42	0,29	0,47	0,62	0,30	3,00	1,10	1,10
	F	0,52	0,93	0,49	0,66	0,42	0,44	0,55	0,51	0,70	0,81	1,33	0,93	0,71	1,16	2,20	0,46
GR$\left[\frac{cmH_2O}{l/s}\right]$	P	10,0	10,0	132,0	64,3	96,3	120,0	48,3	78,3	111,0	214,0	76,0	93,4	147,0	52,0	15,8	38,4
	F	18,0	15,0	88,5	57,6	118,0	165,0	53,0	127,0	83,0	159,0	29,0	88,8	24,5	95,0	34,8	151,0
EP[W]	P	0,17	0,53	0,85	1,03	2,27	1,58	0,97	1,57	1,57	2,07	1,35	3,28	1,68	15,50	1,87	4,55
	F	0,28	0,47	1,19	2,90	1,85	2,64	1,66	2,69	4,54	9,90	7,40	8,73	1,42	6,60	16,5	3,11
S[kGm]	P	0,27	0,48	1,94	1,81	2,70	3,51	1,58	2,58	2,46	4,55	2,00	3,53	3,49	4,59	1,20	2,91
	F	0,40	0,95	2,09	2,61	2,86	3,72	1,95	4,19	4,23	7,40	2,78	5,76	1,23	4,57	5,28	4,78

parameters P = piano , F = forte

particular instruments (4 persons on average) could not be considered a full basis for determining the value of scatter. The results are shown in two tables. Table 1 lists value for the normal play time whereas Table 2 does so for those with shorter play time (pathology).

To illustrate better the results and the mutual relations between particular aerodynamic parameters, Fig. 1 lists graphically the results obtained for persons with normal play time and the values with reduces play time (MPT), mean flow rate (MFR) of air through the reed or lips and expiration power (EP).

Interpreting the relations between these three parameters one should pay attention to the following dependencies. It is known that the power (EP) is the product of strength (here, SP) and the flow rate (MFR). Moreover it should be recognized that the person playing an instrument has a limited air volume in his lungs – so an increase in the flow rate (MFR) must be accompanied by a decrease in the play time (MPT). An increase in the expiration power (EP) corresponds to an increase in the air flow rate. Considered for particular instruments and ways of playing in piano and forte, thes dependencies usually provide a logical justification for the increase in the expiration power (EP) and the flow rate (MFR), and the decrease in the time (MPT) of playing sounds in forte. The results listed in Fig. 2 include the values of pressure before the instrument inlet (SP), the lips or reed resistance (GR) and the performed work (S).

The work (S) is proportional to the flow rate and the lips or reed resistance. It is also known that for decreased resistance the keeping of continuous flow would require the corresponding drop of pressure before the instrument inlet (SP). The person playing the instrument can decrease this pressure only to a small degree, to

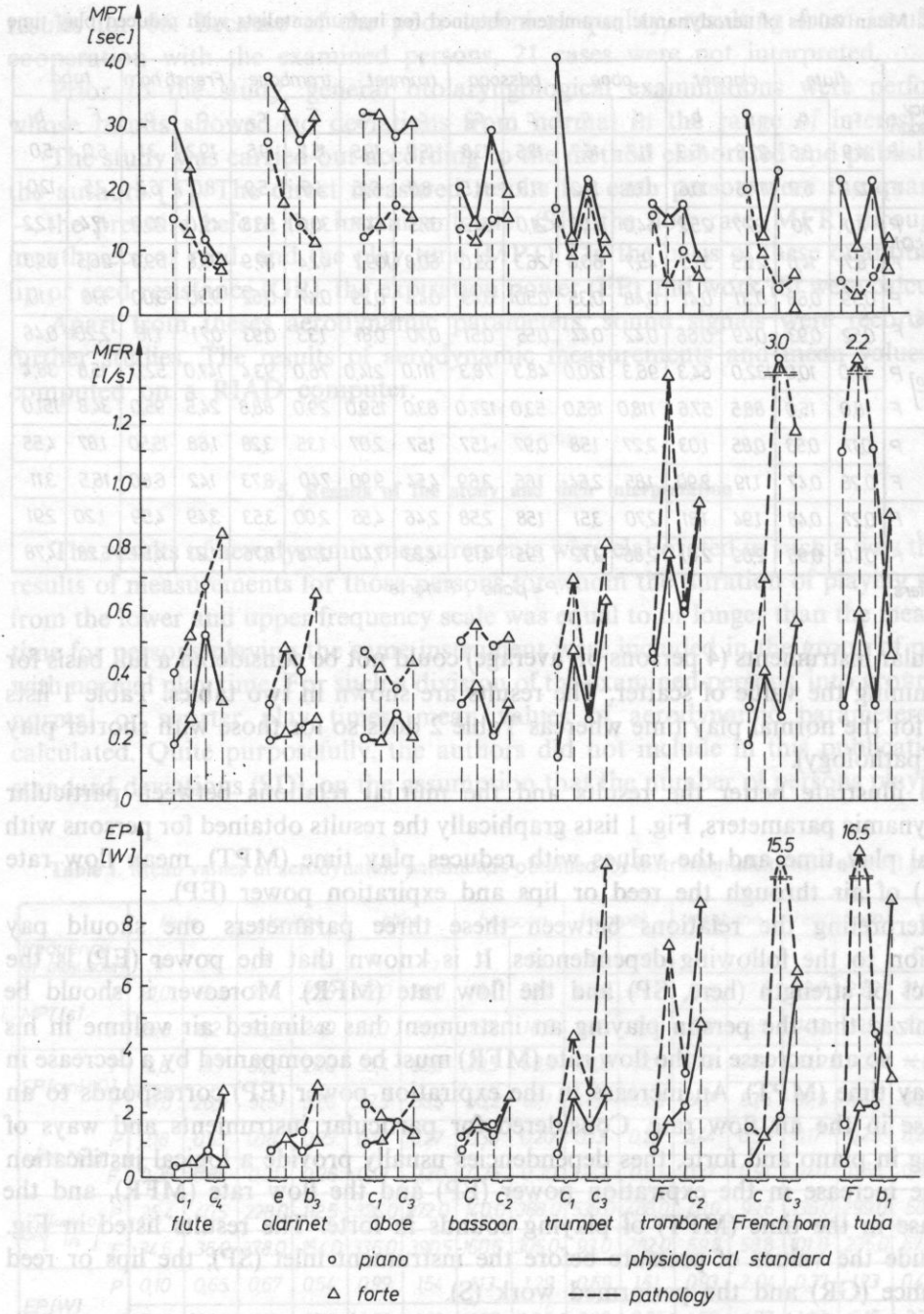

Fig. 1. The values of the maximum play time (MPT), the mean flow rate (MFR) of air through the lips or the reed and the expiration power (EP)

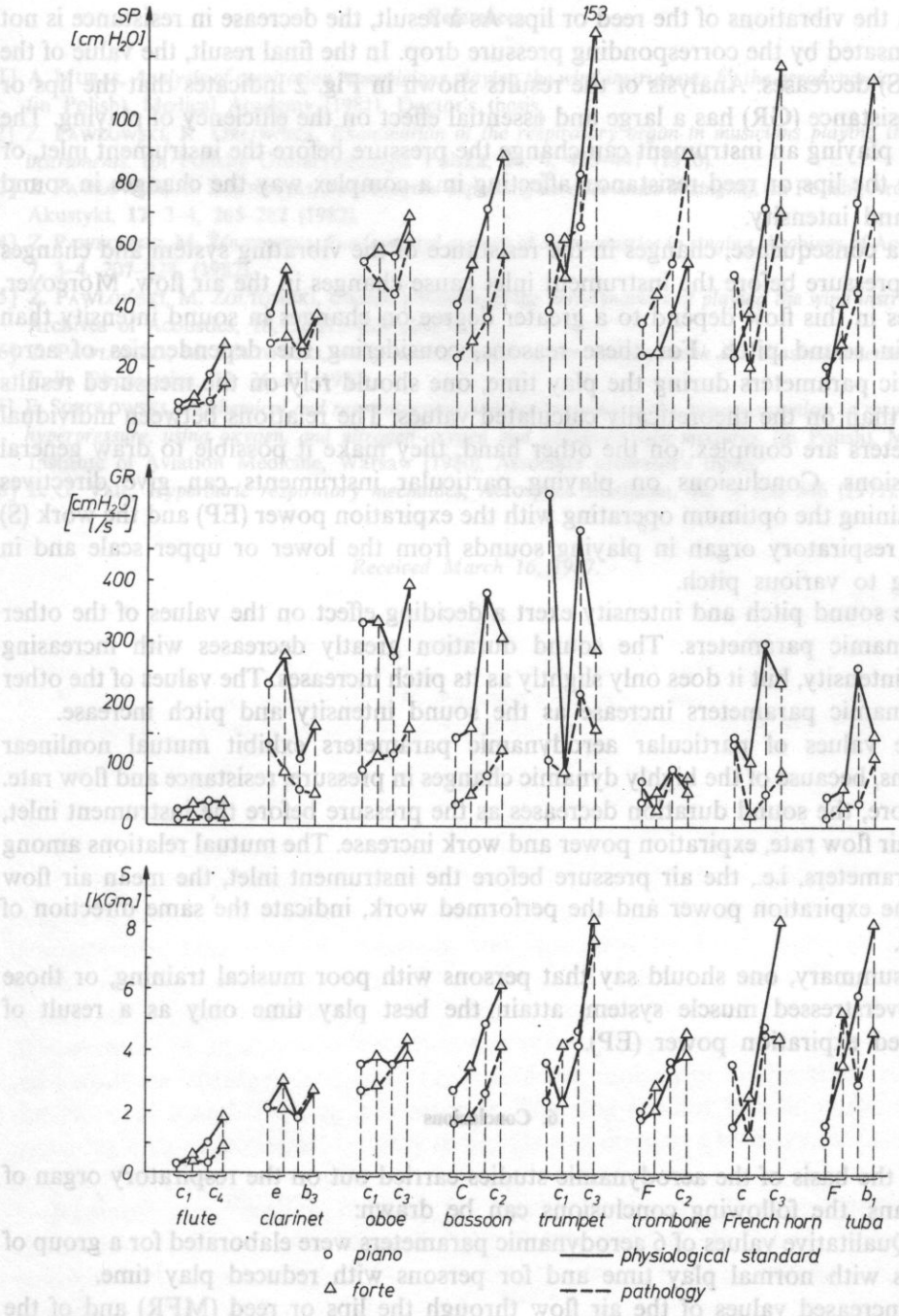

Fig. 2. The values of the air pressure before the instrument inlet (SP), the lips or reed resistance (GR) and the work performed during playing (S)

sustain the vibrations of the reed or lips. As a result, the decrease in resistance is not compensated by the corresponding pressure drop. In the final result, the value of the work (S) decreases. Analysis of the results shown in Fig. 2 indicates that the lips or reed resistance (GR) has a large and essential effect on the efficiency of playing. The person playing an instrument can change the pressure before the instrument inlet, or change the lips or reed resistance, affecting in a complex way the changes in sound pitch and intensity.

As a consequence, changes in the resistance of the vibrating system and changes in the pressure before the instrument inlet cause changes in the air flow. Moreover, changes in this flow depend to a greater degree on changes in sound intensity than those in sound pitch. For these reasons, considering the dependencies of aerodynamic parameters during the play time, one should rely on the measured results rather than on the theoretically calculated values. The relations between individual parameters are complex: on the other hand, they make it possible to draw general conclusions. Conclusions on playing particular instruments can give directives determining the optimum operating with the expiration power (EP) and the work (S) of the respiratory organ in playing sounds from the lower or upper scale and in moving to various pitch.

The sound pitch and intensity exert a deciding effect on the values of the other aerodynamic parameters. The sound duration greatly decreases with increasing sound intensity, but it does only slightly as its pitch increases. The values of the other aerodynamic parameters increase as the sound intensity and pitch increase.

The values of particular aerodynamic parameters exhibit mutual nonlinear relations, because of the highly dynamic changes in pressure, resistance and flow rate. Therefore, the sound duration decreases as the pressure before the instrument inlet, mean air flow rate, expiration power and work increase. The mutual relations among the parameters, i.e., the air pressure before the instrument inlet, the mean air flow rate, the expiration power and the performed work, indicate the same direction of change.

In summary, one should say that persons with poor musical training, or those with overstressed muscle system, attain the best play time only as a result of increased expiration power (EP).

6. Conclusions

On the basis of the aerodynamic studies carried out on the respiratory organ of musicians, the following conclusions can be drawn:

1. Qualitative values of 6 aerodynamic parameters were elaborated for a group of persons with normal play time and for persons with reduced play time.

2. Increased values of the air flow through the lips or reed (MFR) and of the expiration power (EP) occur only for persons exhibiting reduced play time.

3. An increased value of the lips or reed resistance (GR) has an essential effect on the efficiency of playing.

References

[1] A. MURAS, *Analysis of respiration in musicians playing the wind instruments by the aerodynamic method*, (in Polish), Medical Academy (1981), Doctor's thesis.

[2] Z. PAWŁOWSKI, K. ORŁOWSKA, *Examination of the respiratory organ in musicians playing the wind instruments*. (in Polish), Otolaryngologia Polska, **24**, 4, 433–441 (1970).

[3] Z. PAWŁOWSKI, M. ŻÓŁTOWSKI, *Fundamental aspects of aeroacoustics in singing*, (in Polish), Archiwum Akustyki, **17**, 3–4, 265–282 (1982).

[4] Z. PAWŁOWSKI, M. ŻÓŁTOWSKI, *Fundamental aspects of aeroacoustics in singing*, Archives of Acoustics, **7**, 3–4, 207–224, (1982).

[5] Z. PAWŁOWSKI, M. ŻÓŁTOWSKI, *Chosen problems of the aerodynamics of playing the wind instruments*, Archives of Acoustics, **10**, 3, 215–228 (1985).

[6] Z. PAWŁOWSKI, M. ŻÓŁTOWSKI, *Ausgewählte Probleme der Aerodynamik des Blasinstrumentenspiels*, Folia Phoniatrica, **39**, 26–37 (1987).

[7] E. SOKOŁOWSKI, *Biochemical and respiratory-circulatory response of the human organism to respiratory hyperpressure, using oxygen, and nitrogen-oxygen and helium-oxygen mixtures*, (in Polish), Military Institute of Aviation Medicine, Warsaw (1980), Associate professor's thesis.

[8] E. G. VAIL, *Hyperbaric respiratory mechanics*, Aerospace Medicine, **42**, 5, 536–546 (1971).

Received March 16, 1987.

ARCHIVES OF ACOUSTICS
12, 3-4, 301-310 (1987)

A LOW COST SOLID STATE PULSED SYSTEM FOR ULTRASONIC VELOCITY AND ABSORPTION MEASUREMENT

P. K. AGNIHOTRI

Dept. of Physics, Vidarbha Mahavidyalaya
(Amravati – 444 604 India)

C. S. ADGAONKAR, C. Y. BEDARE

Dept. of Physics, Institute of Science
(Nagpur – 440 001, India)

An instrument is described to generate and detect pulsed ultrasonics. The instrument should be useful for ultrasonic measurements in gases for teaching laboratories and for research purpose because of its low cost and ease of construction.

The instrument is tested for ultrasonic wave velocity and absorption in air at frequency 40 kHz and at atmospheric pressure. The results are very much satisfactory.

1. Introduction

Ultrasonic generators are of two types. The first are those designed mainly for industrial flaw detection, produce a sharp voltage pulse of pulse width of few tens of nanoseconds. This type of technique was discussed by G. A. FORSTER [1]. The second are those designed mainly for research purpose where radio frequency pulse is used to ring the transducers of the same frequency. More advanced technique for measurement of ultrasonic attenuation was reviewed by DIGNUM [2]. He concentrated mainly on ultrahigh frequency range and the equipment he described is beyond the scope of many teaching laboratories. The sing-around technique for accurate measurements of ultrasonic velocity in liquids was discussed by SATYABALA et al. [3] and V. S. SOITKAR et al. [4].

Recently reverberation method for measurements of ultrasonic velocity and absorption in liquids was discussed by SATYABALA et al. [5]. A system using non-resonant transducers for absorption measurement in CO_2 and air mixture was described by V. N. BINDAL et al. [6].

So it is clear that more attempts have been made on ultrasonic measurements in liquid than in gases.

The commercial ultrasonic generator and detector would be the most satisfactory solution, but such an item of equipment would be excessively expensive.

In the present paper we described an instrument suitable to generate and detect pulsed ultrasonics at frequency 40KHz in gases. The major financial outlay is single trace oscilloscope with band width 5 MHz, which almost all laboratories possess. The circuit is implemented by using locally available integrated chips. Hence the equipment is useful for demonstration purposes at post-graduate level as well as for research purpose.

2. Acoustical architecture of the system

Quartz transducers having resonant frequency 40 ± 1 kHz and diameter 1 cm are used for ultrasonic velocity and absorption measurements. Sample container is made up of steel and has dimensions 30cm × 30cm × 30cm. The inner surfaces of the walls of container are kept rough to avoid multiple reflection of ultrasound. Sender transducer is rigidly fixed to one side of container and cables are taken out from small hole which is then closed with araldite. Receiver transducer is fixed on hollow movable steel rod to which scale is attached having least count of .01cm. To avoid leakage at the time of movement of receiver transducer, rubber gaskets are used.

In the present case observations are made at room temperature (25° C) and at atmospheric pressure. The change in temperature of medium due to adiabatic compressions is negligible as pulsed system is used [7].

To measure and maintain pressure of gas in the container the elaborate gas handling system described by THOMAS et al [8] may be used. The self explanatory block diagram of the system is shown in Fig. 1.

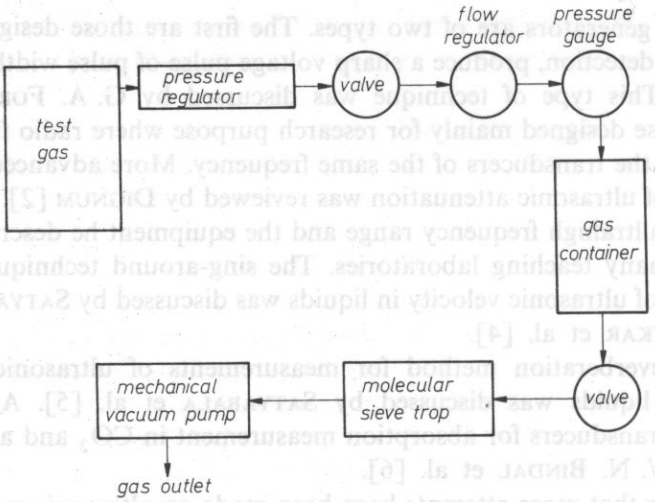

Fig. 1. Gas handling system (Block diagram)

3. Instrumentation

The schematic diagram of the instrument is shown in Fig. 2. The pulse generator generates sharp radio frequency (40 kHz) pulses of pulse width 0.012 ms to 0.86 ms with radio frequency pulse repetition rate of 156.25 Hz.

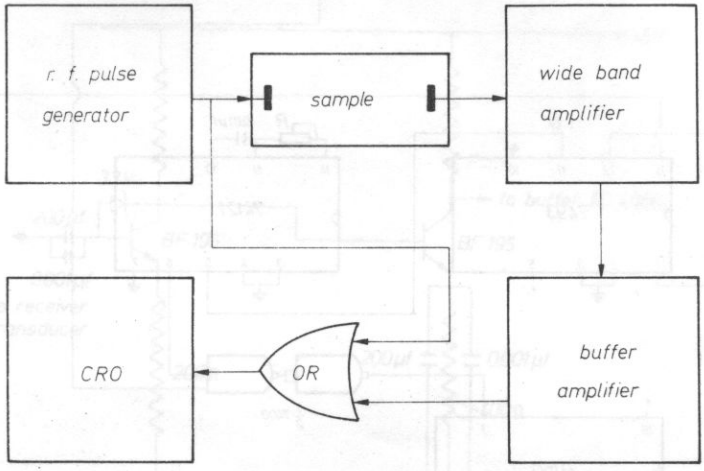

Fig. 2. Block diagram

This radio frequency pulse is placed across sender transducer (whose resonance frequency is the same as that of radio frequency pulse) causing it to ring and send ultrasonic pulse through sample. At the other end of sample the receiver transducer converts ultrasonic pulse into *rf* pulse. This pulse is directly displayed on CRO for absorption measurement. For velocity measurement sender pulse and amplified received pulse through buffer, is connected to OR gate and displayed on CRO screen to measure time delay.

3.1. Pulse generator

A radio frequency pulse generator circuit is shown in Fig. 3 and its wave forms are sketched in Fig. 4 (not to scale). The *rf* generator is designed to generate 40 kHz frequency using two NAND gates of IC 7400 (wave form a). This 40 kHz frequency is divided by two IC 7493 (four bit binary counter). Each IC 7493 divides frequency by 16. So resulting frequency is 156.25 Hz (wave form b). The width of pulse of frequency 156.25 Hz is controlled by monostable multivibrator IC 74121 which produces variation in width from 0.012 ms to 0.86 ms (wave form c). The wave forms a and c are given to AND gate (implemented by using IC 7400) which generates radio frequency pulse of frequency 40 kHz and of sharp width (width can be changed by changing R). This radio frequency pulse is given to buffer IC 4050 with pull up of + 7V which gives 7V peak to peak pulse for ultrasonic generation and is applied to sender transducer.

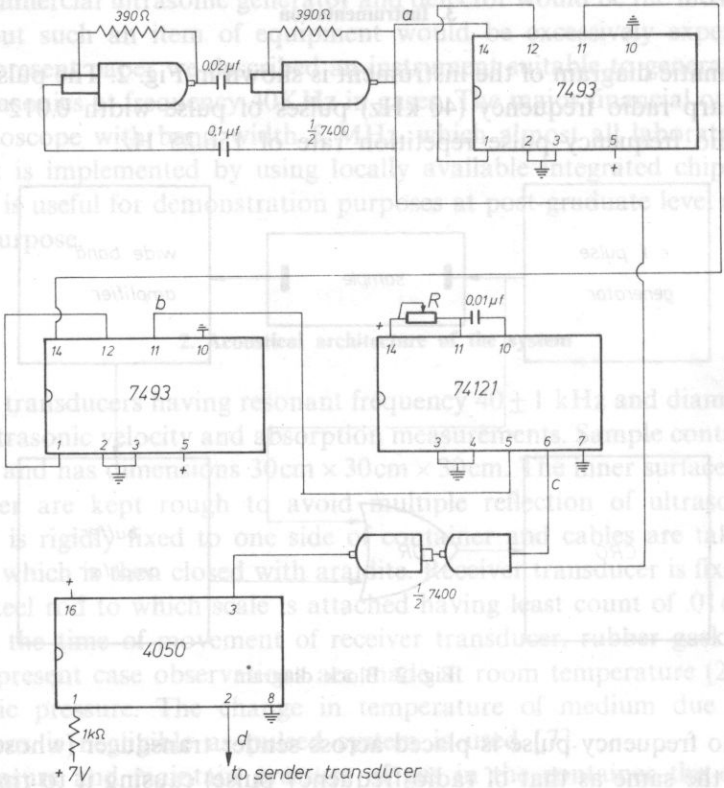

Fig. 3. RF Pulse Generator

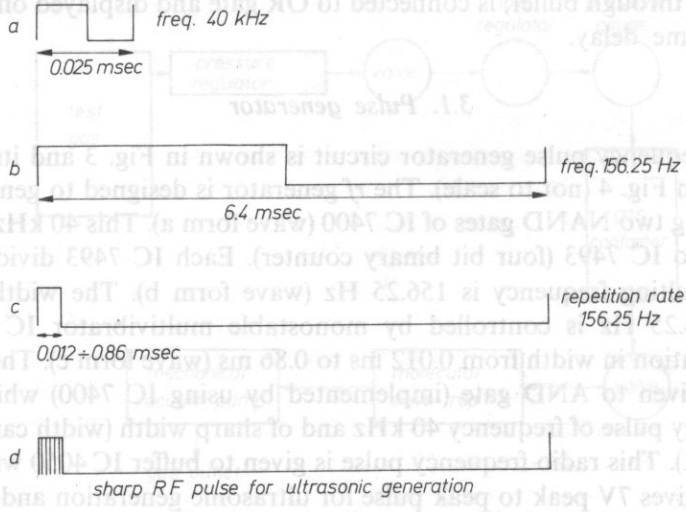

Fig. 4. Wave forms

3.2. *Amplifier*

Amplifier is designed to amplify received *rf* pulse using transistors BF 195 (Fig. 5). The emitter resistance of transistor Q_1 is unby-passed to increase input resistance and band width and to reduce distortion and noise.

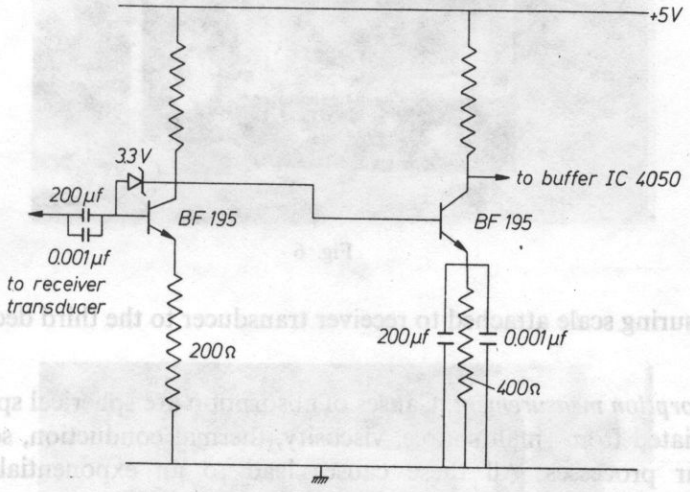

Fig. 5. Amplifier

The Zener diode 3.3 V is connected between base and collector of Q_1 to give proper d.c. bias and stabilise V_{CE}. The output of first amplifier stage is directly coupled to second transistor Q_2. The second stage is by-passed in order to increase voltage gain amplifier. The output of amplifier is given to buffer IC 4050 with pull-up of +7V.

3.3. *Measurement techniques*

3.3.1. Velocity measurement. For velocity measurement sender pulse from buffer and received pulse from amplifier followed by buffer (IC 4050) is given to OR gate and displayed on CRO (Fig. 6). (Pulse on left is sender pulse and on right received pulse). The single beam CRO is sufficient to display both pulses simultaneously because pulse repetition rate of pulse generator is very large as compared to the time required for ultrasonic pulse to travel through sample. As both the transducers are inside the container, the exact distance measurement between the two is not possible. Therefore change in distance Δx with corresponding change in time Δt is measured and velocity is found out by relation $v = \Delta x/\Delta t$. Readings are reported in Table 1. Mean value of ultrasonic velocity at 25°C in air at atmospheric pressure is found out to be 333.31 m/s. Literature value [9] is 331.46 m/s at 0°C. The accuracy in velocity measurement is 0.69%. The accuracy can be further increased by improving least

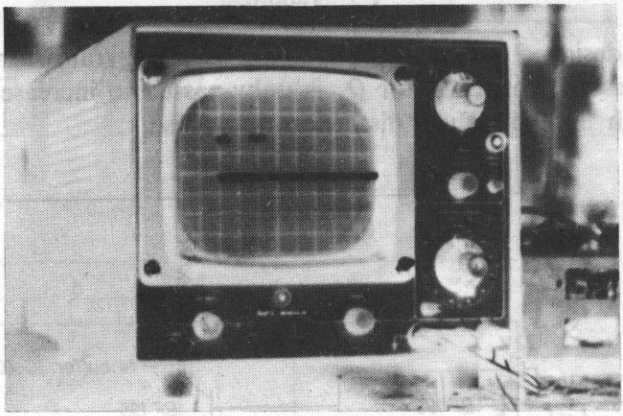

Fig. 6

count of measuring scale attached to receiver transducer to the third decimal place of centimetre.

3.3.2. Absorption measurement. Causes of absorption are spherical spread of beam of sound radiated from small source, viscosity, thermal conduction, scattering and intermolecular processes. All these causes lead to an exponential decrease in amplitude with distance.

For absorption measurement the received pulse is displayed on CRO screen directly (Fig. 2). Fig 8 shows five time expansion of received pulse. Pulse height

Table 1. Ultrasonic velocity in air (frequency 40 kHz and at atmospheric pressure.)

	Δx [m]	Δt [μs]	$v = \frac{\Delta x}{\Delta t}$
1)	.0123	37	332.43
2)	.0224	67	334.32
3)	.0323	97	332.98
4)	.0291	87	334.48
5)	.0127	38	334.21
6)	.0332	100	332.00
7)	.0283	85	332.94
8)	.0314	94	334.04
9)	.0253	76	332.89
10)	.0243	73	332.87

Mean ultrasonic velocity in air at 25°C is found out to be 333.31 m/s.

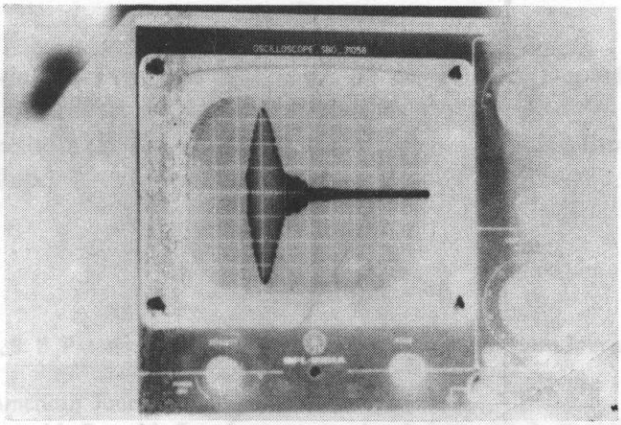

Fig. 7

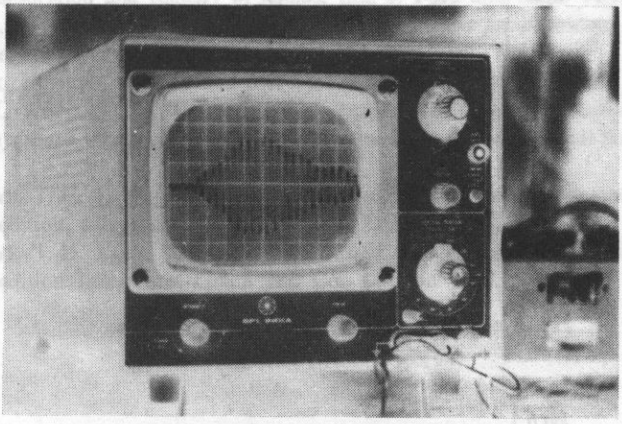

Fig. 8

Fig. 9 measured by changing the distance between transducers. The graph of pulse height vs distance is exponential as expected (Fig. 9). The graph of log e (pulse height) vs distance is shown in Fig. 10. Slope of this straight line is absorption coefficient α in neper/cm and when expressed in dB/cm the value is 8.686 α dB/cm. The attenuation of sound in air is abnormal for frequency variation and also depends greatly on moisture content [10].

In present case the value of α from graph is found out to be 8.53×10^{-3} neper/cm (or .074 dB/cm) at 40 kHz.

Literature value [10] of α for sound waves in air at relative humidity of 40% is 2.26×10^{-3} neper/cm at 50 kHz.

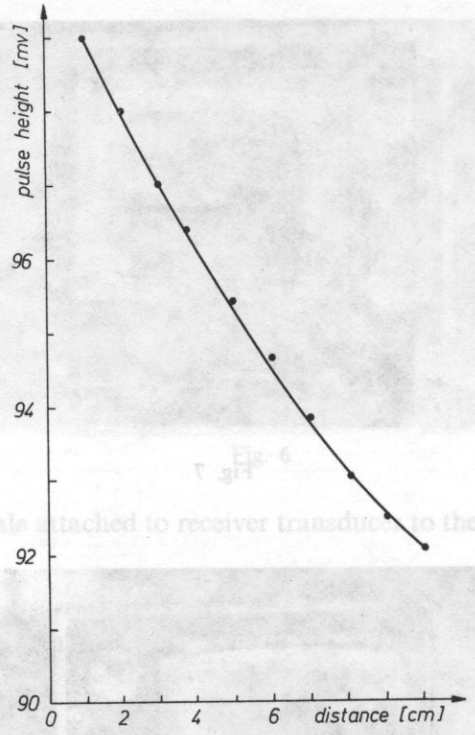

Fig. 9. Graph of pulse height (h) vs distance

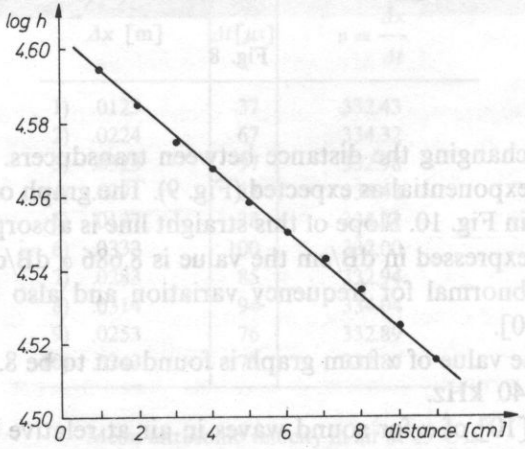

Fig. 10. Graph of log (pulse height) vs distance

Acknowledgement

Thanks are due to Principal and Head of the Physics Department, Vidarbha Mahavidyalaya, Amravati for laboratory facilities.

One of the authors (P. K. Agnihotri) is grateful to CSIR for the award of junior research fellowship.

References

[1] G. A. Forster, S. B. Palmer, *Experiments in pulsed ultrasonics*, American Journal of Physics, **38**, 814 (1970).

[2] R. Dignum, American Journal of Physics, 32, p. 507 (1964).

[3] S. P. Satyabala, M. Rao, M. Suryanarayana, Acust. Lett. GB **2**, 29 (1978).

[4] V. S. Soitkar, K. P. Sunnapwar, G. N. Navaneeth, *A solid state pulsed sing-around system for ultrasonic velocity measurements*, Ind. J. Pure and Appl. Phys., **19**, 555 (1981)

[5] S. P. Satyabala, M. Rao, M. Suryanarayana, *A resonance reverberation technique for measurement of ultrasonic absorption and velocity in liquids*, Ind. J. Pure and Appl. Phys., **23**, 595 (1985).

[6] V. N. Bindal, T. K. Saksena, S. Chandra, *A simple method for ultrasonic relaxation studies in carbon dioxide*, Ind. J. Pure and Appl. Phys., **20**, 196 (1982).

[7] P. Vigeureux, *Ultrasonics*, Chapman and Hall Ltd, London 1952, p. 46.

[8] G. Thomas, L. Winter, L. H. Garnett, *High temperature ultrasonic measurements of rotational relaxation in hydrogen, deuterium, nitrogen and oxygen*, Journal of Acoustical Soc. Am. 42, No. 4, 848 (1967).

[9] G. W. C. Kaye, T. H. Laby, *Tables of physical and chemical constraints and some mathematical functions*, 11 edition, Longmans, Green and Co. London 1956, p. 61.

[10] G. W. C. Kaye, T. H. Laby, *Tables of physical and chemical constraints and some mathematical functions*, 11 edition Longmans, Green and Co., London 1956, p. 60.

Received October 9, 1987.

ARCHIVES OF ACOUSTICS
12, 3–4, 311–318 (1987)

AN ARRAY RECEIVER SCHEME FOR REDUCING REFRACTION INDUCED ARTIFACTS IN ULTRASONIC TOF TOMOGRAPHY

K. SRINIVASA RAO, T. M. SRINIVASAN

Indian Institute of Technology
(Madras 600 036, India)

Different types of errors caused by refraction effects in ultrasonic time-of-flight (TOF) tomography are discussed. The effectiveness of a three element experimental array receiver in reducing refraction induced artifacts in ultrasonic TOF tomography is evaluated. During data acquisition, TOF and peak values of the received signal is measured for each of the three receivers. A peak value index (PVI) is computed for each receiver. The PVIs give an indication of the deviation of the interrogating beam from line-of-sight path. Based on these indices a propagation path is assumed for the ultrasonic beam in the medium and image reconstruction is performed along these assumed propagation paths. These propagation paths are closer to the actual paths than the generally assumed line-of-sight paths and hence superior tomograms are obtained when reconstruction is done along these assumed propagation paths. Tomograms of agar gel objects and excited sheep heart indicate that this method is effective in reducing the geometric distortions in the reconstructions. The tomograms are quantitatively evaluated using two error measures.

1. Introduction

In ultrasonic time-of-flight (TOF) tomography, refraction effects give rise to inaccurate reconstructions, poor resolution and geometric degradations [5]. The origin of these errors can be traced back to the data acquisition schemes used in ultrasonic tomography. Following the conventional X-ray tomography techniques, in ultrasonic tomography a finite aperture receiver is placed opposite to the transmitter along the line-of-sight. However, due to refraction, an ultrasound beam launched at the transmitter, does not travel strictly along the line-of-sight path in the medium. Due to this, a portion of the transmitted beam may fail to reach the finite aperture receiver, thus causing a reduction in the amplitude of the received signal. In TOF tomography, due to time-walk and time-hop phenomenon, variations in received signal amplitude cause errors in estimation of time of flight [6]. Particularly, when the beam is incident upon the boundary of a curved refractive structure, deviation from straight line path is large and time-walk and time-hop errors will be predominant. When these erroneous TOF projections measured over

non-straight line paths are processed with standard straight line reconstruction methods, the quantitative accuracy of the tomograms will further deteriorate.

The finite width of the transmitted beam, refraction and diffraction effects give rise to multiple propagation paths between the transmitter and the receiver [9]. Under multipath conditions the TOF measuring circuit always registers the TOF of the first arriving pulse. Because of this the TOF tomograms show poor resolution and macrostructural geometric degradations [5]. The nature of these geometric degradations is such that regions of higher acoustic speed appear larger and regions of lower acoustic speed appear smaller than their geometric sizes. It has been demonstrated that the magnitude of these geometric degradations are refraction dependent. Multipath also gives rise to errors in TOF estimates. When multiple rays arrive at the receiver at different time instants, there will be phase cancellation effects [5]. This will appear as noise in TOF projection data.

Resolution in TOF tomography depends upon the speed of ultrasound within a resolution cell. For example, very small regions of high acoustic speed will cause some energy to arrive earlier than the bulk of energy through different pathways and hence such regions can be easily detected [8]. Conversely, in case of small regions of low acoustic speed, the energy received from these regions will be masked by the bulk of energy arriving earlier through paths having higher acoustic speed. This masking will occur even if the bulk of the energy is arriving through regions of low acoustic speed. Thus the resolution is poor for regions of low acoustic speed.

Attempts have been made to compensate for refraction effects in velocity tomograms [1, 3, 5]. These are post-reconstructive cleaning up procedures and are iterative in nature. These methods have provided only modest improvement in the image quality, but the resolution is not improved [9]. Moreover, it is preferable to prevent the refraction induced artifacts from entering into the reconstructions rather than trying to refine the corrupted tomograms. A method based on this approach is experimentally investigated and reported in the present work.

In the method presented here, an array receiver is used. By using an array receiver with sufficiently large aperture, artifacts caused by the parts of beam missing the receiver can be reduced [2]. By measuring the signal on each element of the array, beam profile at the receiving plane can be obtained and depending upon the location of the peak amplitude point of the beam profile, a propagation path can be assumed for the interrogating beam through the medium. As a first step in implementing the array receiver system, three closely spaced individual hydrophones are used. The three transducers are placed opposite to the transmitter such that the central receiver is in line with the transmitter as shown in Fig. 1. The line which joins the center of the transmitter with the transducer registering maximum acoustic field amplitude is selected as the propagation path of the ultrasound in the medium. Since usually these assumed propagation paths are closer to the actual in comparison to the generally assumed straight line paths, images of more accurate dimensions are obtained by reconstructing along these paths.

2. Method

Each hydrophone of the receiving array has a 2 MHz PZT element of 2 mm diameter. The center-to-center spacing between the hydrophones is 4 mm. The transmitter consists of a 2 MHz PZT element of 20 mm diameter. During data acquisition, at each step, the TOF and the peak value of the received signal is measured for each of the three hydrophones. The TOF is measured with a resolution of 1 ns and the peak value is measured with 8 bits resolution. A microprocessor controlled data acquisition system is used to acquire the projection data. Thirty projections are measured from the object with an angular spacing of 6° between the projections and the linear sampling interval for each projection is 2 mm. At the end of the experiment, the measured projection data is transferred to a remote image processing computer (PDP 11/23) through a RS 232C communication link.

For a straight line propagation path, the peak amplitude point of the ultrasound beam also shifts to one of the side receivers and the peak value measured from that peak value measured from this receiver will be relatively large. When the propagation path deviates from the straight line path, the peak amplitude point of the beam also shifts to one of the side receivers and the peak value measured from that side receiver will have a relatively larger value. Thus, the peak values measured from the receivers can be used to detect the deviation from the straight line path. In order to compensate for the unequal sensitivities of the receivers a peak value index (PVI) is defined as:

$$\text{peak value index (PVI)} = P_0/P_m, \tag{1}$$

where P_0 – peak value of the signal received with the object in the coupling medium between the transducers; P_m – peak value of the received signal with only the coupling medium between the transducers.

With a straight line propagation path, if the entire cross section of the beam is subjected to the same amount of attenuation, the peak value indices of all the receivers will be equal. When the propagation path is bent towards any of the off central receivers, the corresponding receiver will have a maximum value of PVI. It should be noted that the knowledge of maximum PVI for a given receiver will not provide precise information about the actual propagation path. However, as a first order approximation, the line joining the center of the transmitter and the receiver having maximum PVI is assumed to be the propagation path of the interrogating beam. The TOF recorded by that receiver having maximum PVI is back projected along this assumed propagation path. Since the signal amplitude on this receiver is large, the TOF measured from the receiver will be least affected by the time-walk and time-hop errors [6].

The standard reconstruction algorithms require equiangularly spaced projections measured over a straight line path. The three sets of TOF projections measured with

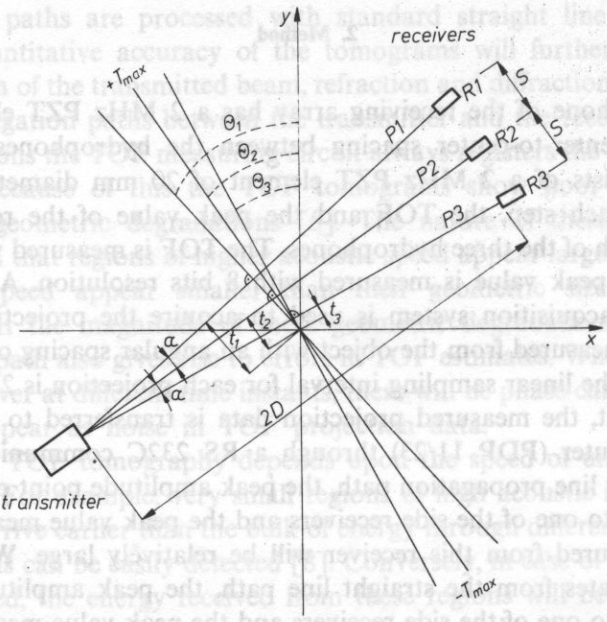

Fig. 1. Transducer configuration for three receiver technique

this three receiver scheme are rearranged using a sorting algorithm to obtain a single modified projection set so that standard reconstruction methods can be used. The sorting algorithm used here is the same as the one used to convert fan beam projections into parallel ray projections [7] and is based on the mathematical relation between the ray sums of the three receivers as given below.

The geometry of the scanning apparatus is shown in Fig. 1. Let the projections be denoted as $P(\Theta, t)$, where Θ and t define the propagation path of the interrogating beam. For the line integral measured over the propagation path $P2$ with the middle receiver $R2$, Θ is equal to Θ_2 and t is equal to t_2 as shown in Fig. 1. From the geometry it can be shown that for small values of α (in the present experimental setup $\alpha = 2°$ and $\cos\alpha$ is taken equal to unity) Θ and t corresponding to the propagation path $P1$ are given by

$$\Theta_1 = \Theta_2 + \alpha \quad \text{and} \quad t_1 = t_2 + S/2. \tag{2}$$

where S is the spacing between the receivers. Similarly, for propagation path $P3$, the corresponding relations are

$$\Theta_3 = \Theta_2 - \alpha \quad \text{and} \quad t_3 = t_2 - S/2. \tag{3}$$

It can be inferred from the above equations that the straight line propagation path $P2$ for a given Θ and t coincides with the propagation path $P1$ or $P3$ for appropriately modified values of Θ and t. Thus we may say that the line integrals measured by the receivers $R1$ or R3 are the same as the one that would be measured

by the middle receiver $R2$ for a suitably modified values of Θ and t. This fact is used in sorting the projection data. When the PVI of, say, receiver $R1$ is more than that of the other two receivers, the TOF by the central receiver $R2$ is ignored and the TOF measured by receiver $R1$ is placed in an appropriate location in the modified projections.

In order to simplify the sorting procedure, the TOF projections and the peak amplitude value projections measured at an angular spacing of 6° are expanded by first order interpolation to obtain projections at 2° spacing, so that the angular spacing is equal to α. The additional projection data thus generated by interpolation also reduces the noise in reconstructed images [7]. While sorting the projections at $\Theta = 2°$ and at $\Theta = 178°$ it is possible that they may give rise to entries in modified projections, at projection angles $\Theta = -2°$ and $\Theta = 180°$. The appropriate location of these values in final projection are selected based on criteria:

$$P(\Theta, t) = P(\Theta + 180, -t). \tag{4}$$

After the sorting is completed, it is found that in some of the locations of the modified projection set, there are no entries. This situation arises when the maximum value of PVI jumps from $R1$ to $R3$ or vice versa. However, the number of such locations is usually less than 10 percent of the total line integrals in the projection. The TOF values corresponding to these locations are computed from the TOF values of the neighbourhood locations, by using first order interpolation.

The conventional filtered back projection algorithm is used to reconstruct a 64×64 pixel image from these 90 modified projections. For comparison, an image is reconstructed from the 90 interpolated projections of the middle receiver alone. This image is the same as the one that would have been generated by a standard tomographic scanner employing a single receiver. For display purpose, these images are expanded by first order interpolation to 256×256 pixels.

3. Results and discussion

The merit of the three receiver technique is evaluated qualitatively using two different objects and quantitatively by two error coefficients namely, the geometric distortion coefficient and the normalized mean squared error. The geometric distortion coefficient δ [4] gives a measure of the macrostructural geometric degradations present in the reconstructions. This is measured by comparing the threshold versions of a reference tomogram and a test tomogram. Thresholding is done such that all pixels below a threshold are set to zero and all pixels above this value are set to one. If I and J are the reference and test tomograms after the above procedure, the distortion measure is given by

$$\delta = \frac{1}{N \cdot N} \sum_{i=1}^{N} \sum_{j=1}^{N} |I(i, j) - J(i, j)|, \tag{5}$$

where i, j are pixel co-ordinate and $N \times N$ is the image dimension. The standard normalised mean squared error (NMSE) [10] between the reference tomogram and the test tomogram is used as a measure of the quantitative accuracy.

To simplify the computation, the error coefficients are evaluated for tomograms of an agar gel cylinder. The tomogram of a cylinder is circular in shape and has a constant TOF value in all pixels. The error free projections of such cross section can be generated mathematically [10]. Tomograms reconstructed from these computed projections are used as reference tomograms for evaluating the error coefficients. The propagation velocity of ultrasound in agar gel is equal to that in water at room temperature. Hence, the refractive nature of the object is controlled by altering the temperature of water bath. Table 1 shows the error coefficients for tomograms of agar gel cylinder obtained at two different values of V_α which is the difference between the propagation velocity of ultrasound in the object and in the coupling medium. For evaluating the geometric distortion coefficient the threshold level is chosen as half the average TOF value across the cross section. It can be observed that the geometric distortion coefficients are less for the tomograms obtained with the proposed three receiver technique in comparison to those of the tomograms obtained using single receiver. The NMSE values are also less for the three receiver tomograms thus indicating that these TOF values are closer to the actual values for these objects.

The two objects used for qualitative evaluation are an agar gel cylinder with a hole (scanned in transformer oil $V_\alpha = 36$ m/s) and an excised sheep heart. TOF tomograms of these objects are shown in Fig. 2 and Fig. 3 respectively. The bright circles superimposed on the images in Fig. 2 represent the boundaries of the original object. The effectiveness of the proposed three receiver technique in reducing the geometric distortions is evident from the three receiver tomograms given in Fig. 2(b) and Fig. 3(b). It may be noticed that the geometric distortion in the tomograms is not eliminated completely. This is due to the limited number of elements in the

Table 1. Geometric distortion coefficient (δ) and normalised mean squared error NMSE for tomograms of an agar gel cylinder

Object	δ	NMSE
Agar gel cylinder $V_\alpha = 24$ m/s		
Single receiver	0.01928	0.0415
Three receivers	0.01733	0.0321
Agar gel cylinder $V_\alpha = -21$ m/s		
Single receiver	0.07885	0.1276
Three receivers	0.06543	0.0997

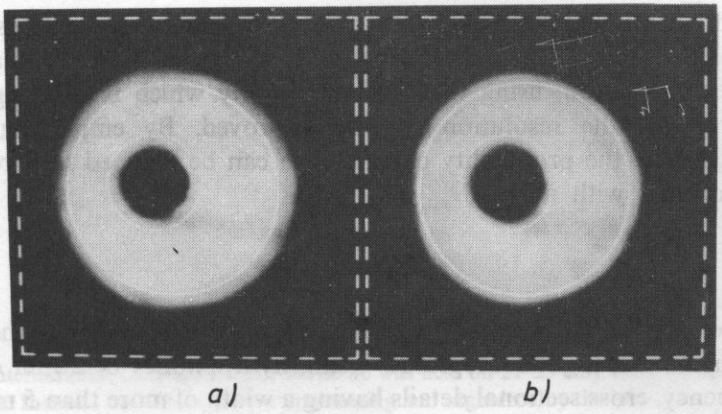

Fig. 2. TOF tomograms of an agar gel object scanned in transformer oil $V_\alpha = 36$ m/s (a) Tomogram obtained using a single receiver. (b) Tomogram obtained using three receivers

receiving array. By using an array with more number of elements the geometric distortion can be further reduced. In the three receiver tomogram of the excised sheep heart, though there is some improvement in the sizes of the left ventricle and that of the whole heart, the size of the right ventricle is reduced. This drawback arises from the fact that the PVI values can detect the deviation from straight line propagation path only if the entire cross section of the beam is subjected to the same amount of attenuation. In the actual sheep heart the width of the right ventricle is only about 5 mm, due to which the above assumption is invalidated. In this case also, by employing an array with more number of elements, actual beam profile in the receiving plane can be obtained and using this information, the deviation from straight line path can be detected with higher accuracy.

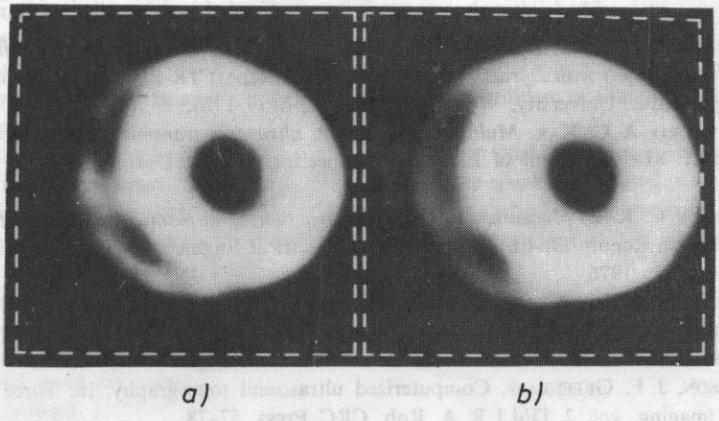

Fig. 3. TOF tomograms of an excised sheep heart. The circular hole is the left ventricle and the elongated hole is the right ventricle. (a) Tomogram obtained using single receiver. (b) Tomogram obtained using three receivers

As already mentioned, limited resolution of the TOF tomograms arises from the method employed for measuring TOF. Instead of using the TOF of first arriving ray for image reconstruction, using the TOF of the ray which is carrying maximum amount of energy the resolution can be improved. By employing a narrow interrogating beam, the probability of multipath can be reduced thus reducing the artifacts associated with it.

4. Conclusions

The three receiver array system used here is effective in reducing the geometric distortions in time-of-flight tomograms. Using hydrophones of 2 mm diameter at 2 MHz frequency, cross sectional details having a width of more than 5 mm could be improved. Details smaller than this dimension are not improved by this scheme. This is thought to be due to the limited number of elements in the receiving array. Optimization of number of receivers and frequency of operation is under progress. Better methods for measuring the TOF are being investigated.

References

[1] S. A. JOHNSON, J. F. GREENLEAF, W. F. SAMAYOA, F. A. DUCK, J. D. SJOSTRAND, *Reconstruction of three dimensional velocity fields and other parameters by acoustic ray tracing*, Ultrasonic Symp. Proc., IEE Cat. 75 CHO 994-3SU, 46–51 (1975).

[2] R. M. SCHMIDT, C. R. MEYER, P. L. CARSON, T. L. CHENVERT, P. H. BLAND, *Error reduction in through transmission tomography using large receiving arrays with phase insensitive signal processing*, IEEE Trans. on Sonics and Ultrasonics, SU-31, 4, 251–248 (1984).

[3] H. SCHOMBERG, *An improved approach to reconstructive ultrasound tomography*, J. Phys. D: Appl. Phys., **11**, 15, L181–L185 (1978).

[4] P. SOBEL, R. M. RANGAYYAN, R. GORDON, *Quantitative and qualitative evaluation of geometric deconvolution of distortion in limited-view computed tomography*, IEEE Trans. on Biomed. Eng., BME-32, 5, 330–335 (1985).

[5] A. H. ANDERSON, A. C. KAK, *The application of ray tracing towards a correction for refraction effects in computed tomography with diffracting sources*, Research Report TR-EE 84–14, School of Electrical Engineering, Purdue University, West Lafayette, IN, May 1984.

[6] C. R. CRAWFORD, A. C. KAK, *Multipath artifacts in ultrasonic transmission tomography*, Research Report TR-EE 81–43 School of Electrical Engineering, Purdue University, West Lafayette, IN, Dec. 1981

[7] K. A. DINES, A. C. KAK, *Measurement and reconstruction of ultrasonic parameters for diagnostic imaging*, Research Report TR-EE 77–4, School of Electrical Engineering, Purdue University, West Lafayette, In, Dec. 1976.

[8] J. F. GREENLAEF, S. A. JOHNSON, R. C. BAHN, B. RAJAGOPOLAN, S. KENUE, Introduction to computed ultrasound tomography, In: Computer aided tomography and ultrasonics in medicine [Eds.] Ravive et al. North-Holland Publ. Co. 1979, 125–136,

[9] B. S. ROBINSON, J. F. GREENLAEF, Computerized ultrasound tomography, In: Three dimensional biomedical imaging, vol. 2, [Ed.] R. A. Rob, CRC Press, 57–78.

[10] A. ROSENFIELD, A. C. KAK, Digital picture processing, vol. 1, Academic Press New York 1976.

Received on October 20, 1986.

C H R O N I C L E

INTER-NOISE 86

The 15 th International Conference Inter-Noise 86 was held on 21–23 July 1986. It was sponsored by the International Institute on Noise Control Engineering and organized by the Massachusetts Institute of Technology in Cambridge, USA.

525 representatives including students from 36 countries from the whole world took part in the Conference, namely from the USA, Japan, West Germany, Denmark, Sweden, France, Belgium, Great Britain, Australia, China, Netherlands, Israel, Norway, Finland and Canada.

Professor Richard H. LYON, the chairman of the Organizing Committee, welcomed the participants in the Conference, asking the President of the International Institute on Noise Control Engineering, Professor Fritz INGERSLEV to open the Conference. Professor INGERSLEV congratulated the Institute on Noise Control Engineering in the USA on the occasion of organizing now the 15th international conference devoted to the problems of noise control, and then presented briefly the history of previous conferences.

The motto of the Inter-Noise 86 Conference was "progress in noise control". At the conference 271 lectures were delivered in the framework of three plenary sessions and sessions denoted to particular subjects. Three lectures were delivered at plenary sessions.

Professor Jens P. BLAUERT from Ruhr University in Bochum West Germany delivered a lecture "Cognitive and aesthetic aspects in technical noise control". The speaker paid particular attention to low noise levels which can essentially interfere with man's environment. He gave a number of examples to support his thesis.

Dr Frank FAHY from the Institute of Sound and Vibration Research, Southampton University Great Britain delivered then the plenary lecture "Sound and structural vibration – a review". Dr FAHY presented a complete review of the problems, based on his recently published book "Sound and Structural Vibration", analyzing the vibration of a body in the acoustic field by applying KIRCHHOFF-HELMHOLTZ differential equations. He also discussed various aspects of the mutual interaction between sound and the structure of a vibrating body. In his discussion, he included the problem of sound radiation by different vibrating bodies.

The third plenary lecture was delivered by Dr George MALING from IBM, Poughkeepsie. In his lecture "The progress in applying sound intensity for noise control", the speaker presented in a brief outline the historical development of the sound intensity problems, beginning with Olson's wattmeter from 1930, and then presented various studies and applications used in many countries for noise control purposes. He also discussed the standardization work.

The other lectures were delivered at 57 sessions within 27 ones on particular subjects. These sessions included:

1. Sound sources, reduction of source emission (4 sessions)
2. Industrial noise (4 sessions)
3. Sound systems
4. Hydraulic systems
5. Diagnostics (2 sessions)
6. Structural noise (2 sessions)

7. External noise – propagations (3 sessions)
8. Sound transmission
9. Control of airport noise (5 sessions)
10. Dampers and absorbers (3 sessions)
11. Signal analysis (3 sessions)
12. Legislation (3 sessions)
13. Influence of airport noise on health
14. Noise reduction (3 sessions)
15. Measurements
16. Computers in measurements of acoustic quantities (2 sessions)
17. Active methods of noise control (2 sessions)
18. Aerodynamic noise (2 sessions)
19. Ventilator noise (3 sessions)
20. Communal noise (3 sessions)
21. Acoustic holography
22. Sound intensity (3 sessions)
23. Standardization
24. Vibration (2 sessions)
25. Transportation noise
26. Psychoacoustics
27. Acoustics in South America

The sessions were held at the same time in 6 rooms. Most interest among the conference participants was enjoyed by sessions on airport noise, industrial noise, reduction of source emission and also those on the problems involved in applying intensity methods. During the conference, there was an exhibition of acoustic equipment and sound-absorbing systems and materials, presented by 18 companies, mainly from the USA, Japan and Denmark, e.g., General Radio, Brüel-Kjaer and Rion.

On 22 July, 1986, there was a plenary session of the members of the Internation Institute on Noise Control Engineering, headed by the president of this organization, Professor Firtz INGERSLEV from Denmark. The president presented a report on the annual activity and then the projected Inter-Noise conferences in the next years.

These conferences will be held as follows: Inter-Noise 87, Peking, China, 15-17 September 1987, Inter-Noise 88, Avignon, France, 30 August–1 September 1988, Inter-Noise 89, Los Angeles, USA.

Z. Engel